Influence of exchange and correlation on the conductance in semi-infinite scattering setups

von

Swantje Heers

Diplomarbeit in Physik

vorgelegt der

Universität Hamburg

im
Juli 2007

angefertigt am

Institut für Festkörperforschung (IFF)
Forschungszentrum Jülich

Summary

As microelectronics turns into nanoelectronics, academic and industrial research aims at the exploration of new concepts and materials such as complex tunnel junctions for spintronics, quantum transport in molecular devices or nanowires and carbon-nanotubes based electronics. Very often, theoretical understanding of these innovative devices and materials is lacking as the calculation of electronic transport on the nanoscale is a very challenging problem. This is due to the complicated interplay of the large number of electrons and to the special geometry of the scattering setup. While *ab initio* transport calculations became possible recently, the conventional mean-field approach might underestimate the influence of the electron-electron interaction in these systems, which is exclusively included in an effective potential. In this thesis I focus on the effects of this interaction, investigating simple three-dimensional infinite model systems with a potential which varies in one direction of space only. They model the physical situation of a thin layer of vacuum, an isolating material or a metal with another electron density sandwiched between two metallic leads.
In the first part of this work I calculate the conductance in the single-particle picture, tackling the problem of the scattering setup. The typical scattering geometry consists of a finite scattering volume, attached to semi-infinite leads at two sides. The special scattering boundary conditions needed in this situation prevent a simple implementation in reciprocal space. One of the possibilities to overcome this challenge is given by the Green-function embedding method developed by Inglesfield [Journal of Physics C, 14:3795 (1981)] for arbitrary, three-dimensional potentials: The addition of a supplementary term to the Hamiltonian ensures the correct boundary conditions.
The Green-function embedding method is tailored to the setup investigated in this thesis and here implemented in a plane-wave basis set to calculate the Green function for non-interacting electrons. For one-dimensional piecewise constant potentials like quantum wells and potential barriers the Green function can be calculated analytically as well, enabling a comparison of the numerical and the analytical results.
In order to include the electron-electron interaction beyond the contribution already contained in the effective potential, the irreducible polarization is calculated. It is related to the non-interacting polarization function via a Dyson-type equation derived in time-dependent density-functional theory, including dynamic electronic interaction effects in the exchange-correlation kernel. The latter is not known exactly and here approximated in the adiabatic local-density approximation. Finally, the conductance is calculated using a relation between the polarization function and the conductance derived by P. Bokes and R. Godby [Physical Review B, 69(24):245420 (2004)]. As this method is based on the linear-response approach, the investigations are restricted to zero-bias conductance.
It is shown that in the case of non-interacting electrons the conductance agrees very well with the analytical result of the Landauer formula. When exchange and correlation are taken into account, an enhancement of the conductance can be observed.

Zusammenfassung

Aufgrund der vielversprechenden Entwicklung von der Mikro- zur Nanoelektronik werden in der universitären und industriellen Forschung größte Anstrengungen unternommen, um neuartige Konzepte und Materialien wie zum Beispiel komplexe Tunnelkontakte für die Spintronik, Quantentransport in molekularen Bauteilen sowie eine auf Nanodrähten und Nanoröhren basierte Elektronik zu erschließen. Häufig fehlt das theoretische Verständnis dieser innovativen Bauteile und Materialien, da die Berechnung von elektronischem Transport in Nanostrukturen sehr kompliziert ist. Die Gründe dafür sind zum einen in der großen Anzahl der miteinander wechselwirkenden Elektronen und zum anderen in der Streugeometrie zu finden. Auch die seit jüngster Zeit möglichen *ab initio* Transportrechnungen lassen die Elektron-Elektron Wechselwirkung nur durch ein effektives Potential in die Rechnungen einfließen.
In dieser Arbeit konzentriere ich mich auf die Auswirkungen der Elektron-Elektron Wechselwirkung und betrachte einfache dreidimensionale, unendliche Modellsysteme mit einem Stufenpotential, welches nur in einer Raumrichtung variiert. Diese Systeme modelieren eine dünne Schicht, die von zwei Metallen eingeschlossen ist und aus Vakuum, einem Isolator oder einem Metall mit einer anderen Elektronendichte besteht. Im ersten Teil der Arbeit werde ich die Leitfähigkeit im Einteilchenbild berechnen. Die typische Streugeometrie besteht aus einer endlichen Streuregion, die von zwei halbunendlichen Leitern umgeben ist. Die in dieser Situation benötigten speziellen Randbedingungen verhindern eine einfache Implementierung im reziproken Raum, können jedoch mit Hilfe der Greenfunktions-embedding Methode [Journal of Physics C, 14:3795 (1981)] integriert werden, die auf beliebige dreidimensionale Potentiale anwendbar ist. Zur Berechnung der Greenfunktion für nichtwechselwirkende Elektronen wird die Embedding Methode auf die zu untersuchenden Systeme zugeschnitten und in einer Basis aus ebenen Wellen implementiert. Die nur in einer Raumrichtung variierenden Stufenpotentiale ermöglichen ebenfalls eine analytische Berechnung der Greenfunktion und den Vergleich mit dem numerischem Ergebnis.
In der Berechnung der irreduziblen Polarisationsfunktion wird nun der Anteil der Elektron-Elektron Wechselwirkung berücksichtigt, der über den bereits im effektiven Potential enthaltenen Beitrag hinausgeht. Die irreduzible Polarisationsfunktion ist über eine Gleichung ähnlich der Dyson-Gleichung mit der Polarisationsfunktion für nichtwechselwirkende Elektronen verknüpft. Der wichtigste Bestandteil dieser aus der zeitabhängen Dichtefunktionaltheorie stammenden Gleichung ist der Austausch-Korrelationskern, welcher die Elektron-Elektron Wechselwirkung enthält, nicht exakt berechnet werden kann und daher in der adiabatischen lokale-Dichte-Näherung approximiert wird. Mit Hilfe der Beziehung zwischen der Polarisationsfunktion und der Leitfähigkeit [Physical Review B, 69(24):245420 (2004)] wird die letztere berechnet. Da diese Beziehung auf der linear-resonse-Theorie basiert, sind die Untersuchungen nur auf den Fall der zero-bias Leitfähigkeit anwendbar. Es wird gezeigt, dass die Leitfähigkeit im nichtwechselwirkenden Fall sehr gut mit dem analytischen Ergebnis der Landauerformel übereinstimmt. Unter dem Einfluss von Austausch und Korrelation wird ein Anstieg der Leitfähigkeit beobachtet.

Contents

1 Introduction **1**

2 Green-Function embedding **7**
2.1 Schrödinger equation in the embedded region 7
2.1.1 The embedding potential 10
2.1.2 Embedded Green function 11

3 Theoretical treatment of electronic exchange and correlation **13**
3.1 Many-body problem in solid-state physics 13
3.2 Quasi-particle picture and the concept of electronic self-energy 15
3.3 Elementary excitations in solids 16
3.4 Green function formalism 17
3.5 The self-energy 21
3.6 Feynman diagrams 23
3.7 The Dyson equation 25
3.8 Hedin's equations 27
3.9 The *GW* approximation 29
3.10 Irreducible polarization 30

4 Concepts of electronic transport **35**
4.1 Single particle view on electronic transport 36
4.2 Conductance and polarization 40
4.2.1 Conductance and conductivity 40
4.2.2 Conductivity and polarization 42
4.2.3 Non-interacting homogeneous electron gas 46
4.2.4 Response to the applied external field 47

5 Application of the Green-function embedding method **49**
5.1 Investigated scattering setup 49
5.2 Equation for the Green function in the embedding region 52
5.3 The embedding potentials 54
5.4 Expanding the Green function in terms of plane waves 56
5.5 Embedding Hamiltonian 56
5.6 Details of the implementation: The numerical parameters 59

6 Test of the Green-function embedding method **61**
6.1 Analytical calculation of the Green function 61

6.1.1 Green function of the homogeneous electron gas 61
6.1.2 One-dimensional Green function 63
6.1.3 Three-dimensional Green function 66
6.2 Determination of the numerical convergence parameters 67
6.2.1 Comparison to homogeneous electron gas 67
6.2.2 Simple one-dimensional potential problems 70
Real energies 70
Complex frequencies 71
6.2.3 Three-dimensional Green function 73

7 Polarization function **79**
7.1 Polarization function in the complex frequency plane 79
7.2 Polarization function of the homogeneous electron gas 83
7.3 Numerical calculation of $\Delta P_0(\mathbf{k}_\parallel, z, z'; i\omega)$ 85
7.3.1 Convolution on the complex frequency axis 85
7.3.2 Two-dimensional Fourier transformation 87
7.3.3 Convergence parameters 87
7.3.4 Extrapolation to $z = z'$ 91
7.4 Total polarization function 93
7.5 Density 95
7.6 Irreducible polarization function 98
7.6.1 Numerical calculation 98
7.6.2 Homogeneous electron gas 100
7.6.3 Potential barrier and quantum well 102

8 Conductance **105**
8.1 Landauer conductance 105
8.1.1 Homogeneous electron gas 106
8.1.2 Potential problems 107
8.2 Inclusion of exchange and correlation effects 110
8.2.1 Homogeneous electron gas 110
8.2.2 Potential barrier and quantum well 111
8.2.3 Discussion 113

9 Summary and outlook **115**

10 Acknowledgments **119**

Bibliography **121**

1 Introduction

Electronic transport in nanostructures, such as tunnel junctions, point contacts, vacuum tunneling microscopy or molecular junctions has become a major subject of both industrial and academic research in the last couple of years. Extending standard semiconductor concepts, new materials such as nanowires, carbon nanotubes [TVD98, HTM$^+$02] or even single molecules [RZM$^+$97, ROB$^+$02] have been explored and probed for electronic transport. They show interesting transport characteristics, which are mostly not understood until now but which are crucial for many technological applications. These new materials might be the key to a new generation of even more powerful computers. For example, carbon nanotubes have raised high hopes due to their combination of unique structural and electronic properties, such as ballistic transport. On the other hand, further shrinking of the structures may be limited by effects such as leakage currents and increasing power consumption [Was03]. As a consequence, transport calculations for nanosize setups moved more and more into the focus of interest. Compared to larger structures on the mesoscopic and macroscopic scale, in this order of magnitude quantum effects start to change and in some cases even to dominate the overall transport properties of the sample. Additionally, atomic details cannot be neglected any more and have to be taken into account.

Therefore, an adequate treatment of systems at nanoscale dimensions requires *ab initio* calculations like density-functional theory (DFT) [HK64, KS65], which was originally developed to investigate structural and electronic properties of stationary systems in equilibrium. Transport calculations (i.e., basically the calculation of the conductance on a microscopic scale) were a new challenge for the electronic-structure community. One of the key problems in transport calculations lies in the special geometry required. In contrast to standard density-functional theory setups, neither can periodic boundary conditions be used to simplify the problem nor is it sufficient to consider a finite volume. Instead one has to treat a scattering setup in which a finite scattering volume is attached to semi-infinite leads at two sides. Due to the broken translational symmetry, the simple description of bulk materials in reciprocal space using Bloch functions is no longer applicable. In contrast, a Green-function formalism is required which entails a much more complicated theoretical framework. The common approach for *ab initio* predictions of conductance is based on the Landauer formula $\Gamma = \frac{2e^2}{\hbar} T(\mu)$ [Lan57, BILP85], which identifies the conductance Γ with the transmission probability $T(\mu)$ for electrons at the chemical potential μ. The Landauer approach is a so-called single-particle approach, which instead of the actual interacting many-particle system only consider the motion of a single particle within the effective potential caused by all other electrons. Nevertheless, the quantization

of the conductance predicted by the Landauer formula is often in good agreement with experimental results and correctly describes effects such as the quantum-Hall effect [KDP80].
In spite of the complications provoked by the scattering boundary conditions, several implementations of density-functional theory tackling the transport problem have been developed. Among them are tight-binding formulations [Mat97, CBLC96], the Korringa-Kohn-Rostoker (KKR) [Kor47, KR54] Green-function approach, and methods in which the Schrödinger equation is integrated on real space mesh-points [HT95]. All of them are real-space implementations and investigate the three different regions (i.e., the two leads and the scattering region) of space separately. The possibility to do so is a direct consequence of the locality of DTF in the conventional local-density approximation (LDA) [KS65, CA80] and generalized gradient approximation (GGA) [PCV$^+$92, PBE96]. A very successful recent implementation of the conductance on a nanosize scale uses a full-potential linearized augmented plane-wave (FLAPW) code [WIB02]. This might initially be surprising, since the FLAPW method explicitly includes periodic boundary conditions in its definition of an augmented plane-wave basis set, and these are contradictory to the special boundary conditions of a scattering problem. Nevertheless, systems with broken translational symmetry can be treated within the FLAPW code using the Green-function embedding method of Inglesfield [Ing81]. The basic idea of the embedding method is to include the boundary conditions imposed on the solution of the Schrödinger equation in the same variational principle from which the Schrödinger equation is derived; in addition to the wave functions the boundary conditions are varied themselves. This procedure yields a supplementary term in the Hamiltonian for the scattering region which ensures the correct boundary conditions.
Although the DFT approach has proved highly valuable for the interpretation of experiments measuring the conductance through nanostructures, some spectacular failures of this approach have also been identified. For example in the case of the current driven through a single molecule, the experimental result for the conductance differs several orders of magnitude from the calculated one [EWK04]. One possible reason for this might be found in the use of single-particle states and the disregard of (non-local) exchange and correlation effects.

In recent years, alternative *ab initio* methods like many-body perturbation theory [FW03, Mah90] have increasingly been used for electronic-structure calculations, often in combination with DFT as a zeroth order approximation. Such approaches allow a more systematic treatment of electronic correlation and led to a (sometimes even qualitative) significant improvement of the numerical results and to a better physical comprehension of spectroscopic experiments. The amelioration is not surprising since DFT by design describes only ground-state properties correctly and considers electronic exchange and correlation effects exclusively by a local exchange-correlation potential [HK64]. Although in DFT theoretically the exact ground state energy of the whole electron system can be calculated, it does not give access to any single-particle properties such as the single-particle energy or the wave function.

Furthermore, the exchange-correlation potential cannot be calculated exactly and has to be approximated. The most common approximations are the local-density approximation and the generalized gradient approximation. Thus, possible failures of DFT might be the consequence of the failure of the chosen exchange-correlation potential. For example, band gaps of semiconductors are systematically underestimated in the local density approximation of DFT, and, in the case of Ge, it even predicts a semi-metal with a negative band gap rather then a semiconductor, whereas the correct result is obtained within many-body perturbation theory [HL86, GSS87]. In contrast to DFT, many-body perturbation theory is suited to the description of excited states. It is based on the Green-function formalism and connects the Green function of a non-interacting system with that of the interacting system. In the case of the one-particle Green function this coupling is described by the Dyson equation which besides the two Green functions contains the electronic self-energy. Incorporating all interaction processes, the electronic self-energy is a very complicated quantity and therefore cannot be calculated exactly. Its most successful approximation is the *GW* approximation [Hed65], derived from the expansion of the electronic self-energy in terms of the screened interaction. It is obtained using a systematic algebraic approach and enables one to calculate the spectrum of quasiparticle excitations measured in photoemission spectroscopy.
As another application of many-body perturbation theory the Bethe-Salpeter equation allows the calculation of the two-particle Green function for the correlated motion of electron-hole pairs [ARDSO98]. Analogously to the Dyson equation the Bethe-Salpeter equation is exact but the relevant correlation term has to be approximated in practical calculations. It gives access to the dielectric polarization and the magnetic susceptibility and can be used to study neutral, particle-conserving excitations such as charge oscillations (plasmons) in metals or bound electron-hole pairs (excitons) in semiconductors. Thus, the Bethe-Salpeter equation is complementary to the *GW* approximation, which describes photoemission processes in which the number of particles changes. Experimentally, excitations calculated with the Bethe-Salpeter equation can be measured in electron energy-loss spectroscopy and optical absorption spectroscopy.
The numerics involved in the *GW* approximation [AG98] and the Bethe Salpeter equation are very complicated [WGAW00]. For periodic systems many operations can be simplified by Fourier transforming the problem to reciprocal space. For that reason almost all implementations were made for periodic (bulk) systems in reciprocal space. There are also some real-space codes for finite systems with localized basis sets, whereas real-space implementations for infinite non-periodic systems are completely lacking.
Another method for spectroscopic quantities outside many-body perturbation theory that includes exchange and correlation effects is time-dependent density-functional theory (TDDFT) [RG84], an extension of static DFT describing the dynamics of a system. Although it was originally developed to describe dynamic phenomena in time-dependent potentials, one of its principal areas of applications today is the analysis of electronic excitations. TDDFT represents an alternative to the Bethe-Salpeter

equation and gives access to the same physical quantities such as the linear density-response function (i.e., the dielectric polarization) and the magnetic susceptibility. In TDDFT, dynamic exchange and correlation effects are included in the exchange-correlation kernel, which just like the exchange-correlation potential in static DFT and the self-energy in the GW approximation is not known exactly and has to approximated.

The integration of electronic exchange and correlation effects in transport calculations is extremely difficult. As pointed out above, the main problem lies in the contradictoriness of the scattering setup with its special scattering boundary conditions (lack of periodicity) and the difficulty to implement a real-space code applicable to infinite systems. However, for the simulation of real devices it is an extremely interesting and important question to go beyond the single-particle Landauer approach and investigate the influence of exchange and correlation on the conductance.
The problem of incompatible boundary conditions, though not in the context of transport, was tackled in a first exploratory work by Fratesi [FBM04]. It deals with the calculation of surface states at a potential step, evaluating the GW approximation with the DFT Green function obtained from the Green-function embedding method. However, although this approach was successful, it does not yield the conductance.
This diploma thesis is a first effort to fill the gap between transport calculations and the treatment of explicit exchange and correlation effects, intending to study the influence of exchange and correlation on the conductance. In order to acquire some experience in this field of research, which is almost unexplored until now, the investigations will be restricted to simple model systems whose numerical treatment is significantly easier than that of realistic ones. I follow the approach of Bokes and co-workers [BG04, BJG06], who derived a relation between the conductance and the irreducible polarization, defined as the linear response of the density to an electric field. This approach to the conductance is especially interesting and promising, since the irreducible polarization is a quantity that can be constructed using *ab initio* methods with inclusion of electronic correlation. However, it has to be emphasized that the linear-response approach limits the validity of the calculations to the zero-bias conductance, thus the slope of the voltage/current characteristics at the origin. Furthermore, only the case of direct current is accessible.
In contrast to the calculations by Bokes and co-workers [BG04], I will investigate three-dimensional infinite systems which should model a realistic scattering setup. They are homogeneous in the xy plane and the potential in the z direction has the shape of a barrier potential or a quantum well. In a first step I calculate the Green function in the single-particle picture, using the embedding method of Inglesfield. It is a universal method valid for arbitrary potentials and can be generalized to realistic systems. However, the simple potentials investigated in this thesis also make it possible to calculate the Green function analytically, and to compare the numerical results obtained with the embedding method to the analytical ones. In order to exclude errors resulting from the inaccuracy of the Green-function embedding method, for further calculations the analytically calculated Green function is taken.

The polarization function in the random-phase approximation (RPA) (i.e., for an effective potential) is related to the irreducible polarization by a Dyson-type equation derived in TDDFT [PGG96]. This irreducible polarization includes exchange and correlation effects via the so-called exchange-correlation kernel, which in general is not known exactly and has to be approximated. For simplicity, in this diploma thesis it is calculated in the simplest non-trivial approximation, the adiabatic local-density approximation (ALDA). Finally, I use the relation between the polarization and the conductance to obtain the latter both with and without the involvement of exchange and correlation effects. I will analyze and discuss the results for the conductance and investigate the possibilities, limits and weak points of the method proposed by Bokes and co-workers. At the end, a short outlook about possible future investigations is given.

2 Green-Function embedding

The Green-function embedding method [Ing81] is one of the very few possibilities to integrate scattering boundary conditions in a reciprocal space implementation. Generally, it enables one to calculate the Green function in a finite volume of space, containing a localized perturbation. This situation occurs in impurity problems, surface problems and scattering setups. For such problems, one is often not interested in the wave function or the Green function in entire space but in a finite region which includes the perturbation potential. Therefore it would be a lot of needless work to solve the Schrödinger equation in whole space, which is often quite complicate and computationally intensive. The basic idea behind the Green-function embedding method is to limit the calculation to the space where the perturbation takes place and thus to save unnecessary work. The restriction of the Hamiltonian to this finite volume leads to a modified Schrödinger equation containing additional terms which make sure that the boundary conditions at the interface between the embedding region and the outer volume are fulfilled. The additional terms include the so-called embedding potential which is a property of the outer volume only. The geometry of an embedding setup is illustrated in figure 2.1. I would like to stress that the embedding method can only be applied to systems with a local potential $V(\mathbf{r})$ in entire space and therefore cannot be used to include e.g. the non-local Coulomb interaction $v(\mathbf{r}, \mathbf{r}')$.
In this chapter I will introduce the technique of Green-function embedding and discuss its central formulas. In chapter 5 I apply the method to the geometry of the systems investigated in this thesis.

2.1 Schrödinger equation in the embedded region

The derivation of the Schrödinger equation in the embedded region is based on the variational principle for the energy expectation value in entire space

$$E = \frac{\int_{V_0+\Omega} d\mathbf{r}\ \Psi^*(\mathbf{r}) H \Psi(\mathbf{r})}{\int_{V_0+\Omega} d\mathbf{r}\ \Psi(\mathbf{r})^* \Psi(\mathbf{r})} = \ \min\ , \tag{2.1}$$

where $\Psi(\mathbf{r})$ denotes the wave function in $V_0 + \Omega$. It subsumes the wave functions of the different regions

$$\Psi(\mathbf{r}) = \begin{cases} \psi(\mathbf{r}) & \forall\ \mathbf{r}\ \in\ V_0 \\ \phi(\mathbf{r}) & \forall\ \mathbf{r}\ \in\ \Omega \end{cases} \quad . \tag{2.2}$$

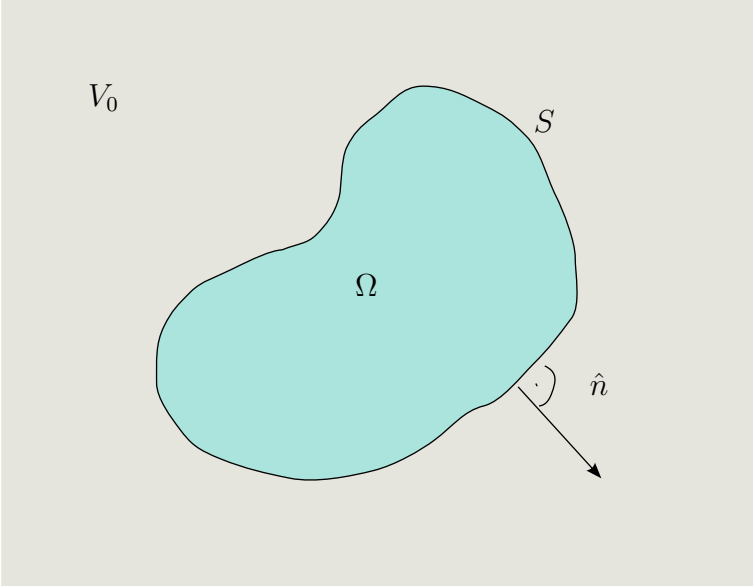

Figure 2.1: Geometry of the embedding method: The so-called embedding region Ω including the 'perturbation' (i.e. the surface, the impurity or the scattering potential) is enclosed by an 'outer' volume V_0, where the perturbation is zero. The two volumes V_0 and Ω are separated by an interface $S = \partial\Omega$. $\hat{n}$ denotes the normalized vector perpendicular to the interface S which points out of the embedding region.

Since the wave function $\Psi(\mathbf{r})$ must be continuous at the interface S, the condition

$$\psi(\mathbf{r}_S) = \phi(\mathbf{r}_S) \tag{2.3}$$

has to be fulfilled.
The wave function $\phi(\mathbf{r})$ in the embedded region is an unknown trial wave function included in trial, whereas the wave function in the outer volume $\psi(\mathbf{r})$ is a solution of the unperturbed Schrödinger equation in V_0 with energy ϵ

$$\left(-\frac{1}{2}\nabla^2 + V(\mathbf{r}) - \epsilon\right)\psi(\mathbf{r}) = 0 \quad \text{in} \quad V_0\,. \tag{2.4}$$

Besides, $\psi(\mathbf{r})$ has to fulfill the outer boundary conditions for the volume V_0.
Since the wave function $\phi(\mathbf{r})$ in Ω is a general trial wave function, the derivative of the wave function $\Psi(\mathbf{r})$ is in general not continuous at the interface S. Otherwise, there would not be any variational freedom. The continuity of the derivative of the wave function $\Psi(\mathbf{r})$ is naturally fulfilled after/through variation.
I will now insert the definition (2.2) in the energy expectation value (2.1). The operator for the kinetic energy included in $H(\mathbf{r})$ leads to an additional surface term (ensuring that the Hamiltonian is hermitian) which can be seen by applying Green's

Theorem

$$\begin{aligned}
&\int_{V_0+\Omega} dV\ \Psi^*(\mathbf{r})\nabla^2\Psi(\mathbf{r}) \qquad (2.5)\\
&= -\int_{V_0+\Omega} dV\ \nabla\Psi^*(\mathbf{r})\nabla\Psi(\mathbf{r})\\
&= -\int_{V_0} dV\ \nabla\psi^*(\mathbf{r})\nabla\psi(\mathbf{r}) - \int_{\Omega} dV\ \nabla\phi^*(\mathbf{r})\nabla\phi(\mathbf{r})\\
&= \int_{V_0} dV\ \psi^*(\mathbf{r})\nabla^2\psi(\mathbf{r}) + \int_S dS\ \psi^*(\mathbf{r})\partial_n\psi(\mathbf{r})\\
&\qquad + \int_{\Omega} dV\ \phi^*(\mathbf{r})\nabla^2\phi(\mathbf{r}) + \int_S dS\ \phi^*(\mathbf{r})(-\partial_n)\phi(\mathbf{r})
\end{aligned}$$

with $\partial_n f(\mathbf{r}) := \hat{n}\cdot(\nabla f(\mathbf{r}))$ and $S = \partial\Omega$. $\hat{n}$ is the projection of the gradient onto the surface normal.
As one can see, the discontinuity of the normal derivative leads to an additional surface term. Introducing eq. (2.5) in the energy expectation value (2.1) results in

$$E = \frac{\int_{V_0} dV\ \psi^*(\mathbf{r})H\psi(\mathbf{r}) + \int_{\Omega} dV\ \phi^*(\mathbf{r})H\phi(\mathbf{r}) + \frac{1}{2}\int_S dS\,\{\psi^*(\mathbf{r})\partial_n\phi(\mathbf{r}) - \phi^*(\mathbf{r})\partial_n\psi(\mathbf{r})\}}{\int_{V_0} dV\ \psi(\mathbf{r})^*\psi(\mathbf{r}) + \int_{\Omega} dV\ \phi(\mathbf{r})^*\phi(\mathbf{r})}\ . \qquad (2.6)$$

The expectation value of the energy E possibly differs from the predefined energy ϵ of the wave function $\psi(\mathbf{r})$ in the outer region. However, since one seeks for a final solution of the Schrödinger equation in entire space $V_0+\Omega$, in the end $E = \epsilon$ has to be valid. Therefore it can be already assumed in order to simplify the further derivation[1]. On that condition, the variation of the energy expectation value regarding the trial wave function $\phi^*(\mathbf{r})$ in Ω leads to

$$(H(\mathbf{r}) - \epsilon)\,\phi(\mathbf{r}) + \frac{1}{2}\delta(n - n_S)\,[\partial_n\phi(\mathbf{r}) - \partial_n\psi(\mathbf{r})] = 0\ . \qquad (2.7)$$

We observe that the two terms which do not depend on $\phi(\mathbf{r})$ vanish. n denotes the normal coordinate perpendicular to the surface and n_S the position of the surface. Thus, the second term contributes on the interface S only. It ensures that the boundary condition (2.3) is fulfilled correctly.
Although eq. (2.7) looks very similar to a common Schrödinger equation, there is an important difference: since the normal derivative of the wave function of the outer volume $\partial_n\psi(\mathbf{r})$ depends on the energy ϵ, the equation does not represent a simple eigenvalue problem any more.
Before eq. (2.7) can be solved, the normal derivative of the wave function of the outer volume $\partial_n\psi(\mathbf{r})$ on the interface S has to be eliminated. This will be done in the next section by introducing the so-called embedding potential.

[1]The correct derivation consists in the self-consistent determination of the energy eigenvalue ϵ of the outer volume V_0 and yields the same result. More details can be found in [Ing81].

2.1.1 The embedding potential

In order to reformulate the normal derivative $\partial_n\psi(\mathbf{r})\,|_S$ in terms of known quantities I will use the Schrödinger equation in V_0 as well as the definition of the Green function

$$\begin{aligned} (H(\mathbf{r})-\epsilon)\,\psi(\mathbf{r}) &= 0 && (2.8)\\ (H(\mathbf{r})-\epsilon)\,G_0(\mathbf{r},\mathbf{r}';\epsilon) &= -\delta(\mathbf{r}-\mathbf{r}')\;. && (2.9)\end{aligned}$$

Writing $H(\mathbf{r})$ as $H(\mathbf{r}) = -\frac{1}{2}\nabla^2 + V(\mathbf{r})$ and multiplying the Schrödinger equation (2.8) with $G_0(\mathbf{r},\mathbf{r}';\epsilon)$, the equation for the Green function (2.9) with $\psi(\mathbf{r})$ and integrating the difference between the two results over the volume V_0 yields

$$\int_{V_0} dV\;\delta(\mathbf{r}-\mathbf{r}')\psi(\mathbf{r}) = -\frac{1}{2}\int_{V_0} dV\;\left[G_0(\mathbf{r},\mathbf{r}';\epsilon)\nabla^2\psi(\mathbf{r}) - \psi(\mathbf{r})\nabla^2 G_0(\mathbf{r},\mathbf{r}';\epsilon)\right]\;. \quad (2.10)$$

At this point the locality of the potential $V(\mathbf{r})$ is required.
Applying Green's theorem to the right side results in

$$\psi(\mathbf{r}') = \frac{1}{2}\int_S dS\;\left[G_0(\mathbf{r},\mathbf{r}';\epsilon)\partial_n\psi(\mathbf{r}) - \psi(\mathbf{r})\partial_n G_0(\mathbf{r},\mathbf{r}';\epsilon)\right]\;. \quad (2.11)$$

In order to simplify eq. (2.11) von-Neumann boundary conditions of vanishing normal derivative on S are applied

$$\partial_n G_0(\mathbf{r},\mathbf{r}';\epsilon) = 0\;. \quad (2.12)$$

Since $\psi(\mathbf{r}')$ is defined for all $\mathbf{r}' \in V_0$, it can be chosen to be on the interface S

$$\psi(\mathbf{r}_S) = \frac{1}{2}\int_S dS'\;G_0(\mathbf{r}_S,\mathbf{r}'_S;\epsilon)\partial_n\psi(\mathbf{r}'_S)\;. \quad (2.13)$$

Inverting this equation for $\partial_n\psi(\mathbf{r}_S)$ results in

$$\partial_n\psi(\mathbf{r}_S) = 2\int_S dS'\;\sigma(\mathbf{r}_S,\mathbf{r}'_S;\epsilon)\psi(\mathbf{r}'_S)\;, \quad (2.14)$$

which because of the boundary condition (2.3) equals

$$\partial_n\psi(\mathbf{r}_S) = 2\int_S dS'\;\sigma(\mathbf{r}_S,\mathbf{r}'_S;\epsilon)\phi(\mathbf{r}'_S)\;. \quad (2.15)$$

The surface inverse of the Green function $\sigma(\mathbf{r}_S,\mathbf{r}'_S;\epsilon) := G_0^{-1}(\mathbf{r}_S,\mathbf{r}'_S;\epsilon)$ is a key quantity of the embedding method which in the original paper of Inglesfield was called embedding potential. It can be interpreted as a generalized logarithmic derivative.
The most important fact about eq. (2.14) is that there is a linear operator which applied to the wave function itself reproduces the normal derivative of the wave function at the interface S.

2.1.2 Embedded Green function

I can now insert the expression for the normal derivative $\partial_n\psi(\mathbf{r}_S)$ of eq. (2.15) in the 'embedded Schrödinger equation' (2.7). As a result, the Schrödinger equation does no longer depend explicitly on the wave function $\psi(\mathbf{r})$

$$(H(\mathbf{r})-\epsilon)\,\phi(\mathbf{r})+\frac{1}{2}\delta(n-n_S)\left[\partial_n\phi(\mathbf{r})-2\int_S dS'\,\sigma(\mathbf{r}_S,\mathbf{r}'_S;\epsilon)\phi(\mathbf{r}'_S)\right]=0\;. \quad (2.16)$$

The equation can be rewritten as

$$(H_{\mathrm{emb}}(\mathbf{r};\epsilon)-\epsilon)\,\phi(\mathbf{r})=0\;, \quad (2.17)$$

combining the common Hamiltonian containing the kinetic energy and the potential with the energy-dependent surface term to the embedding Hamiltonian $H_{\mathrm{emb}}(\mathbf{r};\epsilon)$. The embedding Hamiltonian $H_{\mathrm{emb}}(\mathbf{r};\epsilon)$ does not depend on the normal derivative of the external wave function any more but on the embedding potential which is uniquely defined by the wave function $\psi(\mathbf{r})$ of the outer region V_0.
The reformulation of the 'embedded Schrödinger equation' in terms of the embedding potential instead of the normal derivative shows one advantage. As already mentioned, the embedding potential is a logarithmic derivative and therefore does not include a normalization.
If one tries to solve eq. (2.17) now, one will meet another problem. Since the embedding potential and therefore the Hamiltonian depends on the energy it is not easy to find a general solution for the wave function. For this reason, it makes much more sense to consider energy-dependent Green functions than wave functions. The defining equation for an embedded Green function then becomes

$$\begin{aligned}&(H(\mathbf{r})-\epsilon)\,G(\mathbf{r},\mathbf{r}';\epsilon)\\&\quad+\frac{1}{2}\delta(n-n_S)\left[\partial_n G(\mathbf{r}_S,\mathbf{r}';\epsilon)-2\int_S dS''\,\sigma(\mathbf{r}_S,\mathbf{r}''_S;\epsilon)G(\mathbf{r}''_S,\mathbf{r}'\,;\epsilon)\right]=-\delta(\mathbf{r}-\mathbf{r}')\;,\end{aligned} \quad (2.18)$$

or using the notation of the embedding Hamiltonian $H_{\mathrm{emb}}(\mathbf{r};\epsilon)$

$$(H_{\mathrm{emb}}(\mathbf{r};\epsilon)-\epsilon)\,G(\mathbf{r},\mathbf{r}';\epsilon)=-\delta(\mathbf{r}-\mathbf{r}')\;. \quad (2.19)$$

Between the normal derivative of the Green function at the interface and the Green function itself there exists a similar relation as for the corresponding quantities of the wave function (see eq. (2.13))

$$\partial_n G(\mathbf{r}_S,\mathbf{r}'_S;\epsilon)=2\int_S dS''\,\sigma(\mathbf{r}_S,\mathbf{r}''_S,\epsilon)G(\mathbf{r}''_S,\mathbf{r}'_S;\epsilon)\;. \quad (2.20)$$

The application of the same linear operator σ to the Green function results in its normal derivative. This is easy to understand, since the Green function $G(\mathbf{r},\mathbf{r}';\epsilon)$ with one argument fixed (for example $\mathbf{r}=\mathbf{r}_0$) and $\mathbf{r}'\neq\mathbf{r}$ fulfills the Schrödinger equation for the wave function. Therefore $G(\mathbf{r},\mathbf{r}';\epsilon)$ has to fulfill the same boundary conditions and eq. (2.20) is valid.

3 Theoretical treatment of electronic exchange and correlation

3.1 Many-body problem in solid-state physics

Whenever a solid has to be described at a fundamental level, one faces a difficult many-particle problem, because a crystalline solid typically consists of a vast number of interacting particles (approximately 10^{23} atoms per cubic centimeter). Governed by the laws of quantum mechanics, the Schrödinger equation can be written down quite easily. However, its exact solution is sheer impossible, taking into account that due to their mutual Coulomb interaction the particles do not act independently from each other. For that reason the question arises how to reduce the complexity of the problem but nevertheless describe the macroscopic properties almost correctly.
Considering a solid, one can distinguish two sorts of particles: the positively charged nuclei and the negatively charged electrons. In principle, one has to solve the Schrödinger equation containing both the motion of the nuclei and the electrons as well as the interactions with each other. But in practice it turns out that it is possible to treat the two systems separately. This is of course an approximation but it can be justified as follows: Compared to the mass of an electron, the mass of a nucleus is three to four orders of magnitude larger. Thus, the electronic system adapts almost instantaneously to any change in the atomic configuration. In practice, the lowest-energy state of the electronic system is calculated as a function of the atomic configuration, and afterward the ground state is found by minimizing this energy function with respect to the atomic coordinates. This first simplification, which describes the actual situation very accurately, is called Born-Oppenheimer approximation.
In the following, only the electronic system will be considered. Naturally, writing down the Hamiltonian of the electronic system, the Coulomb interaction between the positively charged nuclei and the negatively charged electrons has to be taken into account. The interaction terms of one electron at position $\mathbf{r}_i$ with all nuclei at $\mathbf{R}_A$ are subsumed into an external potential $v_{\mathrm{ext}(r)}$, since they depend on the single variable $\mathbf{r}_i$. The coordinates of the positions of the nuclei enter as parameters and no longer as variables

$$v_{\mathrm{ext}}(\mathbf{r}_i) = -\frac{e^2}{4\pi\varepsilon_0} \sum_A \frac{Z_A}{|\mathbf{R}_A - \mathbf{r}_i|} \,. \tag{3.1}$$

In the Born-Oppenheimer approximation, the Hamiltonian of the electronic system can be thus written as

$$H = \sum_i \left[-\frac{\hbar^2}{2m_\mathrm{e}} \nabla_i^2 + v_\mathrm{ext}(\mathbf{r}_i) \right] + \frac{1}{2} \sum_{i \neq j} \frac{e^2}{4\pi\varepsilon_0 \left| \mathbf{r}_i - \mathbf{r}_j \right|} \, . \tag{3.2}$$

In the following, Hartree atomic units will be used, thus $\hbar \equiv m_\mathrm{e} \equiv e \equiv 4\pi\varepsilon_0 \equiv 1$.
The last term of the Hamiltonian, the strong repulsive Coulomb interaction, keeps any two electrons apart in space and gives rise to several energy terms. The most important one is the Hartree energy, followed by the exchange and the relatively weak correlation energy.
The exchange energy contributes only for electrons with the same spin, since the Pauli exclusion principle does not allow two electrons with the same spin to be simultaneously at the same place in space.
The exclusion principle is taken into account by the antisymmetrization of the N-particle wave function $\Psi_N(\mathbf{x}_1, ..., \mathbf{x}_N)$, which is a solution of the time-independent Schrödinger equation

$$H \Psi_N(\mathbf{x}_1, ..., \mathbf{x}_N) = E_N \Psi_N(\mathbf{x}_1, ..., \mathbf{x}_N) \tag{3.3}$$

and which has to fulfill the antisymmetry relation

$$\Psi_N(..., \mathbf{x}_i, ..., \mathbf{x}_j, ...) = -\Psi_N(..., \mathbf{x}_j, ..., \mathbf{x}_i, ...) \, . \tag{3.4}$$

Here, N denotes the particle number (thus the number of electrons) and $\mathbf{x}_i = (\mathbf{r}_i, \sigma_i)$ the spatial and spin coordinates of the ith electron.
In order to solve the Schrödinger equation (3.3), one could transform the problem to an effective one-particle problem by treating the mutual Coulomb interaction in the form of a self-consistent mean field. Examples for such single-particle approximations are the Hartree and the Hartree-Fock approximation (HFA). In the first one the non-local Coulomb term is replaced by an average local Coulomb potential from all other electrons. Although the Hartree approximation does not take exchange and correlation effects into account, it may still lead to useful and qualitatively correct results, for example for the homogeneous electron gas. An extension of the Hartree approximation taking the fermionic nature of the electrons into account is the HFA, which adds to the Hartree potential a non-local exchange potential reflecting the Pauli exclusion principle. Whereas the exchange term of the energy is treated exactly in this way, the correlation term is entirely ignored.
Methods like density-functional theory (DFT) [HK64], which in principle includes all exchange and correlation effects via a local exchange-correlation potential, give access to ground-state properties of many-electron systems[1]. But although the solution of

[1] The exchange-correlation potential in general cannot be calculated exactly, but there are different approximations for it, which work quite well for some systems. The most common ones are the local density approximation (LDA) [CA80] and the generalized gradient approximation (GGA) [PCV+92], [PBE96].

the Kohn-Sham equation of DFT [KS65] yields a spectrum of single-particle states, it is not possible to identify the corresponding eigenvalues with excitation energies. They are simply mathematical tools, Lagrange parameters introduced to enforce the normalization of the wave function, without any physical meaning. Instead, excited states as well as excited-state properties can be calculated using many-body perturbation theory, which is outside DFT and based on the Green function formalism [FW03].

3.2 Quasi-particle picture and the concept of electronic self-energy

Exchange and correlation effects whose origins have been already described in the previous section cause a positively charged region around each electron (with a smaller electron density than the average), the so-called Coulomb hole. Since the Coulomb hole does not exist independently from the bare electron, the electron and the Coulomb hole are often treated as a single entity, the so-called quasi-particle. It is important to state that the interaction between quasi-particles is much weaker than the interaction between bare electrons, because the hole surrounding the electron screens the strong Coulomb potential caused by the bare electron itself. For that reason, the independent-particle picture leads often to quite good results. Although the particles interact strongly with each other, the quasi-particles are almost independent. The interaction between quasi-particles therefore is called screened interaction and denoted by W instead of the pure Coulomb interaction v. Hence, from a physical point of view it is more reasonable to calculate the energy of one quasi-particle instead of one bare electron. Furthermore, the description in terms of quasi-particles correspond exactly to the experimental situation, for example in photoemission. As explained in detail in section 3.3, the quasi-particle spectrum can be measured experimentally, which is not the case for the bare electron spectrum.
The energy difference between the energy of one quasi-particle and the corresponding bare particle itself is called self-energy. The name can be explained in the following way: The bare electron interacts with the many-body system and creates a Coulomb hole. This Coulomb hole in turn reacts back on the electron and disturbs its motion. Therefore the particle interacts with itself via the many-body system and changes its own energy.
The self-energy is a very important quantity since theoretically it enables one to calculate the eigenvalues of the many-body system including correlation and exchange effects exactly. In practice, however, it turns out that the exact calculation of the self-energy of a given system is very difficult or even impossible. Therefore several approximations for the self-energy have been developed.
In the following sections of this chapter one possible approximation — the so-called GW approximation — for the electronic self-energy will be introduced. In the framework of the GW approximation exchange effects are treated exactly and a large part

of correlation effects are included.
Since the GW approximation serves to calculate excitation spectra, in the next section the nature of electronic excitations is analyzed.

3.3 Elementary excitations in solids

There are two kinds of excitations which have to be distinguished: quasi-particle and collective excitations. Whenever the excitation can be described by the elevation of a single particle to an excited eigenstate, the excitation is called a quasi-particle excitation. In the opposite case, when a large number of particles are involved, the excitation is denoted as a collective excitation. For example plasmons, which describe the long-lived resonant charge-oscillations in a system induced by a spatially and temporary varying electric field fall within this category. Other examples are phonons, magnons and excitons. Excitons are a bound states between an electron and a hole which propagate as a pair.
Whereas quasi-particle excitations can qualitatively be described in a single-particle picture, in which the electron-electron interaction is included via an effective potential, collective excitations result directly from the electron-electron interaction and are therefore absent in mean-field theories.
Experimentally, electronic excitation spectra can be measured using angle-resolved photoemission spectroscopy. In direct photoelectron spectroscopy, photons with energy $\hbar\omega$ impinge on the sample and — if their energy is sufficient — eject electrons from the sample, leaving a quasi-hole behind. Measuring the kinetic energy of the emitted electron enables one to reconstruct the quasi-particle band structure $E_k = E_{kin} - \hbar\omega$ below the chemical potential μ, since the momentum of the photons is negligible and thus the $\mathbf{k}$ vector of the electron does not change in a relevant way. Equivalently, inverse photoelectron spectroscopy allows one to obtain the quasi-particle bandstructure E_k above the chemical potential μ. In this case, electrons are injected into the sample and the energy of the ejected photons is measured. Naturally, the resulting spectrum does not only contain quasi-particle excitations but includes collective excitations as well, since the injected/ejected electrons as well as the photons can create or absorb collective excitations. In the resulting spectrum quasi-particle excitations can be distinguished from collective ones through their high intensity and the width of the peak. The width of the peak is related to the lifetime of the state by the uncertainty relation, thus a narrow peak correspond to a long lifetime. Since quasi-particle excitations typically have a much longer lifetime than collective excitations, their peaks are much narrower.
In order to describe excitations mathematically, it is convenient to use the Green function formalism, which will be introduced in the next section.

3.4 Green function formalism

There are several reasons why the Green function formalism is useful when dealing with various aspects of the many-body problem in solids. As opposed to common wave functions, Green functions allow us to calculate the many-body eigenvalues without having explicitly calculated the eigenstates of the Hamiltonian. Supplementary to ground-state properties like the electronic density and the expectation value of any single-particle operator of the system, the time-ordered one-particle Green function contains the whole excitation spectrum as well as the corresponding excitation lifetimes. As Green functions link the N-particle with the $N \pm 1$-particle system, they are closely related to photoemission spectroscopy based on the injection/ejection of electrons. In general, the close connection between Green functions and experiments is a valued property.
Because of all these characteristics, many-body perturbation theory including the GW approximation draws on the concept of Green functions. Unfortunately, Green functions are often quite complicated to calculate. For that reason the Green-function formalism is rarely applied to calculate ground-state properties only. Most often, Green functions are calculated in order to obtain properties of the system related to excited states.
Green-function formalism is based on the concept of second quantization which is equivalent to common quantum mechanics and only uses a different mathematical formulation. For the treatment of statistical problems which involve a large and variable number of particles this approach is more practical, since it provides a more economical language than conventional quantum mechanics.
In the following I will consider a N-electron system with the N-electron ground state $\left|\Psi_0^N(t')\right\rangle$. For the manipulation of the number of particles the so-called field operators

$$\hat{\psi}^\dagger(\mathbf{x}) \qquad \text{and} \qquad \hat{\psi}(\mathbf{x}) \tag{3.5}$$

are required. They cause the creation/annihilation of an electron at position $\mathbf{r}$ with spin σ, subsumed into $\mathbf{x} = (\mathbf{r}, \sigma)$. Alternatively, the annihilation of an electron is interpreted as creation of a hole. The time development of the system is described by the time evolution operator $\hat{U}(t, t') = e^{-i\hat{H}(t-t')}$, which propagates an arbitrary system, characterized by the Hamiltonian $\hat{H}$, from t' to a later time t.
In general, one has to distinct between several kinds of Green functions, which are all equivalent to each other — knowing one of them (regardless which one), all others can be calculated. The most popular Green function is the time-ordered one. Physically, it describes the propagation of an electron and a hole.
In the following, the electron Green function will be derived. It is defined such that $iG^{\text{electron}}(\mathbf{x}t, \mathbf{x}'t')$ is the probability amplitude for an additional electron to propagate from $\mathbf{r}'$ with spin σ' at time t' to the state $\mathbf{x}$ at time t. Therefore first the creation operator $\hat{\psi}^\dagger(\mathbf{x}')$ (for an electron in the state $\mathbf{x}'$) is applied to the N-electron ground state $\left|\Psi_0^N(t')\right\rangle$ and then the system is propagated in time by applying the time evolution operator $\hat{U}(t, t')$. Finally the annihilation operator $\hat{\psi}(\mathbf{x})$ for an electron in

the state $\mathbf{x}$ has to be applied to return to an N-electron-system. The overlap of this product $\hat{\psi}(\mathbf{x})\hat{U}(t,t')\hat{\psi}^\dagger(\mathbf{x}')\left|\Psi_0^N(t')\right\rangle$ representing the final state with $\left|\Psi_0^N(t)\right\rangle$ has to be calculated in order to obtain the electron Green function. This yields

$$G^{\text{electron}}(\mathbf{x}t,\mathbf{x}'t') = -i\left\langle \Psi_0^N(t)\left|\hat{\psi}(\mathbf{x})\hat{U}(t,t')\hat{\psi}^\dagger(\mathbf{x}')\right|\Psi_0^N(t')\right\rangle \Theta(t-t')\ . \tag{3.6}$$

The Heaviside step function

$$\Theta(t-t') = \begin{cases} 1 & \text{if} \quad t > t' \\ 0 & \text{if} \quad t < t' \end{cases} \tag{3.7}$$

makes sure that the electron has only a finite amplitude to propagate if the time t of arrival at $\mathbf{x}$ is later than the time t' of departure at $\mathbf{x}'$.
Naturally, formula (3.6) can be reformulated in the Heisenberg picture, too, where operators are time-dependent

$$\hat{A}_{\text{H}}(t) = \hat{U}(0,t)\hat{A}_{\text{S}}\hat{U}(t',0)\ , \tag{3.8}$$

whereas states are time-independent like

$$|\Psi_{\text{H}}\rangle = \hat{U}(0,t)\,|\Psi_{\text{S}}(t)\rangle\ . \tag{3.9}$$

Inserting the two definitions (3.8) and (3.9) in (3.6) I obtain the Green function in the Heisenberg picture

$$G^{\text{electron}}(\mathbf{x}t,\mathbf{x}'t') = -i\left\langle \Psi_0^N\left|\hat{\psi}(\mathbf{x},t)\hat{\psi}^\dagger(\mathbf{x}',t')\right|\Psi_0^N\right\rangle \Theta(t-t')\ . \tag{3.10}$$

The hole Green function, describing the propagation of an additional hole can be derived equivalently and results in

$$G^{\text{hole}}(\mathbf{x}t,\mathbf{x}'t') = -i\left\langle \Psi_0^N\left|\hat{\psi}^\dagger(\mathbf{x}',t')\hat{\psi}(\mathbf{x}.t)\right|\Psi_0^N\right\rangle \Theta(t'-t)\ . \tag{3.11}$$

As already announced, the time-ordered Green function implies electron propagation as well as hole propagation, and is therefore composed of the electron and the hole Green function to

$$\begin{aligned} G(\mathbf{x}t,\mathbf{x}'t') &= G^{\text{electron}}(\mathbf{x}t,\mathbf{x}'t') - G^{\text{hole}}(\mathbf{x}'t',\mathbf{x}t) \\ &= -i\left\langle \Psi_0^N\left|\hat{T}\left[\hat{\psi}(\mathbf{x},t)\hat{\psi}^\dagger(\mathbf{x}',t')\right]\right|\Psi_0^N\right\rangle\ . \end{aligned} \tag{3.12}$$

The time-ordering operator $\hat{T}$ puts the field operators in such an order that the time increases from the right to the left. If field operators must be commuted, a factor (-1) has to be added for each permutation. The time-ordering operator $\hat{T}$ ensures that the Green function describes either the propagation of an electron (for $t > t'$) or the propagation of a hole (for $t < t'$).
I will now consider the time-ordered Green function of a stationary system with a

Hamiltonian which does not depend explicitly on the time. Consequently, the Green function depends only on the time difference $\tau = t - t'$ between the initial and the final state and therefore in the following will be written as

$$G(\mathbf{x}t, \mathbf{x}'t') = G(\mathbf{x}, \mathbf{x}'; \tau) \; . \tag{3.13}$$

In order to obtain the Green function in terms of excited states of the $(N \pm 1)$-particle system I will insert the closure relation

$$\sum_i \left|\Psi_i^{N\pm1}\right\rangle \left\langle\Psi_i^{N\pm1}\right| = 1 \tag{3.14}$$

between the field operators, where $\left\{\left|\Psi_i^{N\pm1}\right\rangle\right\}$ is the complete set of state vectors of the $(N \pm 1)$-particle system. The excitation energies will be denoted as

$$\epsilon_i^{N-1} = E_0^N - E_i^{N-1} \qquad \text{or} \qquad \epsilon_i^{N+1} = E_i^{N+1} - E_0^N \; , \tag{3.15}$$

respectively. Thus, the time-ordered Green function in the Schrödinger picture becomes

$$\begin{aligned} G(\mathbf{x}, \mathbf{x}'; \tau) = -i \sum_i \left\langle \Psi_0^N \left| \hat{\psi}(\mathbf{x}) \right| \Psi_i^{N+1} \right\rangle \left\langle \Psi_i^{N+1} \left| \hat{\psi}^\dagger(\mathbf{x}') \right| \Psi_0^N \right\rangle e^{-i\epsilon_i^{N+1}\tau} \Theta(\tau) \\ +i \sum_i \left\langle \Psi_0^N \left| \hat{\psi}^\dagger(\mathbf{x}) \right| \Psi_i^{N-1} \right\rangle \left\langle \Psi_i^{N-1} \left| \hat{\psi}(\mathbf{x}') \right| \Psi_0^N \right\rangle e^{-i\epsilon_i^{N-1}\tau} \Theta(-\tau) \; . \end{aligned} \tag{3.16}$$

Using the following definitions

$$\psi_i^{N-1}(\mathbf{x}) = \left\langle \Psi_i^{N-1} \left| \hat{\psi}(\mathbf{x}) \right| \Psi_0^N \right\rangle \tag{3.17}$$

and

$$\psi_i^{N+1}(\mathbf{x}) = \left\langle \Psi_0^N \left| \hat{\psi}(\mathbf{x}) \right| \Psi_i^{N+1} \right\rangle \; , \tag{3.18}$$

the time-ordered Green function can be rewritten as

$$\begin{aligned} G(\mathbf{x}, \mathbf{x}'; \tau) = -i \sum_i \psi_i^{N+1}(\mathbf{x}) \psi_i^{N+1\,\star}(\mathbf{x}') e^{-i\epsilon_i^{N+1}\tau} \Theta(\tau) \\ +i \sum_i \psi_i^{N-1}(\mathbf{x}) \psi_i^{N-1\,\star}(\mathbf{x}') e^{-\frac{i}{\hbar}\epsilon_i^{N-1}\tau} \Theta(-\tau) \; . \end{aligned} \tag{3.19}$$

The summation has to be executed over the ground state and all excited states of the $(N-1)$ or the $(N+1)$ particle system, respectively.
Expression (3.19) shows that the Green function in fact contains the whole excitation spectrum: The resulting states evolve according to their phase factors $e^{-i\epsilon_i^{N\pm1}\tau}$ containing the excitation energies ϵ_i^{N+1} or ϵ_i^{N-1} and are then probed in the state $\mathbf{x}$ by the projections $\psi_i^{N+1}(\mathbf{x})$ or $\psi_i^{N-1}(\mathbf{x})$, respectively.
In the next step, the Green function is Fourier transformed to frequency space, thus

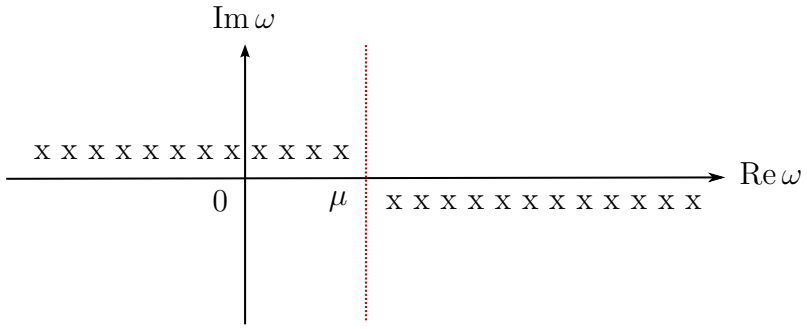

Figure 3.1: The poles of the time-ordered Green function (represented as crosses) are situated close to the real frequency axis. For frequencies with $\mathrm{Re}\,\omega < \mu$ they are located infinitesimally above the real frequency axis, whereas for frequencies with $\mathrm{Re}\,\omega > \mu$ they are in the lower half-plane of the complex frequency plane.

to $G(\mathbf{x}, \mathbf{x}'; \omega)$.
The only terms in (3.19) which depend on τ are the phase factors and the Heaviside step functions. With the Fourier transform of the Heaviside step function

$$\Theta(\omega) = \int_{-\infty}^{\infty} \Theta(\tau) e^{i\omega\tau - \eta|\tau|} d\tau = \frac{i}{(\omega + i\eta)} \tag{3.20}$$

(with an infinitesimally small real η, $\eta > 0$) the time-ordered Green function in Fourier space results in

$$G(\mathbf{x}, \mathbf{x}'; \omega) = \sum_i \frac{\psi_i^{N+1}(\mathbf{x}) \psi_i^{N+1\star}(\mathbf{x}')}{\omega - \epsilon_i^{N+1} + i\eta} + \sum_i \frac{\psi_i^{N-1}(\mathbf{x}) \psi_i^{N-1\star}(\mathbf{x}')}{\omega - \epsilon_i^{N-1} - i\eta} \,. \tag{3.21}$$

This representation of the Green function is called the Lehmann representation. It is very useful, because it shows that the Green function has poles at the true many-particle excitation energies $\epsilon_i^{N\pm1}$. Their position in the complex plane, infinitesimally below the real axis for energies greater than the chemical potential μ and above otherwise, are schematically shown in figure 3.1.
Eq. (3.21) can be interpreted for the special case of non-interacting systems: In this case the ψ_i^{N+1} are simply the unoccupied states whereas the ψ_i^{N-1} represent the occupied wave functions. Furthermore, the excitation energies $\epsilon_i^{N\pm1}$ become simply the single-particle energies.

Spectral function In order to analyze the excitation spectrum it is useful to introduce the spectral function $A(\mathbf{x}, \mathbf{x}'; \omega)$ which is defined through the spectral representation of the Green function

$$G(\mathbf{x}, \mathbf{x}'; \omega) = \int_{-\infty}^{\infty} \frac{A(\mathbf{x}, \mathbf{x}'; \omega')}{\omega - \omega' + i\,\mathrm{sgn}\,(\omega' - \mu)\,\eta} \, d\omega' \,. \tag{3.22}$$

Inserting the identity

$$\frac{1}{x \mp i\eta} = P\left(\frac{1}{x}\right) \pm i\pi\delta(x) \tag{3.23}$$

in equation (3.22), where P denotes the principal value, and taking the limit $\eta \to 0$ yields

$$A(\mathbf{x}, \mathbf{x}'; \omega) = -\frac{1}{\pi} \operatorname{sgn}(\omega - \mu) \operatorname{Im} G(\mathbf{x}, \mathbf{x}'; \omega) \; . \tag{3.24}$$

This formula enables one to calculate the spectral function explicitly using the Lehmann representation of the Green function

$$\begin{aligned} A(\mathbf{x}, \mathbf{x}'; \omega) = &\sum_i \psi_i^{N+1}(\mathbf{x}) \psi_i^{N+1\,\star}(\mathbf{x}') \delta(\omega - \epsilon_i^{N+1}) \\ &+ \sum_i \psi_i^{N-1}(\mathbf{x}) \psi_i^{N-1\,\star}(\mathbf{x}') \delta(\omega - \epsilon_i^{N-1}) \; . \end{aligned} \tag{3.25}$$

The spectral function is closely related to the distribution function measured by photoemission experiments. It can be interpreted as the density of excited (or quasi-particle) states that contribute to the electron or hole propagation.

3.5 The self-energy

In section 3.1 the physical meaning of the self-energy was explained. Now, a defining equation for the self-energy will be derived. The self-energy is important for the calculation of the Green function since the original definition of the Green function (3.12) is not very useful for practical calculations — it is expressed in terms of the wave functions, which we want to avoid.
In the following a procedure to obtain the Green function without calculating the wave functions will be derived. This procedure is based on the equation of motion of the Green function.
In order to derive the equation of motion, the time derivative of the Green function given by eq. (3.12) is calculated. Therefore the time derivative of the field operators is needed. It can be obtained using the equation of motion for an arbitrary Heisenberg operator $O_{\mathrm{H}}(t)$

$$i\frac{d}{dt}\hat{O}_{\mathrm{H}}(t) = \left[\hat{O}_{\mathrm{H}}(t), \hat{H}\right]_- + i\frac{\partial \hat{O}_{\mathrm{H}}(t)}{\partial t} \tag{3.26}$$

and the derivative of the Heaviside step function $\frac{d\Theta(t)}{dt} = \delta(t)$, hence

$$i\frac{d\psi(\mathbf{x}, t)}{dt} = \left[h(\mathbf{r}) + \int \psi^\dagger(\mathbf{x}', t) v(\mathbf{r}, \mathbf{r}') \psi(\mathbf{x}', t) d^3x'\right] \psi(\mathbf{x}, t) \; . \tag{3.27}$$

Here, the one-particle contribution to the Hamiltonian is denoted by $h(\mathbf{r}) = -\frac{1}{2}\nabla^2 + v_{\mathrm{ext}}(\mathbf{r})$ and the Coulomb potential is written as $v(\mathbf{r}, \mathbf{r}') = \frac{1}{|\mathbf{r}-\mathbf{r}'|}$.

With the help of eq. (3.27) and the anticommutation relations of the field operators an equation of motion of the Green function can be derived

$$\left[i\frac{\partial}{\partial t} - h(\mathbf{r})\right] G(\mathbf{x}t, \mathbf{x}'t') = \delta(\mathbf{x}-\mathbf{x}')\delta(t-t') - i\int v(\mathbf{r},\mathbf{r}'')\langle\Psi_N\left|T\left[\psi^\dagger(\mathbf{x}'',t)\psi(\mathbf{x}'',t)\psi(\mathbf{x},t)\psi^\dagger(\mathbf{x}',t')\right]\right|\Psi_N\rangle d^3x'' \ . \quad (3.28)$$

The last term which contains a product of four field operators is yet another Green function but of higher order. Since the one-particle Green function contains two field operators, we have to deal here with a two-particle Green function describing two-particle correlations. One could set up a new equation of motion to obtain this two-particle Green function, but this would result in an equation similar to (3.28), including now a Green function of still higher order. This procedure would lead to an infinite chain of differential equations: In order to determine the one-particle propagator exactly an infinite number of differential equations has to be solved, which is just as impossible as finding the many-electron wave function.
There are now at least two possibilities to deal with this problem. The first one would be to terminate the chain of equations by approximating the highest-order Green function through lower-order terms. The second one, which will be the method of choice here, decouples the equations by introducing a set of non-linear equations. This method follows the standard procedure in field theory and invokes the concept of the self-energy.
Therefore, the dominant interaction term, denoted by the Hartree potential is written as

$$V^{\mathrm{H}}(\mathbf{r}) = \int v(\mathbf{r},\mathbf{r}')\langle\Psi_N\left|\psi^\dagger(\mathbf{x}',t)\psi(\mathbf{x}',t)\right|\Psi_N\rangle d^3x' \ . \quad (3.29)$$

Then, the self-energy operator Σ is defined by

$$\left[i\frac{\partial}{\partial t} - h(\mathbf{r}) - V^{\mathrm{H}}(\mathbf{r})\right] G(\mathbf{x}t, \mathbf{x}'t') = \delta(\mathbf{x}-\mathbf{x}')\delta(t-t') + \int \Sigma(\mathbf{x}t, \mathbf{x}''t'')G(\mathbf{x}''t'', \mathbf{x}'t')d^3x''dt'' \quad (3.30)$$

and a strict comparison to (3.28). It is a non-local time- (or energy-) dependent quantity, which accounts for the interaction between a particle and the rest of the system and generalizes the notion of a local potential. As already illustrated in section 3.1, the self-energy specifies the difference in energy between the quasi-particle and the bare particle.
If the potential does not depend explicitly on time, the self-energy as well as the Green function depends only on the relative difference between its two temporal arguments.
Although in principle the self-energy incorporates all exchange and correlation effects exactly, in practice it is often approximated. The *GW* approximation for Σ, which

is used in this diploma thesis, will be presented in detail in section 3.9. Much easier approximations which were obtained by educated guesses are the Hartree and the Hartree-Fock approximation which have been already described in section 3.1. In the first one the self-energy is chosen to be zero

$$\Sigma^{\mathrm{H}}(\mathbf{x}t, \mathbf{x}'t') = 0 \ , \tag{3.31}$$

whereas in the second one the self-energy gives rise to the non-local exchange potential, thus

$$\Sigma^{\mathrm{HF}}(\mathbf{x}t, \mathbf{x}'t') = iG(\mathbf{x}t, \mathbf{x}'t')v(\mathbf{r}, \mathbf{r}')\delta(t - t') \ . \tag{3.32}$$

In these two mean-field approximations the self-energy does not depend on frequency. The self-energy of the GW approximation, which will be introduced in section 3.9, resembles the Hartree-Fock self-energy, but the Coulomb potential is replaced by the time- (or frequency-) dependent screened interaction W

$$\Sigma^{GW}(\mathbf{x}t, \mathbf{x}'t') = iG(\mathbf{x}t, \mathbf{x}'t')W(\mathbf{r}t, \mathbf{r}'t') \ . \tag{3.33}$$

3.6 Feynman diagrams

Feynman diagrams are a very useful tool for the description of many-body interaction processes. They display complex mathematical expressions in a concise picture using the framework of Green functions. Since Feynman diagrams are a means to describe mathematical formulas, they can be translated back to mathematical expressions. Each symbol is associated with a variable. Thus a mathematical expression can be translated into the language of diagrams, then changed or simplified and in the end translated back to a mathematical formula without losing its validity.
The basic ingredients of Feynman diagrams are the Green function $G(\mathbf{x}t, \mathbf{x}'t')$ of the interacting system and the Green function $G_0(\mathbf{x}t, \mathbf{x}'t')$ of the independent-particle system. The latter is also called the free-particle propagator and drawn by a single-line arrow, connecting two vertices associated with different coordinates in space and time. For $t > t'$ it describes the propagation of a free particle from $(\mathbf{x}'t')$ to $(\mathbf{x}t)$, whereas for reverse time-order the free propagation of a hole in the opposite direction is represented by the same symbol. Although a time axis is often included in Feynman diagrams, in this work no time axis is drawn for reasons of simplicity. The Green function of the interacting-particle system is represented by a double-line arrow. In contrast to to the free-particle propagator, it describes the propagation of a particle influenced by all other particles.
The Coulomb interaction $v(\mathbf{r}, \mathbf{r}')\delta(t - t')$ is represented by a wiggly line and assumed to happen instantaneously in time. It is no fermion propagator and hence drawn without arrow.
The symbols for the three basic ingredients introduced until now are shown in the following table.

Symbol	Formula	Description
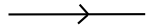	$-iG$	Green function of the interacting system
	$-iG_0$	Green function of the non-interacting system
	iv	Coulomb interaction

There are different criteria which can be used to characterize Feynman diagrams. One of them is the distinction between connected and disconnected diagrams. Examples for these two types are diagrams are shown in figure 3.2. The value of a disconnected diagram is just the product of its subunits. Hence, for the evaluation of the self-energy only connected diagrams have to be considered. Additionally, in order to avoid double-counting, only diagrams which are topologically distinct have to be included.

Connected diagrams can often be broken into two unconnected parts by removing one particle or hole line. This kind of diagrams is called reducible, whereas diagrams like the Hartree and the Fock-type diagram displayed in the middle and on the right side of figure 3.3 are called irreducible, because they cannot be split into two parts by cutting a single particle or hole line. As I will present in the next section, these irreducible diagrams play an important role in the calculation of the self-energy (or the full propagator $G(\mathbf{x}t, \mathbf{x}'t')$, respectively), since they are the basic modules of which all relevant Feynman diagrams are composed of.

Furthermore, Feynman diagrams can be classified by their order, i.e. the number of interactions which are included in the diagram and represented by the number of Coulomb (wiggly) lines. Since each Coulomb line connects two vertices, each diagram of order n contains $2n+1$ free-particle propagators G_0 (single-arrow lines). Therefore, the only diagram of zeroth order is the free propagator. In first order, there are already two possible diagrams: the Hartree- and the Fock-type diagram. The latter represents the exchange term, which can be interpreted as an electron which emits a photon and absorbs it at the same time but at a different location. The 'bubble' in the Hartree diagram (right diagram in figure 3.3) is a so-called closed fermion loop and represents the electron density. Translating it back into mathematical formulas, it also contains an additional phase factor -1. As I will show in the next section, these two first-order diagrams are the only irreducible diagrams appearing in the Hartree-Fock approximation. All other diagrams of higher order are reducible and composed of these two diagrams only. More detailed information about Feynman diagrams can be found in [FW03] and [Ink84].

Figure 3.2: Feynman diagrams can be characterized as to whether they are connected (right diagram) or whether they are disconnected (left diagram).

3.7 The Dyson equation

In order to obtain the complete Green function, one has to include all possible interactions. In the language of Feynman diagrams that implies the summation over all diagrams up to infinite order.
This issue is described mathematically by the Dyson equation

$$G(\mathbf{x}t,\mathbf{x}'t') = G_0(\mathbf{x}t,\mathbf{x}'t') + \int\int G_0(\mathbf{x}t,\mathbf{x}''t'')\left[V^{\mathrm{H}}(\mathbf{x}'')\delta(\mathbf{x}''-\mathbf{x}''')\delta(t''-t''') + \Sigma(\mathbf{x}''t'',\mathbf{x}'''t''')\right] G(\mathbf{x}'''t''',\mathbf{x}'t')d^3x''d^3x'''dt''dt''' \ , \quad (3.34)$$

which relates the Green function of the interacting-particle system $G(\mathbf{x}t,\mathbf{x}'t')$ to the free-particle propagator $G_0(\mathbf{x}t,\mathbf{x}'t')$ via the electronic self-energy $\Sigma(\mathbf{x}t,\mathbf{x}'t')$. For a time-invariant system $G(\mathbf{x}t,\mathbf{x}'t')$ can be written as $G(\mathbf{x},\mathbf{x}';t-t')$, and it is more comfortable to Fourier transform the Dyson equation to frequency space, because in this case the integrations over the time variables reduce to a product

$$G(\mathbf{x},\mathbf{x}';\omega) = G_0(\mathbf{x},\mathbf{x}';\omega) + \int\int G_0(\mathbf{x},\mathbf{x}'';\omega)\left[V^{\mathrm{H}}(\mathbf{x}'')\delta(\mathbf{x}''-\mathbf{x}''') + \Sigma(\mathbf{x}'',\mathbf{x}''';\omega)\right] G(\mathbf{x}''',\mathbf{x}';\omega)d^3x''d^3x''' \ . \quad (3.35)$$

The irreducible self-energy Σ is given by the sum over all single scattering processes. In terms of diagrams this equals the sum over all irreducible diagrams. One can convince oneself that the Dyson equation includes all single, double, triple, etc., scattering processes composed of these irreducible diagrams by replacing the Green function on the right side under the integral by the expression for the whole Green function, thus in the first step by $G^{(0)} + G^{(0)}\tilde{\Sigma}G$ with $\tilde{\Sigma}(\mathbf{x},\mathbf{x}';\omega) = V^{\mathrm{H}}(\mathbf{x})\delta(\mathbf{x}-\mathbf{x}') + \Sigma(\mathbf{x},\mathbf{x}';\omega)$. Repeating this procedure several times will lead to an infinite sum of scattering terms

$$G = G_0 + G_0\tilde{\Sigma}G_0 + G_0\tilde{\Sigma}G_0\tilde{\Sigma}G_0 + G_0\tilde{\Sigma}G_0\tilde{\Sigma}G_0\tilde{\Sigma}G_0 + ... \quad (3.36)$$

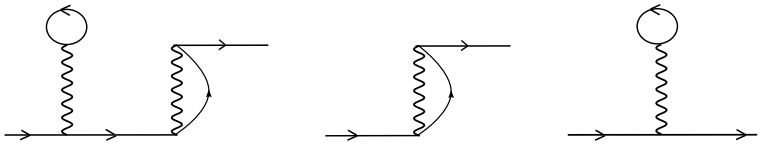

Figure 3.3: Example of a reducible diagram (left), which can be broken into two irreducible diagrams, the Hartree- (right) and the Fock-type diagram (middle). They represent the first scattering process of the Hartree-Fock approximation, hence $G_0\tilde{\Sigma}G_0$.

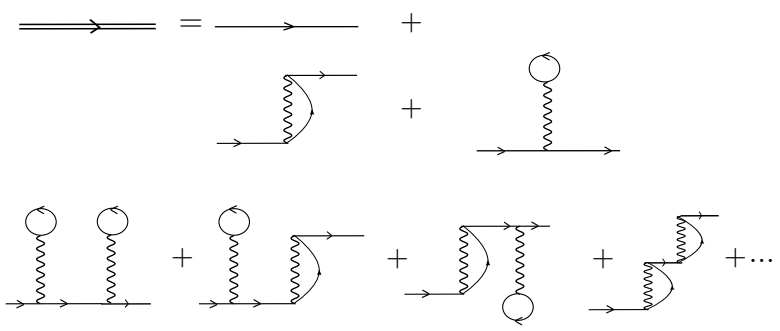

Figure 3.4: Zeroth-, first- and second-order terms of the Hartree-Fock approximation

Although the Dyson equation (3.34) is exact, in practice it is not possible to calculate the Green function exactly since the self-energy comprising a sum over an infinite number of diagrams cannot be calculated exactly. On the other hand, the Dyson equation is a good starting point for many-body approximations: The interpretation in terms of scattering processes allows one to construct approximations for Σ by the summation of diagrams considered essential for a given electronic system. In practice, the irreducible self-energy is approximated by one or several irreducible self-energy parts which yield (or which are assumed to yield) the dominant contribution. Unfortunately, a straightforward application of finite-order perturbation theory does not work for infinite systems with a long-range interaction. In this case the value of individual diagrams of any given order may be infinite and the sum may not converge. However, the divergences of individual diagrams cancel out when summing up the entire subclass of diagrams until infinite order.
An example for the successful application of the Dyson equation is the Hartree-Fock approximation. In this approximation, the irreducible self-energy consists of the two diagrams of first order already displayed in figure 3.3. The zeroth, first and second-order terms of the infinite sum (3.36) are presented in figure 3.4.
Another approximation for the irreducible self-energy which can be obtained by the means of physical intuition and diagrammatic technique is presented in figure 3.5. Its basic compound is the – divergent – second order diagram (the second in the sum)[2]. However, since all other diagrams of higher order diverge as well, the divergences of the individual diagrams cancel out when calculating the sum over all of them. The 'ring'

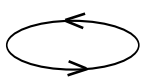

in this second order diagram corresponds to the polarization

$$P_0(\mathbf{x}t, \mathbf{x}'t') = -iG_0(\mathbf{x}t, \mathbf{x}'t')G_0(\mathbf{x}'t', \mathbf{x}t) \tag{3.37}$$

[2]It is the only diagram of second order which diverges

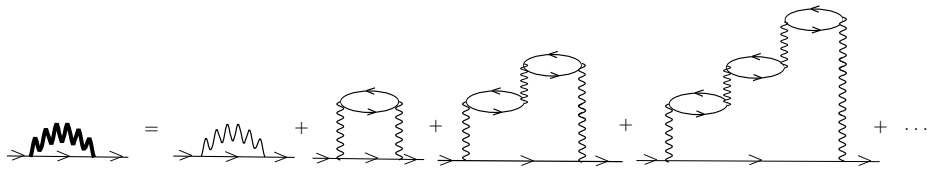

Figure 3.5: Diagrammatic expansion of the self-energy in the GW approximation. Going from the nth-order diagram to the next highest order, one more Coulomb line and one more ring has to be added. Except the first-order exchange diagram all summands contain the ring, representing the polarization. Removing the free-particle particle propagator results in the screened interaction in the RPA (see 3.6).

and describes the simultaneous creation of an electron and a hole and their subsequent annihilation. This fits to the classical idea of the polarization process as the production of positive and negative charges in a medium and the resulting reduction of the applied field. The upper part of the sum presented in figure 3.5 without the free-particle propagator represents the screened interaction (shown in figure 3.6) between quasi-particles and is denoted by W. It is an expansion in terms of the bare Coulomb interaction reduced by the polarization process. This approximation for the screened interaction is called the Random Phase Approximation (RPA). Symbolically, it can be written as the infinite sum

$$W = v + vPv + vPvPv + vPvPvPv + \cdots \ . \tag{3.38}$$

The electronic self-energy approximated by the infinite sum in figure 3.5 equals the electronic self-energy in the GW approximation. Originally, it was developed to describe the high-density electron gas, because in this case it can be shown mathematically that it represents a good approximation. However, it leads to reasonable results even for intermediate and low densities (for example in the case of metals). Although this approximation was developed by a diagrammatic approach, the GW approximation is obtained by a systematic algebraic method instead. It will be introduced in section 3.9.

3.8 Hedin's equations

In 1965 Hedin derived a set of five self-consistent integral equations for the formally exact calculation of the Green function of a system of interacting particles [Hed65]. These equations link the self-energy to the full particle propagator and include the calculation of the polarization function as well as the screened interaction.
There are different methods how to derive these equations. In the original paper of Hedin, they were obtained with the help of Schwinger's functional derivative method

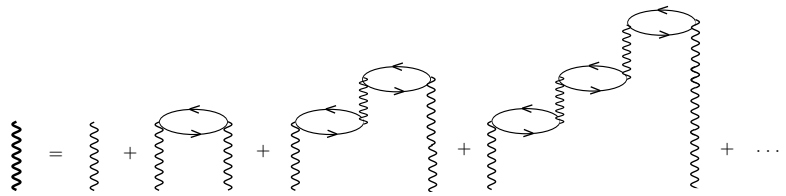

Figure 3.6: Diagrammatic expansion of the screened interaction in the RPA. The bare Coulomb interaction is reduced by the polarization process, represented by the ring.

[Sch51], [MS59] which makes use of an artificial potential (in the derivation) which is set to zero at the end. Hedin developed the self-energy in terms of the screened interaction $W(\mathbf{r}, \mathbf{r}', \omega)$ (and not the bare Coulomb potential $v(\mathbf{r}, \mathbf{r}')$). Since the exact derivation is very complicated and lengthy, just the results are written down here. A detailed derivation can be found in [AG98].
In the following the notation will be simplified by subsuming the position, time and spin variables $(\mathbf{r}_1, t_1, \sigma_1)$ into a single symbol 1 (or 2, 3,..., respectively). In this notation the first of Hedin's equation for the vertex function — a three-point operator — can be written as

$$\Gamma(1,2;3) = \delta(1,2)\delta(1,3) + \int\int\int\int \frac{\delta\Sigma(1,2)}{\delta G(4,5)} G(5,6)\Gamma(6,7;3)G(7,4)\, d4\; d5\; d6\; d7\; . \tag{3.39}$$

With the help of the vertex function, the irreducible polarization propagator is given by

$$P(1,2) = -i \int\int G(1,3)\Gamma(3,4;2)G(4,1)\, d3\; d4\; . \tag{3.40}$$

The dielectric function which quantifies the screening is then given by

$$\epsilon(1,2) = \delta(1,2) - \int v(1,3)P(3,2)\; . \tag{3.41}$$

Although eq. (3.41) is not counted among Hedin's equations, it is written down here because the dielectric function is an important property. Its inverse relates the bare Coulomb interaction to the dynamically screened interaction

$$W(1,2) = \int \epsilon^{-1}(1,3)v(3,2)\, d3 = v(1,2) + \int\int v(1,3)P(3,4)W(4,2)\, d3\; d4\; . \tag{3.42}$$

As already explained in the last section, W quantifies the interaction between quasi-particles since the interaction between bare particles is screened through their polarization clouds.
The self-energy Σ is then given by

$$\Sigma(1,2) = i \int\int W(1,3)G(1,4)\Gamma(4,2;3)\, d3\; d4\; . \tag{3.43}$$

Finally, the Dyson equation (3.34) yields the complete Green function including all exchange and correlation effects.
In principle, this set of five coupled integral equations (3.39), (3.40), (3.42), (3.43) and (3.34) solves the many body problem exactly. Unfortunately, the nature of the relations is not just numerical, since eq. (3.39) contains a functional derivative. Therefore the equations cannot be solved self-consistently by computer codes. However, they are a good starting point for approximations, which are intrinsically different from the diagrammatic approach. For example, they may be iterated analytically in order to derive useful approximations. One possible approximation is the GW approximation, which will be presented in the next section.

3.9 The GW approximation

In order to iterate Hedin's equations analytically, a starting point is required. Therefore a zeroth-order self-energy $\Sigma^{(0)}$ and a corresponding Green function $G^{(0)}$ are chosen, which may already include certain exchange and/or correlation effects. In order to avoid double-counting, Dyson's equation must be modified to

$$G(1,2) = G^{(0)}(1,2) + \int\int G^{(0)}(1,3)\left[V^{\mathrm{H}}(3)\delta(3,4) + \Sigma(3,4) - \Sigma^{(0)}(3,4) - V^{\mathrm{H}(0)}(3)\delta(3,4)\right] G(4,2)\, d3\, d4\ . \tag{3.44}$$

In the original version of the GW approximation proposed by Hedin, the Hartree approximation is chosen as starting point, thus $G^{(0)} = G^{\mathrm{H}}$ and $\Sigma^{(0)} = \Sigma^{\mathrm{H}}$. This choice leads to a strong simplification, since the vertex function reduces to a product of two delta functions

$$\Gamma(1,2;3) = \delta(1,2)\delta(1,3)\ . \tag{3.45}$$

Inserting the simplified vertex function in eq. (3.40) leads to the polarization function

$$P(1,2) = -iG^{(0)}(1,2)G^{(0)}(2,1)\ , \tag{3.46}$$

which corresponds to the ring already introduced in section 3.7, eq. (3.37). In order to distinguish this approximated polarization function from the irreducible polarization as defined in eq. (3.40), in the following I will denote it with $P_0(1,2)$. With $P(1,2) = P_0(1,2)$, the screened interaction equals the corresponding quantity in the random-phase approximation (compare the schematic expression eq. (3.38) and figure 3.6). It results in

$$W(1,2) = v(1,2) + \int\int v(1,2)P_0(3,4)W(4,2)\, d3\, d4$$

and stays formally the same as defined in eq. (3.42), just with P_0 instead of P. The self-energy reduces to a product of G and W

$$\Sigma^{GW}(1,2) = iG^{(0)}(1,2)W(1,2)\ . \tag{3.47}$$

Since the self-energy of the Hartree-approximation is zero, the Green function $G^{(1)}$ after one iteration becomes

$$G^{(1)}(1,2) = G^{(0)}(1,2) + \int\int G^{(0)}(13)\Sigma^{GW}(3,4)G^{(1)}(42)\, d3\; d4\; . \tag{3.48}$$

Practical applications of the GW approximation often start from a different initial Green function. In particular, the Green function obtained by mean-field theories like DFT, which already includes exchange and correlations effects, is often taken. The comparison to experimental results shows that the choice of a different, 'better' starting point leads to a real improvement of the results of the GW calculations.

3.10 Irreducible polarization

The irreducible polarization as defined in eq. (3.40) can be obtained in another way without calculating the three-point vertex function $\Gamma(1,2;3)$ (see eq. (3.39)) as well. It satisfies a Dyson-type equation [PGG96] and therefore (for a time-invariant system) in frequency space

$$P(\mathbf{r},\mathbf{r}';\omega) = P_0(\mathbf{r},\mathbf{r}';\omega) + \int d^3r'' \int d^3r''' P_0(\mathbf{r},\mathbf{r}'';\omega) f_{\mathrm{xc}}(\mathbf{r}'',\mathbf{r}''';\omega) P(\mathbf{r}''',\mathbf{r}';\omega)\; , \tag{3.49}$$

where $P_0(\mathbf{x},\mathbf{x}';\omega)$ is the polarization function calculated for an effective potential according to eq. (3.46)[3]. In eq. (3.49) I have neglected the spin dependence of the polarization. This is valid for non-magnetic systems and will be discussed in chapter 7.

The function $f_{\mathrm{xc}}(\mathbf{r},\mathbf{r}';\omega)$ which appears for the first time in eq. (3.49) is the so-called exchange-correlation kernel. In direct space it is defined as the derivative of the time-dependent exchange-correlation potential $V_{\mathrm{xc}}(\mathbf{r}t)$ with respect to the density $n(\mathbf{r}'t')$

$$f_{\mathrm{xc}}(\mathbf{r},\mathbf{r}';t-t') = \left.\frac{\delta V_{\mathrm{xc}}(\mathbf{r},t)}{\delta n(\mathbf{r}',t')}\right|_{n(\mathbf{r}',t')=n^{(0)}(\mathbf{r}')}\; , \tag{3.50}$$

where $n^{(0)}(\mathbf{r}')$ is the static ground-state density of the system. Although eq. (3.49) is in principle exact, the practical evaluation requires to make some approximations, since the exchange-correlation kernel cannot be calculated exactly.

In order to obtain an approximation for the kernel any explicit approximate formula for the potential can be used to derive a matching approximation for the kernel. The most common approximation for the exchange-correlation potential $V_{\mathrm{xc}}(\mathbf{r},t)$ is the adiabatic local-density approximation (ALDA) which replaces the exchange-correlation potential at the coordinates $\mathbf{r}$ and t by that of the homogeneous electron gas with the same local density $n(\mathbf{r},t)$. It is readily expressed in terms of the

[3] More precisely, it is the polarization function calculated according to eq. (3.46) with a Green function calculated within DFT.

exchange-correlation energy density $\epsilon_{\rm xc}^{\rm hom}(n)$ of the homogeneous electron gas according to

$$V_{\rm xc}^{\rm ALDA}(\mathbf{r},t) = \frac{d}{dn}\left[n\epsilon_{\rm xc}^{\rm hom}(n)\right]_{n=n(\mathbf{r},t)} \ . \tag{3.51}$$

The ALDA is a rather drastic approximation that ignores the non-local dependence of $V_{\rm xc}(\mathbf{r},t)$ on the density elsewhere in space as well as the memory of the density distribution at earlier times. Nevertheless, the static exchange-correlation potential in bulk solids is typically quite well modeled in the ALDA; in the case of the homogeneous electron gas it yields the correct constant potential.
Inserting formula (3.51) for $V_{\rm xc}^{\rm ALDA}(\mathbf{r},t)$ in eq. (3.50), one obtains the exchange-correlation kernel in the adiabatic local-density approximation [ZS80]

$$f_{\rm xc}^{\rm ALDA}(\mathbf{r},\mathbf{r}';t-t') = \frac{\delta V_{\rm xc}^{\rm ALDA}(\mathbf{r},t)}{\delta n(\mathbf{r}',t')} = \delta(\mathbf{r}-\mathbf{r}')\delta(t-t')\frac{d^2}{dn^2}\left[n\epsilon_{\rm xc}^{\rm hom}(n)\right]_{n=n^{(0)}(\mathbf{r})} \ . \tag{3.52}$$

In order to calculate this kernel, I will in a first step calculate the exchange-correlation energy-density of the homogeneous electron gas. It is given as the sum of the exchange and the correlation part

$$\epsilon_{\rm xc}^{\rm hom}(n) = \epsilon_{\rm x}^{\rm hom}(n) + \epsilon_{\rm c}^{\rm hom}(n) \ . \tag{3.53}$$

I start with the (analytical) calculation of the exchange part. In the Hartree-Fock approximation, one obtains the exact result for the exchange-energy of the homogeneous electron gas

$$E_{\rm x} = -N\frac{3}{4}\frac{k_{\rm F}}{\pi} \ . \tag{3.54}$$

Expressing the number of particles as an integral over the density $N = \int_V n\ d^3r$ and the Fermi wave-vector in terms of the density $k_{\rm F} = (3\pi^2 n)^{1/3}$ one obtains

$$E_{\rm x} = \int_V d^3r\ n(\mathbf{r})\left[-\frac{3}{4\pi}(3\pi^2 n)^{1/3}\right] = \int_V d^3r\ n\epsilon_{\rm x}(n) \ . \tag{3.55}$$

The exchange-energy density is thus given by

$$\epsilon_{\rm x}^{\rm ALDA}(n) = -\frac{3}{4\pi}(3\pi^2 n)^{1/3} \ . \tag{3.56}$$

Finally, the exchange part of the exchange-correlation kernel is obtained following eq. (3.52) as

$$f_{\rm x}^{\rm ALDA}(n) = \frac{d^2}{dn^2}\left[n\epsilon_{\rm x}^{\rm hom}(n)\right] = -\frac{\pi}{(3\pi^2 n)^{2/3}} \ . \tag{3.57}$$

The correlation part of the exchange-correlation energy density $\epsilon_{\mathrm{c}}^{\mathrm{ALDA}}(n)$ is known numerically from quantum Monte-Carlo calculations [CA80] and parametrized in the form [PW92]

$$\epsilon_{\mathrm{c}}(r_s) = -2A(1+\alpha_1 r_s)\ln\left[1+\frac{1}{X(r_s)}\right] \tag{3.58}$$

$$X(r_s) = 2A(\beta_1 r_s^{1/2} + \beta_2 r_s + \beta_3 r_s^{3/2} + \beta_4 r_s^{p+1}), \tag{3.59}$$

with a set of parameters $p, A, \alpha_1, \beta_1, \beta_2, \beta_3, \beta_4$.
The function ϵ_{c} depends on the density radius r_s which is related to the density by

$$r_s = \left(\frac{3}{4\pi n}\right)^{1/3} \tag{3.60}$$

The constants are

p	A	α_1	β_1	β_2	β_3	β_4
1	0.031091	0.21370	7.5957	3.5876	1.6382	0.49294

In order to obtain the correlation part of the kernel I have to calculate

$$f_{\mathrm{c}}(n) = 2\frac{\partial\epsilon_{\mathrm{c}}}{\partial n} + n\frac{\partial^2\epsilon_{\mathrm{c}}}{\partial n^2}\ . \tag{3.61}$$

This involves the derivatives

$$\frac{\partial}{\partial n} = \frac{\partial\epsilon_{\mathrm{c}}}{\partial r_s}\frac{\partial r_s}{\partial n}, \qquad \frac{\partial^2\epsilon_{\mathrm{c}}}{\partial n^2} = \frac{\partial^2\epsilon_{\mathrm{c}}}{\partial r_s^2}\left(\frac{\partial r_s}{\partial n}\right)^2 + \frac{\partial\epsilon_{\mathrm{c}}}{\partial r_s}\frac{\partial^2 r_s}{\partial n^2} \tag{3.62}$$

with

$$\frac{\partial r_s}{\partial n} = -\frac{1}{3}\left(\frac{3}{4\pi}\right)^{1/3} n^{-4/3}, \qquad \frac{\partial^2 r_s}{\partial n^2} = \frac{4}{9}\left(\frac{3}{4\pi}\right)^{1/3} n^{-7/3}. \tag{3.63}$$

The derivatives of the function ϵ_{c}

$$\frac{\partial\epsilon_{\mathrm{c}}}{\partial r_s} = -2A\alpha_1\ln\left[1+\frac{1}{X}\right] + 2A(1+\alpha_1 r_s)\frac{1}{X^2+X}\frac{\partial X}{\partial r_s} \tag{3.64}$$

$$\frac{\partial^2\epsilon_{\mathrm{c}}}{\partial r_s^2} = 4A\alpha_1\frac{1}{X^2+X}\frac{\partial X}{\partial r_s} + 2A(1+\alpha_1 r_s)\left[\frac{1}{X^2+X}\frac{\partial^2 X}{\partial r_s^2} - \frac{2X+1}{(X^2+X)^2}\left(\frac{\partial X}{\partial r_s}\right)^2\right] \tag{3.65}$$

incorporate derivatives of X as well:

$$\frac{\partial X}{\partial r_s} = 2A\left(\frac{1}{2}\beta_1 r_s^{-1/2} + \beta_2 + \frac{3}{2}\beta_3 r_s^{1/2} + (p+1)\beta_4 r_s^{p}\right) \tag{3.66}$$

$$\frac{\partial^2 X}{\partial r_s^2} = 2A\left(-\frac{1}{4}\beta_1 r_s^{-3/2} + \frac{3}{4}\beta_3 r_s^{-1/2} + p(p+1)\beta_4 r_s^{p-1}\right) \tag{3.67}$$

Substituting all derivatives in eq. (3.61) and adding the exchange part (3.57) results in the exchange-correlation kernel $f_{\mathrm{xc}}^{\mathrm{ALDA}}(n)$.
Although the ALDA is based on a numerically exact parametrization of the exchange-correlation energy density $\epsilon_{\mathrm{xc}}^{\mathrm{hom}}(n)$, it actually constitutes a very poor representation of the kernel even for homogeneous systems. In contrast to the true exchange-correlation kernel $f_{\mathrm{xc}}(|\mathbf{r}-\mathbf{r}'|, t-t')$ of the homogeneous electron gas it is both local in time and space coordinates, and thus ignores essential physical features like the non-local dependence on the global density distribution. In reciprocal space, the ALDA corresponds only to the long-wavelength limit $f_{\mathrm{xc}}^{\mathrm{ALDA}}(q,\omega) = \lim_{q\to 0} f_{\mathrm{xc}}^{\mathrm{hom}}(q,\omega=0)$.
One can conclude that although the static exchange-correlation potential in the ALDA in many cases leads to quite reasonable results, the exchange-correlation kernel is not well represented in this approximation. Therefore often one seeks for separate approximations for these both quantities [Sch06]. Nevertheless, since there are few alternatives for practical calculations and very little is known about the true exchange-correlation kernel, in this diploma thesis the exchange-correlation kernel is approximated in the ALDA.

4 Concepts of electronic transport

The calculation of the current flowing in a system due to some bias voltage is one of the most difficult problems in theoretical solid state physics [BB06]. Therefore different levels of approximations have been applied to the problem and theoretical models for many different aspects of the problem have been developed.
The Boltzmann formalism provides a classical description of electronic transport. It describes the time-dependent change in the electronic distribution function due to the applied electric field $\mathbf{E}$. It is a classical approximation, since it neglects interference effects caused by the quantum-mechanical nature of electrons are neglected and assumes the electrons to move freely between individual scattering events. Nevertheless, the description of electrons as quasi-particles moving around freely without scattering at atomic sites is of course a quantum-mechanical phenomenon.
Very often, the Boltzmann formalism is used in the so-called time-relaxation approximation in order to describe inelastic scattering processes. In this approximation the scattering rate of the conducting electrons is assumed to depend linearly on the change Δf of the distribution function f. The basic input parameter is the so-called mean-free path L, which represents the characteristic average length between two scattering events.
With the help of the Boltzmann-equation for example the low-temperature dependence of the resistance of simple metals due to electron-phonon scattering can be derived, yielding the famous Bloch T^5 law. Because of the characteristics described so far, the Boltzmann formalism represents a good description of systems, in which the sample dimensions are much larger than the mean-free path and the scattering events can be viewed as independent of each other so that quantum interference effects can be neglected[1]. Therefore it is appropriate to describe diffusive transport in large structures.
Another more basic starting point to describe electronic transport is made in the linear-response theory, where the current is treated as (linear) response of the quantum system to the applied electric field. The conductance of the system is obtained with the help of the so-called Kubo formalism, a quantum mechanical formalism appropriate to time-dependent system. This approach will be described in more detail in section 4.2. Unlike the Boltzmann formalism, it is not only appropriate to describe transport in the diffusive transport regime but also in the ballistic regime[2]. Although this is a very general approach and allows to include all kinds of scattering, it is not easy to apply it to realistic systems.

[1] Such quantum interference can lead to a drastic variation of the resistance of the sample in an effect known as Anderson localization.
[2] The ballistic regime deals with elastic scattering processes only.

In the following, electronic transport will be considered from a quantum-mechanical point of view. I, however, chose a more intuitive approach than that of the Kubo-formalism. Nevertheless, the same results could be obtained within the Kubo-formalism, too.
The investigated systems are assumed to be small enough, so that the resistance is only due to the scattering of the electrons on the potential in some scattering volume. Therefore, the dimensions of the considered systems have to be chosen such that they are much smaller than the mean-free path due to scattering on impurities, interface roughness, phonons, magnons and other temperature dependent excitations.
Nevertheless, the calculation of the conductance is still complicate even when imposing the latter restrictions, since one has to deal with a complicated many-electron problem of a system in non-equilibrium. On the macroscopic scale, different quantities like the current and the charge density can be defined. Unfortunately, the thermodynamical averaging makes it quite complicate to scale these quantities down to microscopic dimensions. Therefore on different time and length scales different theoretical approaches are required and different effects have to be included.
However, in the following I will treat microscopic systems which can be described by pure wave functions without any statistical averaging. Naturally, these pure wave-functions are no simple one-electron wave functions but complicated time-dependent many-electron wave functions containing information about the whole electron system. Knowing these wave-functions one can calculate the probability $P_{\mathrm{i,f}}$ of the system changing its state from an initial multi-electron state Φ_{i} to a different final state Φ_{f}, corresponding to a different charge distribution than the initial state Φ_{i}. Unfortunately, the calculation of the time dependent many-electron wave functions is a very difficult problem which cannot be solved in general.
In order to overcome this obstacle I will in a first step treat the electrons as independent from each other and calculate the conductance in the single-electron picture. In this case, the conductance is given by the famous Landauer equation. Subsequently, exchange and correlation effects are included (see section 4.2) via the irreducible polarization (as already introduced in chapter 3, eq. (3.49)). Using linear response theory, a relation between the conductivity and the irreducible polarization will be derived. Finally, the conductivity including exchange and correlation effects will be calculated.

4.1 Single particle view on electronic transport: The Landauer approach

In the following I will restrict the discussion to scattering processes without energy-dissipation, i.e. treat only elastic scattering. This so-called ballistic transport is well described in the Landauer approach [Lan57]. The derivation presented here follows the derivation in [Wor03].
The setup described in the Landauer approach (see figure 4.1) consists of a region

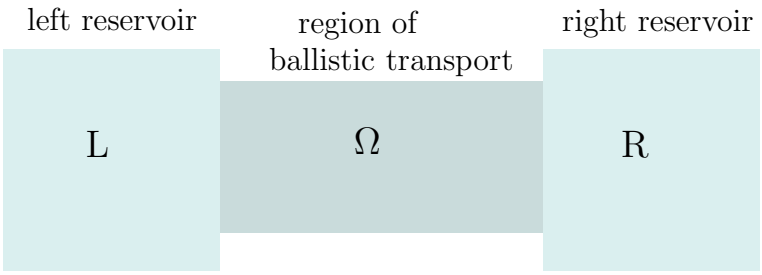

Figure 4.1: Basic setup of the Landauer approach to electronic transport. The two reservoirs are assumed to be in thermal equilibrium.

Ω, the so-called scattering region, in which the electrons travel ballistic. It is located between two reservoirs, situated at the left and the right side of the scattering volume Ω. For an easy derivation of the conductance Γ of the region Ω, a simple one-dimensional model is assumed. The conductance Γ is then defined by the net current I_{LR} divided by the potential difference between the two reservoirs L and R. The net current I_{LR} is given by the difference of the current due to electrons traveling from the right to the left reservoir and the current due to electrons traveling vice versa

$$I_{\mathrm{LR}} = I_{\mathrm{L}\to\mathrm{R}} - I_{\mathrm{R}\to\mathrm{L}} \; . \tag{4.1}$$

Assuming that the electronic structure of the region Ω can be described by a single band, the current from the left to the right reservoir is given by the sum over all states with $k > 0$ up to the Fermi wave vector k_{F}

$$\begin{aligned} I_{\mathrm{L}\to\mathrm{R}} &= \sum_{0}^{k_{\mathrm{F}}} v(k) \\ &= \frac{1}{2\pi} \int_0^{k_{\mathrm{F}}} dk \, v(k) \; , \end{aligned} \tag{4.2}$$

where $v(k)$ denotes the group velocity of the state given by

$$v(k) = \frac{\partial E}{\partial k} \; . \tag{4.3}$$

The transformation of the sum to the integral in eq. (4.2) requires the additional factor $\frac{1}{2\pi}$ which is the one-dimensional volume of one state in reciprocal space. The integral over k can be transformed to an energy integration resulting in

$$\begin{aligned} I_{\mathrm{L}\to\mathrm{R}} &= \frac{1}{2\pi} \int_0^{k_{\mathrm{F}}} dk \, v(k) \\ &= \int_0^{\mu_{\mathrm{L}}} dE \, \frac{\partial E}{\partial k} \frac{1}{\frac{1}{2\pi} \partial E / \partial k} \\ &= \int_0^{\mu_{\mathrm{L}}} dE \, \frac{1}{2\pi} = \frac{1}{2\pi} \mu_{\mathrm{L}} \; , \end{aligned} \tag{4.4}$$

where $\frac{1}{\frac{1}{2\pi}\partial E/\partial k}$ can be interpreted as the density of states $n(E)$. The upper limit of the energy-dependent integral is given by the chemical potential of the left side, since only occupied electronic states contribute to the electric current.
For the states incoming from the right one obtains equivalently

$$I_{\mathrm{R}\to\mathrm{L}} = \frac{1}{2\pi}\mu_{\mathrm{R}} \tag{4.5}$$

and therefore

$$I_{\mathrm{LR}} = \frac{1}{2\pi}\left(\mu_{\mathrm{L}} - \mu_{\mathrm{R}}\right) \ . \tag{4.6}$$

Since the difference of the chemical potentials equals the applied voltage $V = \mu_{\mathrm{L}} - \mu_{\mathrm{R}}$, the conductance results in

$$\Gamma = \frac{I_{\mathrm{LR}}}{V} = \frac{1}{2\pi} \ . \tag{4.7}$$

This is a striking result, since the conductance neither depends on the group velocity $v(k)$ nor on the density of states $n(E)$. The derivation shows that a low group velocity and therefore a low current j is compensated by a high density of states (and vice versa) such that the conductance does not change.
Since in general the electronic structure of the region of ballistic transport has to be described not only by a single band but by multiple bands, the derivation has to be extended and an extra sum over the different bands has to be included. Since each band contributes the same value $\Gamma = \frac{1}{2\pi}$, the conductance of N conducting bands results in

$$\Gamma = N\frac{1}{2\pi} \ . \tag{4.8}$$

At this point, one can argue that the description of the electronic structure in the region Ω with the help of bands including a dispersion relation $E(\mathbf{k})$ is not valid because of the lack of periodicity of the system. This is true and will be corrected now. Although one cannot speak of Bloch states in the region of ballistic transport, one can correctly speak of Bloch states in the two reservoirs. We will assume the typical scattering problem for a Bloch state in the left lead incoming from the left ($-\infty$), thus with a current flowing towards Ω. (In the following it will be denoted by a state propagating towards Ω.) In the left reservoir, the resulting scattering state can be written as a sum over the incoming and the reflected bulk Bloch states of the reservoir, whereas in the right lead the state is given by the sum over transmitted Bloch states

$$\psi(\mathbf{r}) = \begin{cases} \psi_{\mathrm{in}}(\mathbf{r}) + \sum_n r_{\mathrm{in},n}\psi_{\mathrm{r}}^n(\mathbf{r}) & \mathbf{r} \text{ in left reservoir} \\ \sum_{n'} t_{\mathrm{in},n'}\psi_{\mathrm{t}}^{n'}(\mathbf{r}) & \mathbf{r} \text{ in right reservoir.} \end{cases} \tag{4.9}$$

States which are decaying away from the interfaces into the reservoirs can be neglected since (in the semi-infinite reservoirs) they do not carry any current. They can simply be eliminated by shifting the interfaces far enough in the reservoirs.
Now, I go back to the derivation of the Landauer formula. The evaluation of the current in eq. (4.2) has to be modified such that the integration has to be performed

over all states labeled with an 'in' in the definition (4.9). However, since the current is conserved and all states are normalized to carry unit current, the integration can be as well performed in the right lead, where it is much simpler. Exploiting the orthogonality of the Bloch states, one obtains the correct Landauer equation for ballistic transport in the presence of some scattering of the incoming electrons

$$\Gamma = \frac{1}{2\pi} \sum_{i,j} |t_{ij}|^2 \ . \tag{4.10}$$

The indices i, j label the Bloch states traveling from the left to the right side. The square of the absolute value of the transmission coefficient $|t_{ij}|^2$ can be interpreted as the quantum mechanical transmission probability $P_{i,j} = |t_{ij}|^2$ for an electron from the incoming Bloch state i into the transmitted Bloch state j.
For a homogeneous transport region without any scattering – hence $\sum P_{i,j} = 1$ – eq. (4.10) reduces to eq. (4.8), i.e. to the finite conductance $\Gamma = \frac{N}{2\pi}$. Similarly, one obtains a finite conductance in the case of the free electron gas. This is a striking result, since only elastic scattering without energy dissipation was assumed — quite the contrary, an infinite conductance could have been expected for a perfect bulk crystal!
Since the finite conductance cannot be explained by the scattering in the region of ballistic transport, the explication has to be searched elsewhere. In fact, the answer can be found at the interfaces between the ballistic region and the leads. The finite conductance can be interpreted as due to the finite conductance at the interface between the reservoirs and the ballistic region. It is also called the Sharvin-resistance of the system.
The Landauer equation is valid in many cases reaching from systems with a high conductivity to systems in the tunneling regime. Nevertheless, the validity may break down in the limit of a very low transmission. This is due to the fact, that the Landauer formalism includes only incoming and transmitted states which can be described by Bloch states. Therefore all states localized in the ballistic region of transport are neglected. However, coupling of these localized states to the otherwise orthogonal Bloch states in the reservoirs can be provided by effects like many-body electron-electron interaction, electron-phonon scattering or structural defects. Transport caused by such processes may become important in the limit of very low transmission probability through Bloch states, whereas in the case of high transmission probability through Bloch states the Landauer approach represents a good description of the physical process. In the one-electron picture transport through localized states can be imagined as a transition of one electron from the left reservoir into a localized state in the region Ω, followed by one or more transitions of the electron to the other side of Ω and finally a transition into a Bloch state of the other reservoir. Hence, it is reasonable that the validity of the Landauer equation breaks down if the transmission probability between reservoirs states and localized states becomes comparable to the probabilities $P_{i,j} = |t_{ij}|^2$.
The limit of very small transition probabilities is treated in the so-called Bardeen

approach [Bar61]. In this limit, the details of the scattering processes which couple the states can be neglected and the physical situation is that of a quantum mechanical tunneling process. In the Bardeen approach to tunneling both localized and Bloch states contribute to the conductance. Whereas in the limit of small conductance the results for localized states obtained within the Bardeen approach are in good agreement with the values calculated with the Landauer formula, in the case of higher conductance the validity of the Bardeen approach breaks down since we are no longer in the tunneling regime and the result obtained within the Bardeen approach rises above the conductance Γ evaluated according to eq. (4.10).
Until now, all results were obtained within the single-electron picture. However, one should keep in mind that the validity of the single-electron approach is restricted by many effects. Additionally to electron-electron scattering effects of different conducting electrons, electron-phonon scattering, screening and charging effects or many-particle interactions in magnetic systems have to be named. Furthermore, as soon as quantum mechanical many-body effects become dominant, qualitatively different phenomena can be observed, which cannot be described in the single-particle picture. One of them is the Kondo-effect [Kon64] which describes conductance abnormalities at low-temperatures in metals. Another example is the Coulomb blockade.
In the next section, exchange and correlation effects will be included via the irreducible polarization. Therefore linear response theory will be used to relate the conductance to the irreducible polarization of the system. I follow the derivation of P.Bokes and R.Godby [BG04].

4.2 Conductance and polarization

In order to relate the irreducible polarization to the conductance, in the first part of this section I will derive the dependence of the conductance on the conductivity. In the second part, the equation of continuity is used to connect the polarization function to the conductivity and therefore also to the conductance. For the simple case of non-interacting electrons and homogeneous electron gas I will show that the result equals the conductance calculated with the Landauer formula.

4.2.1 Conductance and conductivity

In Kubo linear response theory [Kub59], the electric current density $\mathbf{j}(\mathbf{r},t)$ is given as a linear answer of the electronic system to an external electric field $\mathbf{E}(\mathbf{r},t)$

$$\mathbf{j}(\mathbf{r},t) = \int_{-\infty}^{\infty} dt' \int d^3r' \overleftrightarrow{\sigma}(\mathbf{r},\mathbf{r}';t-t') \cdot \mathbf{E}(\mathbf{r}',t') \;, \tag{4.11}$$

where $\overleftrightarrow{\sigma}(\mathbf{r},\mathbf{r}';t)$ is the nonlocal tensor of conductivity given by

$$\overleftrightarrow{\sigma}(\mathbf{r},\mathbf{r}';t) = i\Theta(t) \int_{0}^{-i\beta} d\tau \, \mathrm{Tr}\left\{\rho_{\mathrm{eq}} \mathbf{j}(\mathbf{r}',t+\tau)\mathbf{j}(\mathbf{r},0)\right\} \tag{4.12}$$

with the equilibrium density matrix ρ_{eq}.
In the following derivation exclusively the case of an infinitesimally weak external field will be considered which acts only in z direction, i.e. $E_z(\mathbf{r},t) = E(z)\Theta(t)$ and $E_x = E_y = 0$.
Integration of the current density over the surface perpendicular to z leads to the current

$$\begin{aligned}
I(z,t) &= \int d\mathbf{S}\cdot\mathbf{j}(\mathbf{r},t) \\
&= \int_{-\infty}^{\infty} dt' \int d^3r' \int d\mathbf{S}\cdot\overleftrightarrow{\sigma}(\mathbf{r},\mathbf{r}';t-t')\cdot\mathbf{E}(\mathbf{r}',t') \\
&= \int_{-\infty}^{\infty} dt' \int dz' \int d\mathbf{S}\cdot\overleftrightarrow{\sigma}(\mathbf{r},\mathbf{r}';t-t')\cdot d\mathbf{S}'E(z')\Theta(t') \\
&= \int_{0}^{\infty} dt' \int_{-\infty}^{\infty} dz'\,\sigma(z,z';t-t')E(z') \\
&= \int_{t}^{-\infty} (-dt') \int_{-\infty}^{\infty} dz'\,\sigma(z,z';t')E(z') \\
&= \int_{-\infty}^{t} dt' \int_{-\infty}^{\infty} dz'\,\sigma(z,z';t')E(z')\ , \qquad (4.13)
\end{aligned}$$

where I have introduced the effective one-dimensional conductivity

$$\sigma(z,z';t) = \int d\mathbf{S}\cdot\overleftrightarrow{\sigma}(\mathbf{r},\mathbf{r}';t)\cdot d\mathbf{S}'\ . \qquad (4.14)$$

I am now interested in the steady state current $I(z)$. Therefore I assume, that the electric field is switched on adiabatically, i.e. $E(z,t) = E(z)e^{\alpha t}$, as t approaches 0 from below and measure the current at $t = 0^-$. This results in the steady state current

$$\begin{aligned}
I(z) &= \int_{-\infty}^{\infty} dz' \lim_{\alpha\to 0^+} \int_{-\infty}^{\infty} dt'\, e^{-\alpha t}\sigma(z,z';t')E(z') \\
&= \int_{-\infty}^{\infty} dz' \lim_{\alpha\to 0^+} \sigma(z,z';\omega = i\alpha)E(z') \\
&= \int_{-\infty}^{\infty} dz'\ \sigma(z,z';\omega = i0^+)E(z')\ . \qquad (4.15)
\end{aligned}$$

In order to calculate the conductance of the system given through $\Gamma = \frac{I}{U}$ with the electric current I and the tension U I will Fourier transform eq. (4.15) to reciprocal space

$$I(q) = \frac{1}{2\pi}\int dq'\sigma(q,q';\omega = i0^+)E(q') \qquad (4.16)$$

with

$$\sigma(q,q',\omega = i0^+) = \int_{-\infty}^{\infty} dz \int_{-\infty}^{\infty} dz' e^{-iqz+iq'z'}\sigma(z,z';\omega = i0^+)\ . \qquad (4.17)$$

As a consequence of the equation of continuity the steady-state current has to be independent from z, thus $I(z) = I$, so that $I(q) = 2\pi I\delta(q)$. According to eq. (4.16) it follows that also $\sigma(q, q'; \omega = i0^+) \sim \delta(q)$. Moreover, the linearity of the theory demands that the steady-state current is uniquely given by the bias $U = E(q = 0)$. This is equivalent to the fact, that the steady-state is only influenced by the long-range part of the external electric field. Due to eq. (4.16) this is achieved, when $\sigma(q, q'; \omega = i0^+) \sim \delta(q')$.
When calculating the conductance

$$\Gamma = \frac{I}{U} \,, \tag{4.18}$$

it is not sufficient to divide the current through the impressed voltage but through the voltage of the total electric field $E^{\mathrm{t}}(\mathbf{r})$. This is simply the sum of the external and the induced field $E^{\mathrm{t}}(\mathbf{r}) = E^{\mathrm{ext}}(\mathbf{r}) + E^{\mathrm{i}}(\mathbf{r})$. Combining all this considerations one can conclude

$$\begin{aligned}
\Gamma &= \frac{I}{U} = \frac{I(z=0)}{U} \\
&= \frac{\frac{1}{2\pi}\int dq\ I(q)}{E(q=0)} \\
&= \frac{\frac{1}{2\pi}\int dq\ \frac{1}{2\pi}\int dq' \sigma(q, q'; \omega = i0^+) E(q')}{E(q=0)} \\
&= \frac{\frac{1}{4\pi^2}\int dq \int dq'\ \sigma(q, q'; \omega = i0^+) E(q'=0)}{E(q=0)} \\
&= \frac{1}{4\pi^2}\int dq \int dq'\ \sigma(q, q'; \omega = i0^+) \,.
\end{aligned} \tag{4.19}$$

This result can be reformulated using $\sigma(q, q'; \omega = i0^+) \sim \delta(q)\delta(q')$

$$\lim_{\alpha \to 0^+} \sigma(q, q'; i\alpha) = 4\pi^2 \Gamma \delta(q)\delta(q') \,. \tag{4.20}$$

Eq. (4.20) shows that the conductance Γ is the weight of the Drude singularity. However, for numerical evaluation eq. (4.19) is more useful, since it serves for interpolation of the conductance at small imaginary frequency. Because the conductivity is a peaked function in q, q', it has to be evaluated for small values of these variables only.
Unfortunately, the calculation of the conductivity given by eq. (4.12) and (4.14) is very difficult. Therefore in the next section I will relate the conductivity to the irreducible polarization function $P(\mathbf{r}, \mathbf{r}'; t - t')$, which can be even evaluated efficiently using *ab initio* methods.

4.2.2 Conductivity and polarization

The irreducible polarization function $P(\mathbf{r}, \mathbf{r}'; t - t')$ defined in chapter 3 is given by

$$P(\mathbf{r}, \mathbf{r}'; t - t') = \frac{\delta n(\mathbf{r}, t)}{\delta V(\mathbf{r}', t')} \tag{4.21}$$

and is interpreted as the change in electron density $\delta n(\mathbf{r},t)$ due to the classical electrodynamic potential $V(\mathbf{r},t) = -U$ composed of the external potential and the Hartree term. The equation of continuity[3] integrated over the cross-sectional area

$$\partial_z I(z,t) - \partial_t N(z,t) = 0 \tag{4.22}$$

relates the conductivity to the polarization, since the number of particles $N(z,t)$ consists in

$$N(z,t) = \int_{-\infty}^{t} dt' \int dz'\, P(z,z';t-t')V(z',t') \;, \tag{4.23}$$

where $P(z,z';t-t')$ is defined similarly to $\sigma(z,z';t-t')$ as the effective one-dimensional polarization integrated over the cross-sectional area

$$P(z,z';t) = \int\int dS\, P(\mathbf{r},\mathbf{r}';t)\, dS' \;. \tag{4.24}$$

Since the following calculation is quite lengthy, I will in a first step consider the first summand of eq. (4.22)

$$\begin{aligned}
\partial_z I(z,t) &= \frac{\partial}{\partial z}\int_{-\infty}^{t} dt' \int_{-\infty}^{\infty} dz'\; \sigma(z,z';t')E(z') \\
&= \int_{-\infty}^{t} dt' \int_{-\infty}^{\infty} dz'\; \frac{\partial}{\partial z}\frac{1}{4\pi^2}\int_{-\infty}^{\infty} dq \int_{-\infty}^{\infty} dq'\; e^{iqz-iq'z'}\sigma(q,q';t') \\
&\qquad\qquad \left[\left(\frac{d}{dz'}\right)\frac{1}{2\pi}\int_{-\infty}^{\infty} dq''\; e^{iq''z'}V(q'')\right] \\
&= -\frac{1}{4\pi^2}\int_{-\infty}^{t} dt' \int_{-\infty}^{\infty} dq \int_{-\infty}^{\infty} dq'\; e^{iqz} qq'\sigma(q,q';t')V(q') \;.
\end{aligned} \tag{4.25}$$

In the second step I exploited that the potential V is related to the electric field E according to $E = \nabla V$. In the steady-state limit eq. (4.25) simplifies to

$$\partial_z I(z) = -\frac{1}{4\pi^2}\int_{-\infty}^{\infty} dq \int_{-\infty}^{\infty} dq' e^{-iqz} qq'\sigma(q,q';\omega = i0^+)V(q') \;. \tag{4.26}$$

[3]Usually, the equation of continuity is formulated or for the particle current I_n and the particle density n or for the electric current $I = -eI_n$ and the current density $\rho = -en$. In this case the sign in front of both summands is the same. Here, in contrast, the equation of continuity relates the electric current to the particle density and therefore a factor $-e$ (which in atomic units reduces to -1) in front of the derivative $\partial_t N(z,t)$ has to be added.

The second summand of the equation of continuity (4.22) is rewritten as

$$\begin{aligned}
\partial_t N(z,t) &= \frac{\partial}{\partial t}\int_{-\infty}^{\infty} dt' \int_{-\infty}^{\infty} dz' P(z,z';t-t')V(z',t') \\
&= \int_{-\infty}^{\infty} dt' \int_{-\infty}^{\infty} dz' \frac{\partial}{\partial t} P(z,z';t-t')V(z')\Theta(t') \\
&= \int_{-\infty}^{t} dt' \int_{-\infty}^{\infty} dz' \frac{\partial}{\partial t'} P(z,z';t')V(z') \\
&= \int_{-\infty}^{t} dt' \frac{1}{4\pi^2} \int_{-\infty}^{\infty} dq \int_{-\infty}^{\infty} dq' e^{iqz} \frac{\partial}{\partial t'} P(q,q';t')V(q') \\
&= \frac{1}{4\pi^2} \int_{-\infty}^{t} dt' \int_{-\infty}^{\infty} dq \int_{-\infty}^{\infty} dq' e^{iqz} \frac{\partial}{\partial t'} \frac{1}{2\pi} \int_{-\infty}^{\infty} d\omega e^{-i\omega t'} P(q,q';\omega)V(q') \\
&= \frac{1}{4\pi^2} \int_{-\infty}^{t} dt' \int_{-\infty}^{\infty} dq \int_{-\infty}^{\infty} dq' e^{iqz} \frac{1}{2\pi} \int_{-\infty}^{\infty} d\omega (-i\omega) e^{-i\omega t'} P(q,q';\omega)V(q') \,,
\end{aligned} \tag{4.27}$$

where I have replaced the upper limit t of the integration over the variable t' with ∞. This replacement does not change the value of the integral, since $P(t-t') \propto \Theta(t-t')$. For the steady-state limit I obtain

$$\partial_t N(z) = \frac{1}{4\pi^2} \lim_{\alpha\to 0^+} \alpha \int_{-\infty}^{\infty} dq \int_{-\infty}^{\infty} dq' e^{iqz} P(q,q';i\alpha)V(q') \,. \tag{4.28}$$

Inserting this and the result obtained in eq. (4.26) in the continuity equation (4.22) one finds that

$$\sigma(q,q';i\alpha \to 0^+) = -\lim_{\alpha\to 0^+} \frac{\alpha}{qq'} P(q,q';i\alpha) \,. \tag{4.29}$$

In order to obtain the desired relation between the polarization function and the conductance, this result simply has to be inserted in eq. (4.19)

$$\Gamma = -\lim_{\alpha\to 0^+} \frac{\alpha}{4\pi^2} \int dq\, dq' \frac{P(q,q';i\alpha)}{qq'} \,. \tag{4.30}$$

It has to be stressed once more, that the irreducible polarization P includes exchange and correlation effects and calculates according to eq. (3.49). Hence, formula (4.30) is particularly suited to the treatment of a system of interacting electrons.

Irreducible polarization in reciprocal space In the special case of a system which is invariant under translations along the x, y directions, I can express the conductance in terms of the $\mathbf{k}_\parallel = \mathbf{0}$ component of the irreducible polarization transforming the effective one-dimensional irreducible polarization (or the conductivity, respectively) as defined in eq. (4.14) to reciprocal space. Regarding the time dependence, I will

switch to frequency space and obtain

$$\begin{aligned}
P(z,z';i\omega) &= \int\int dS P(\mathbf{r},\mathbf{r}';i\omega) dS' \\
&= \int d^2r'_\parallel \int d^2r_\parallel P(\mathbf{r}_\parallel - \mathbf{r}'_\parallel, z, z'; i\omega) \\
&= \int d^2r'_\parallel \int d^2r_\parallel \frac{1}{(2\pi)^2} \int d^2k_\parallel e^{i\mathbf{k}_\parallel \cdot (\mathbf{r}_\parallel - \mathbf{r}'_\parallel)} P(\mathbf{k}_\parallel, z, z'; i\omega) \\
&= \int d^2r'_\parallel \frac{1}{(2\pi)^2} \int d^2k_\parallel (2\pi)^2 \delta(\mathbf{k}_\parallel) e^{-i\mathbf{k}_\parallel \cdot \mathbf{r}_\parallel} P(\mathbf{k}_\parallel, z, z'; i\omega) \\
&= \int d^2r'_\parallel P(\mathbf{k}_\parallel = \mathbf{0}, z, z'; i\omega) \\
&= A P(\mathbf{k}_\parallel = \mathbf{0}, z, z'; i\omega)
\end{aligned} \tag{4.31}$$

and

$$\sigma(z,z';i\omega) = A\,\sigma(\mathbf{k}_\parallel = \mathbf{0}, z, z'; i\omega)\ , \tag{4.32}$$

respectively. The unit area $A = \int d^2r_\parallel$ is obtained with the help of the cross-sectional area of the Fermi sphere (in reciprocal space) of the homogeneous electron gas

$$A_{\text{reciprocal}} = \pi k_{\text{F}}^2 = 2\pi\mu\ . \tag{4.33}$$

This corresponds to the area

$$A = \frac{(2\pi)^2}{A_{\text{reciprocal}}} = \frac{2\pi}{\mu} \tag{4.34}$$

in direct space.
Inserting the result of eq. (4.31) in eq. (4.30) leads to the conductance of a system which is periodic in x and y directions

$$\begin{aligned}
\Gamma &= -A \lim_{\alpha\to 0^+} \frac{\alpha}{4\pi^2} \int dq \int dq' \frac{P(\mathbf{k}_\parallel = \mathbf{0}, q, q'; i\alpha)}{qq'} \\
&= -\lim_{\alpha\to 0^+} \frac{\alpha}{2\pi\mu} \int dq \int dq' \frac{P(\mathbf{k}_\parallel = \mathbf{0}, q, q'; i\alpha)}{qq'}\ .
\end{aligned} \tag{4.35}$$

This equation shows that only the irreducible polarization for $\mathbf{k}_\parallel = \mathbf{0}$ enters into the conductance. It is therefore sufficient to evaluate it for this special coordinate only.

Irreducible polarization in mixed representation For the numerical calculation of the conductance it is more convenient to evaluate it in real space according to

$$\Gamma = \frac{2\pi}{\mu} \lim_{\alpha\to 0^+} \alpha \int_0^\infty dz \int_{-\infty}^0 dz' P(\mathbf{k}_\parallel = \mathbf{0}, z, z'; i\alpha)\ . \tag{4.36}$$

In order to prove the equivalence of the expression on the right-hand side to eq. (4.35), the Fourier transformation of the Heaviside step function is required

$$\Theta(z) = \frac{1}{2\pi} \lim_{\eta \to 0} \int_{-\infty}^{\infty} dk \, \frac{i}{k + i\eta} e^{-ikz} \; . \tag{4.37}$$

I start from eq. (4.36) and calculate

$$\begin{aligned}
&\int_0^\infty dz \int_{-\infty}^0 dz' P(\mathbf{k}_\parallel = \mathbf{0}, z, z'; i\alpha) \\
&= \int_{-\infty}^\infty dz \int_{-\infty}^\infty dz' \Theta(z) P(\mathbf{k}_\parallel = \mathbf{0}, z, z'; i\alpha) \Theta(-z') \\
&= \frac{-1}{(2\pi)^4} \lim_{\eta \to 0} \lim_{\eta' \to 0} \int_{-\infty}^\infty dz \int_{-\infty}^\infty dz' \int_{-\infty}^\infty dq \int_{-\infty}^\infty dq' \int_{-\infty}^\infty dk \int_{-\infty}^\infty dk' \\
&\qquad \frac{e^{i(q-k)z}}{k + i\eta} P(\mathbf{k}_\parallel = \mathbf{0}, q, q'; i\alpha) \frac{e^{-i(q'-k')z'}}{k' + i\eta'} \\
&= \frac{-1}{(2\pi)^2} \lim_{\eta \to 0} \lim_{\eta' \to 0} \int_{-\infty}^\infty dq \int_{-\infty}^\infty dq' \int_{-\infty}^\infty dk \int_{-\infty}^\infty dk' \frac{\delta(q-k)}{k + i\eta} P(\mathbf{k}_\parallel = \mathbf{0}, q, q'; i\alpha) \frac{\delta(q'-k')}{k' + i\eta'} \\
&= \frac{-1}{(2\pi)^2} \lim_{\eta \to 0} \lim_{\eta' \to 0} \int_{-\infty}^\infty dq \int_{-\infty}^\infty dq' \frac{1}{q + i\eta} P(\mathbf{k}_\parallel = \mathbf{0}, q, q'; i\alpha) \frac{1}{q' + i\eta'} \\
&= \frac{-1}{(2\pi)^2} \int_{-\infty}^\infty dq \int_{-\infty}^\infty dq' \left[P(\frac{1}{q}) - 2\pi i \delta(q) \right] P(\mathbf{k}_\parallel = \mathbf{0}, q, q'; i\alpha) \left[P(\frac{1}{q'}) - 2\pi i \delta(q') \right] \\
&= \frac{-1}{4\pi^2} \int_{-\infty}^\infty dq \int_{-\infty}^\infty dq' \frac{1}{q} P(\mathbf{k}_\parallel = \mathbf{0}, q, q'; i\alpha) \frac{1}{q'} \; .
\end{aligned} \tag{4.38}$$

In the last step of the derivation I exploited the fact that $P(\mathbf{k}_\parallel = \mathbf{0}, 0, q'; i\alpha) = P(\mathbf{k}_\parallel = \mathbf{0}, q, 0; i\alpha) = 0$. Multiplication of the result with $\frac{2\pi\alpha}{\mu}$ in the limit $\alpha \to 0^+$ proves the asserted equivalence of eq. (4.35) and eq. (4.36).

4.2.3 Conductance of the homogeneous electron gas in the single-particle picture

I will now prove the validity of eq. (4.35) for the homogeneous electron gas in the non-interacting single-particle picture, showing that it yields the result of the Landauer formula for perfect transmission, i.e. $\Gamma = \frac{1}{\pi}$. In this case the exchange-correlation kernel f_{xc} is zero, and hence $P^{\mathrm{hom}}(\mathbf{k}_\parallel = \mathbf{0}, q, q'; i\alpha) = P_0^{\mathrm{hom}}(\mathbf{k}_\parallel = \mathbf{0}, q, q'; i\alpha)$ (compare eq. (3.49)). Due to the complete three-dimensional translational invariance, the polarization

$$P_0^{\mathrm{hom}}(\mathbf{k}_\parallel = \mathbf{0}, q, q'; i\alpha) = 2\pi\delta(q - q') P_0^{\mathrm{hom}}(q; i\alpha) \tag{4.39}$$

is diagonal in the wave vectors and thus the conductance simplifies to

$$\Gamma_0^{\mathrm{hom}} = - \lim_{\alpha \to 0^+} \frac{\alpha}{\mu} \int dq \frac{P_0^{\mathrm{hom}}(q; i\alpha)}{q^2} \; . \tag{4.40}$$

To simplify the integral I introduce dimensionless scaled variables $\tilde{q} = q/k_\mathrm{F}$ and $\omega = \alpha/k_\mathrm{F}^2$, obtaining

$$\Gamma_0^\mathrm{hom} = -\lim_{\omega\to 0^+} \frac{\omega k_\mathrm{F}}{\mu} \int d\tilde{q} \frac{P_0^\mathrm{hom}(\tilde{q}k_\mathrm{F}; i\omega k_\mathrm{F}^2)}{\tilde{q}^2} \,. \tag{4.41}$$

As the order of the operations is significant, the limit $\omega \to 0$ can only be taken after the integration. However, it is possible to overcome this problem by scaling the wave vectors simultaneously and substituting $x = \tilde{q}/\omega$:

$$\Gamma_0^\mathrm{hom} = -\lim_{\omega\to 0^+} \frac{k_\mathrm{F}}{\mu} \int dx \frac{P_0^\mathrm{hom}(x\omega k_\mathrm{F}; i\omega k_\mathrm{F}^2)}{x^2} = -\frac{k_\mathrm{F}}{\mu} \int dx \frac{1}{x^2} \lim_{\omega\to 0^+} P_0^\mathrm{hom}(x\omega k_\mathrm{F}; i\omega k_\mathrm{F}^2) \,. \tag{4.42}$$

The polarization function of the non-interacting electron gas is known analytically (see eq. (7.12)) and given by

$$\begin{aligned} P_0^\mathrm{hom}(x\omega k_\mathrm{F}; i\omega k_\mathrm{F}^2) = -\frac{k_\mathrm{F}}{2\pi^2} \Bigg(1 + \frac{1 + x^2 - \frac{1}{4}\omega^2 x^4}{2\omega x^3} \ln \frac{1 + (x + \frac{1}{2}\omega x^2)^2}{1 + (x - \frac{1}{2}\omega x^2)^2} \\ \frac{1}{x} \left[\arctan(x + \frac{1}{2}\omega x^2) - \arctan(x - \frac{1}{2}\omega x^2) \right] \Bigg) \,. \end{aligned} \tag{4.43}$$

in the notation used here. For further information see chapter 7. Apart from the factor k_F, the right-hand function is a universal function that does not depend on the density parameter. Only the limit

$$\lim_{\omega\to 0} P_0^\mathrm{hom}(x\omega k_\mathrm{F}; i\omega k_\mathrm{F}^2) = -\frac{k_\mathrm{F}}{\pi^2} \left(1 - \frac{\arctan x}{x} \right) \tag{4.44}$$

contributes to the conductance, which can be calculated analytically and yields

$$\Gamma_0^\mathrm{hom} = \frac{k_\mathrm{F}^2}{\pi^2 \mu} \int dx \frac{1}{x^2} \left(1 - \frac{\arctan x}{x} \right) = \frac{1}{\pi} \tag{4.45}$$

since $\mu = \frac{k_\mathrm{F}^2}{2}$. This equals the result of the Landauer formula. Hence, I have verified the validity of eq. (4.35) for the special case of the homogeneous electron gas in the single-particle picture.

4.2.4 Response to the applied external field

The polarization function $\tilde{P}(q; i\omega)$ which describes the linear response of the density to changes in the external field

$$\delta n(q;\omega) = \tilde{P}(q;\omega) \delta V_\mathrm{ext}(q;\omega) \tag{4.46}$$

is related to the irreducible polarization function $P(q;i\omega)$ according to

$$\tilde{P}(q;i\omega) = \frac{P(q;i\omega)}{1 - v(q)P(q;i\omega)} \,. \tag{4.47}$$

Thus, for the homogeneous electron gas the conductance describing the current with respect to the applied external field is given by

$$\Gamma^{\mathrm{hom}} = -\lim_{\omega\to 0^+} \frac{k_{\mathrm{F}}}{\mu} \int dx \frac{1}{x^2} \frac{P^{\mathrm{hom}}(x\omega k_{\mathrm{F}}; i\omega k_{\mathrm{F}}^2)}{1 - v(x\omega k_{\mathrm{F}}) P^{\mathrm{hom}}(x\omega k_{\mathrm{F}}; i\omega k_{\mathrm{F}}^2)} \,. \tag{4.48}$$

As $P^{\mathrm{hom}}(x\omega k_{\mathrm{F}}; i\omega k_{\mathrm{F}}^2)$ approaches a finite value for small ω while $v(x\omega k_{\mathrm{F}}) \propto \frac{1}{\omega^2}$ in the denominator diverges, the entire integrand is asymptotically proportional to ω^2 and hence vanishes in the limit $\omega \to 0$. Therefore, one invariably obtains $\Gamma^{\mathrm{hom}} = 0$.

5 Application of the Green-function embedding method to the investigated scattering setup

In this chapter the Green-function embedding technique is applied and tailored to the investigated scattering setup presented in figure 5.1. Because of its simplicity, some calculations can be done analytically.
After having introduced in some detail the setup under consideration, I will Fourier transform the defining equation for the embedded Green function (2.18) to reciprocal space with respect to the parallel coordinates. Afterwards, I calculate the embedding potentials. Finally, I introduce a basis set for the z dependence of the Green function and expand the Hamiltonian in this basis.

5.1 Investigated scattering setup

The system investigated in this thesis is presented schematically in figure 5.1. In two directions of space — the x and the y direction — the potential is chosen to be constant. In the third, the z direction, the space is divided into three regions: Two semi-infinite leads L and R, separated by a finite layer Ω. In this finite region, fixed between the two z coordinates z_{L} and z_{R}, a z dependent potential $V(z)$ is applied. Beyond this finite layer, the potential is set constant, but the potential on the left side V_{L} may differ from the potential on the right side V_{R}.

Although in principle the calculation of the Green function with the embedding method is possible for an arbitrary potential $V(z)$ with $V(z) \neq 0$ for $z \in [z_{\mathrm{L}}, z_{\mathrm{R}}]$, in this thesis only simple step potentials (i.e. quantum wells and potential barriers) will be investigated. For these simple, piecewise constant potentials the Green function can be easily calculated analytically[1]. This enables one to compare the results obtained with the Green-function embedding method to the analytical ones, and the quality of the method can be evaluated.
In detail, the systems investigated in this thesis are quantum wells and potential barriers with different values of the potential but the same width and the same chemical potential $\mu = 0.1$ Htr. They can be subsumed to

$$V(z) = \begin{cases} V & \text{if } -1 \leq z \leq 1 \\ 0 & \text{otherwise} \end{cases} \tag{5.1}$$

[1]For arbitrary potentials the Green function can be obtained by numerical integration. More details can be found in section 6.1.2.

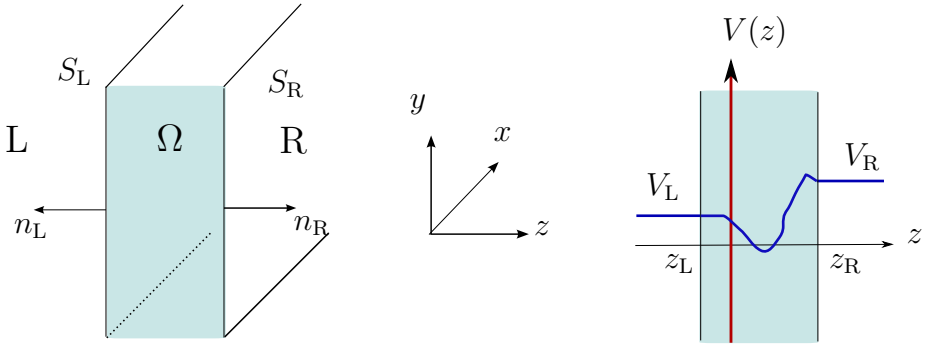

Figure 5.1: The geometry of the scattering setup investigated in this thesis. *Left:* The three-dimensional space is divided into two semi-infinite leads L and R separated by a finite layer Ω. This finite layer Ω, infinite in x and y directions and localized in $[z_\mathrm{L}, z_\mathrm{R}]$ in z direction represents the embedding region. The interfaces S_L and S_R between the embedding region and the leads are defined through $z = z_\mathrm{L}$ and $z = z_\mathrm{R}$. The vectors $n_\mathrm{L/R}$ are normal vectors on $S_\mathrm{L/R}$ pointing out of the embedding region Ω. *Right:* Projection on the xy plane: The Green function embedding method does not impose any restriction on the potential $V(z)$, $z \in [z_\mathrm{L}, z_\mathrm{R}]$. It can be an arbitrary potential, which even does not have to be continuous at z_L and z_R.

where the value of V varies between the two limiting cases $V = -0.1$ Htr and $V = 0.15$ Htr in steps of $\Delta V = 0.025$ Htr (i.e. $V = -0.1, -0.075, -0.05, \cdots, 0.1$, 0.125, 0.15 Htr). Thus, I consider the transition between a quantum well and a potential barrier, including the case $V = 0$ Htr of the homogeneous electron gas. The two setups with the largest positive and negative potentials are presented in figure 5.2.

Although such model systems might seem far away from a realistic physical situation, they comprehend and can reveal new physics. The first point to mention is that the homogeneous electron gas describes the physical situation of simple metals like aluminum quite well. Secondly, the chosen potentials are not far away from realistic setups. The potential barrier is a simple model for a thin film of vacuum or any isolating material sandwiched between two metals. On the other hand, the quantum well describes the physical situation of a material with a higher electron density embedded in two conducting materials.

Additionally, the parameters of the investigated setups are chosen in such a way that they have the same dimensions as in real metals. The chemical potential $\mu = 0.1$ Htr corresponds to the electron density $n = 3.02 \cdot 10^{-3}$ and the Wigner-Seitz radius[2] $r_\mathrm{s} = 4.29$, respectively. This value is comparable to characteristic values of real metals, for which the Wigner-Seitz radius is between $r_\mathrm{s} \approx 2$ and $r_\mathrm{s} \approx 5$.

The thickness of the potentials $d = 2$ Bohr is chosen in such a way that it has the

[2]The Wigner-Seitz radius is defined as the radius of one sphere which contains one particle. Since n denotes the number of particles per unit volume, it calculates according to $\frac{4\pi}{3} r_\mathrm{s}^3 = \frac{1}{n}$ (in 3D).

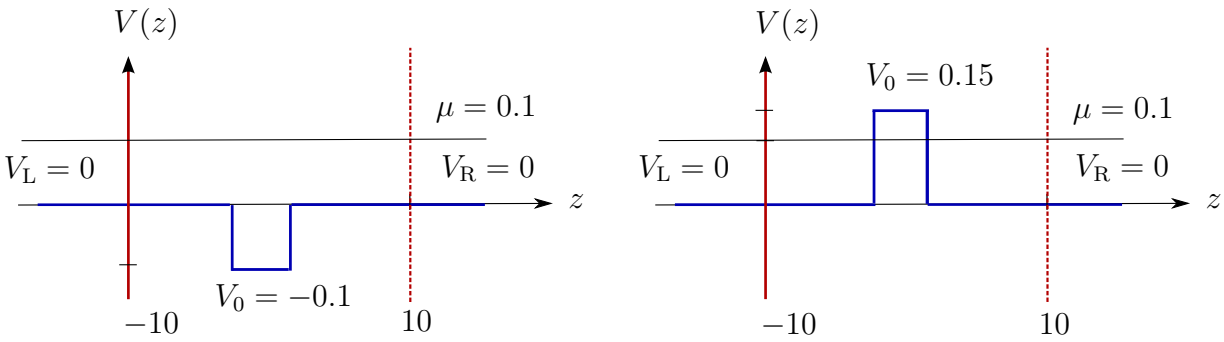

Figure 5.2: The quantum well (*left*) and the potential barrier (*right*) with the largest positive and negative values investigated in this thesis with $z_\mathrm{L} = -10$ and $z_\mathrm{R} = 10$. All quantities are given in atomic units (i.e. energies in Htr, lengths in Bohr).

same order of magnitude as atomic layers. For comparison, in the case of aluminum e.g. which crystallizes in the face-centered cubic structure with a lattice constant $a = 7.6$ Bohr, one atomic layer has a thickness of approximately 4.4 Bohr, since its unit cell has an extension $\frac{a}{\sqrt{3}}$ along the z direction. For simplicity, in the following all units will be omitted.

Considering the geometry of the investigated setups, the choice of the embedding region is quite obvious: It is a slab limited in the z direction by the interfaces S_L and S_R defined through $z = z_\mathrm{L}$ and $z = z_\mathrm{R}$. Although the potential varies in the interval $[-1, 1]$ only, the embedding region is chosen much larger, i.e. $z_\mathrm{L} = -10$ and $z_\mathrm{R} = 10$ (see figure 5.2) in order to evaluate the behavior of the Green function in the region close to the region where the potential $V \neq 0$. It has to be stressed, that this is not necessary for the embedding method – for the application of the embedding method, the choice $z_\mathrm{L} = -1$ and $z_\mathrm{R} = 1$ would be sufficient. In the x and y directions, the embedding region is infinite. Since in these directions the potential is constant, they can be treated partly analytically, whereas the z direction has to be treated numerically.
The geometry of the embedding region slightly differs from that of chapter 2. The outer volume V_0 of figure 2.1 is separated into two volumes L and R. Instead of one connected interface between the embedding region and the outer volume there are now two interfaces parallel to each other. Therefore I have to deal with two embedding potentials (one for each interface) which are independent and may differ from each other. The reason can be found in equation (2.14): Each embedding potential depends exclusively on the wave function, or alternatively the Green function, of its side of the outer volume. Since the constant potential V_L in L might be different from V_R in R, in this case the Green functions in L and R will be different as well.

5.2 Equation for the Green function in the embedding region

As explained in chapter 2, one should solve the equation for the Green function instead of that for the wave function because of the energy dependence of the embedding Hamiltonian. The equation which I have to solve is thus (2.18), rewritten here in more detail

$$\begin{aligned}&\frac{1}{2}\nabla^2 G\left(\mathbf{r},\mathbf{r}';\epsilon\right) - V\left(\mathbf{r}\right) G\left(\mathbf{r},\mathbf{r}';\epsilon\right) + \epsilon G\left(\mathbf{r},\mathbf{r}';\epsilon\right)\\ &-\frac{1}{2}\delta\left(n-n_S\right)\left(\frac{\partial G\left(\mathbf{r}_S,\mathbf{r}';\epsilon\right)}{\partial n_S} + 2\int_S d^2 r''_{\parallel}\sigma\left(\mathbf{r},\mathbf{r}''_S;\epsilon\right) G\left(\mathbf{r}''_S,\mathbf{r}';\epsilon\right)\right) = \delta\left(\mathbf{r}-\mathbf{r}'\right)\ . \quad (5.2)\end{aligned}$$

As the potential is constant in x and y directions, the Green function is invariant under translations in these two directions. As a consequence, it depends only on the difference of the x and y arguments, and I can combine the x and y coordinates to $\mathbf{r}_{\parallel} := (x-x', y-y')$, with $r_{\parallel}$ given by $r_{\parallel} = \sqrt{(x-x')^2+(y-y')^2}$.
Inserting this in eq. (5.2) leads to

$$\begin{aligned}&\frac{1}{2}\nabla^2 G\left(\mathbf{r}_{\parallel},z,z';\epsilon\right) - V\left(z\right) G\left(\mathbf{r}_{\parallel},z,z';\epsilon\right) + \epsilon G\left(\mathbf{r}_{\parallel},z,z';\epsilon\right)\\ &\quad-\frac{1}{2}\delta\left(n-n_S\right)\left(\frac{\partial G\left(\mathbf{r}_{\parallel},z,z';\epsilon\right)}{\partial n_S} + 2\int_S d^2 r''_{\parallel}\sigma\left(\mathbf{r}_{\parallel}-\mathbf{r}''_{\parallel},z,z''_S;\epsilon\right) G\left(\mathbf{r}''_{\parallel},z''_S,z';\epsilon\right)\right)\\ &\qquad\qquad = \delta\left(\mathbf{r}_{\parallel}\right)\delta\left(z-z'\right)\ . \quad (5.3)\end{aligned}$$

As presented in figure 5.1, the interfaces between the embedding region and the outer volume are infinite planes located at $z = z_{\mathrm{L}}$ and $z = z_{\mathrm{R}}$. The projections of the gradient onto the interface normals thus become derivatives in $-z$ and z direction, respectively. For the investigated setup, eq. (5.3) yields

$$\begin{aligned}&\frac{1}{2}\nabla^2 G\left(\mathbf{r}_{\parallel},z,z';\epsilon\right) - V\left(z\right) G\left(\mathbf{r}_{\parallel},z,z';\epsilon\right) + \epsilon G\left(\mathbf{r}_{\parallel},z,z';\epsilon\right)\\ &-\frac{1}{2}\delta\left(z-z_{\mathrm{L}}\right)\left(\frac{\partial G\left(\mathbf{r}_{\parallel},z,z';\epsilon\right)}{\partial(-z)} + 2\int_{z=z_{\mathrm{L}}} d^2 r''_{\parallel}\sigma_{\mathrm{L}}\left(\mathbf{r}_{\parallel}-\mathbf{r}''_{\parallel},z,z_{\mathrm{L}};\epsilon\right) G\left(\mathbf{r}''_{\parallel},z_{\mathrm{L}},z';\epsilon\right)\right)\\ &-\frac{1}{2}\delta\left(z-z_{\mathrm{R}}\right)\left(\frac{\partial G\left(\mathbf{r}_{\parallel},z,z';\epsilon\right)}{\partial(z)} + 2\int_{z=z_{\mathrm{R}}} d^2 r''_{\parallel}\sigma_{\mathrm{R}}\left(\mathbf{r}_{\parallel}-\mathbf{r}''_{\parallel},z,z_{\mathrm{R}};\epsilon\right) G\left(\mathbf{r}''_{\parallel},z_{\mathrm{R}},z';\epsilon\right)\right)\\ &\qquad\qquad = \delta\left(\mathbf{r}_{\parallel}\right)\delta\left(z-z'\right)\ . \quad (5.4)\end{aligned}$$

Two-dimensional Fourier transformation of the equation for the embedded Green function The aim of this section is to calculate the two-dimensional Fourier transform of (5.4) with respect to the parallel coordinates. I want to obtain a differential equation for $G(\mathbf{k}_{\parallel}, z, z';\epsilon)$ instead of $G(\mathbf{r}_{\parallel}, z, z';\epsilon)$, since the resulting equation is

much simpler than eq. (5.4). The two Green functions $G(\mathbf{k}_\parallel, z, z'; \epsilon)$ and $G(\mathbf{r}_\parallel, z, z'; \epsilon)$ are related through

$$G(\mathbf{r}_\parallel, z, z'; \epsilon) = \frac{1}{(2\pi)^2} \int d^2k_\parallel e^{i\mathbf{k}_\parallel \cdot \mathbf{r}_\parallel} G(\mathbf{k}_\parallel, z, z'; \epsilon) \; , \tag{5.5}$$

or

$$G(\mathbf{k}_\parallel, z, z'; \epsilon) = \int d^2r_\parallel e^{-i\mathbf{k}_\parallel \cdot \mathbf{r}_\parallel} G\left(\mathbf{r}_\parallel, z, z'; \epsilon\right) \; , \tag{5.6}$$

respectively. Therefore the Fourier transform of the terms of eq. (5.4) which do not depend on $\mathbf{r}_\parallel$ simply are

$$\int d^2r_\parallel e^{-i\mathbf{k}_\parallel \cdot \mathbf{r}_\parallel} \left(-V(z) + \epsilon\right) G\left(\mathbf{r}_\parallel, z, z'; \epsilon\right) = \left(-V(z) + \epsilon\right) G(\mathbf{k}_\parallel, z, z'; \epsilon) \; . \tag{5.7}$$

The two-dimensional Fourier transform of the first term of eq. (5.4) which contains the kinetic energy is obtained by replacing $G(\mathbf{r}_\parallel, z, z'; \epsilon)$ by its Fourier representation (eq. 5.5)

$$\begin{aligned}
& \int d^2r_\parallel \; e^{-i\mathbf{k}_\parallel \cdot \mathbf{r}_\parallel} \; \frac{1}{2} \nabla^2 G(\mathbf{r}_\parallel, z, z'; \epsilon) \qquad (5.8) \\
= & \int d^2r_\parallel \; e^{-i\mathbf{k}_\parallel \cdot \mathbf{r}_\parallel} \; \frac{1}{(2\pi)^2} \int d^2k'_\parallel \; \frac{1}{2} \left(\nabla^2_{\mathbf{r}_\parallel} + \nabla^2_z\right) e^{i\mathbf{k}'_\parallel \cdot \mathbf{r}_\parallel} G(\mathbf{k}'_\parallel, z, z'; \epsilon) \\
= & \int d^2r_\parallel \; e^{-i\mathbf{k}_\parallel \cdot \mathbf{r}_\parallel} \; \frac{1}{(2\pi)^2} \int d^2k'_\parallel \; \frac{1}{2} \left(-\mathbf{k}'^2_\parallel + \nabla^2_z\right) e^{i\mathbf{k}'_\parallel \cdot \mathbf{r}_\parallel} G(\mathbf{k}'_\parallel, z, z'; \epsilon) \\
= & \; \frac{1}{2} \left(-\mathbf{k}^2_\parallel + \nabla^2_z\right) G(\mathbf{k}_\parallel, z, z'; \epsilon) \; .
\end{aligned}$$

The remaining terms are the additional surface terms which contribute only in the case when the first of the two z arguments is located at an interface, i.e. $z = z_{\mathrm{L,R}}$. For each interface there are two terms. The Fourier transformation of the first of them does not pose any problem, because the derivative acts on the z component only

$$\int d^2r_\parallel \, e^{-i\mathbf{k}_\parallel \cdot \mathbf{r}_\parallel} \left(-\frac{1}{2}\delta\left(z - z_{\mathrm{L,R}}\right) \frac{\partial G\left(\mathbf{r}_\parallel, z, z'; \epsilon\right)}{\partial(\pm z)}\right) = -\frac{1}{2}\delta\left(z - z_{\mathrm{L,R}}\right) \frac{\partial G\left(\mathbf{k}_\parallel, z, z'; \epsilon\right)}{\partial(\pm z)} \; . \tag{5.9}$$

The second one is a convolution of the embedding potential with the Green function, which in Fourier space becomes a simple multiplication

$$-\delta(z-z_{\mathrm{L,R}})\int d^2r_\parallel\; e^{-i\mathbf{k}_\parallel\cdot\mathbf{r}_\parallel}\int d^2r''_\parallel\;\sigma_{\mathrm{L,R}}(\mathbf{r}_\parallel-\mathbf{r}''_\parallel,z,z_{\mathrm{L,R}};\epsilon)G(\mathbf{r}''_\parallel-\mathbf{r}'_\parallel,z_{\mathrm{L,R}},z';\epsilon) \tag{5.10}$$

$$\begin{aligned}
&= -\delta(z-z_{\mathrm{L,R}})\int d^2r_\parallel\int d^2r''_\parallel\; e^{-i\mathbf{k}_\parallel\cdot(\mathbf{r}_\parallel-\mathbf{r}'_\parallel)}\\
&\quad\frac{1}{(2\pi)^2}\int d^2k'_\parallel\; e^{i\mathbf{k}'_\parallel\cdot(\mathbf{r}_\parallel-\mathbf{r}''_\parallel)}\sigma_{\mathrm{L,R}}(\mathbf{k}'_\parallel,z_{\mathrm{L,R}},z_{\mathrm{L,R}};\epsilon)\frac{1}{(2\pi)^2}\int d^2k''_\parallel\; e^{i\mathbf{k}''_\parallel\cdot(\mathbf{r}''_\parallel-\mathbf{r}'_\parallel)}G(\mathbf{k}_\parallel,z_{\mathrm{L,R}},z';\epsilon)\\
&= -\delta(z-z_{\mathrm{L,R}})\sigma_{\mathrm{L,R}}(\mathbf{k}_\parallel,z_{\mathrm{L,R}},z_{\mathrm{L,R}})G(\mathbf{k}_\parallel,z_{\mathrm{L,R}},z';\epsilon)\;.
\end{aligned}$$

In the first step the Fourier representations of $\sigma_{\mathrm{L,R}}(\mathbf{r}_\parallel-\mathbf{r}''_\parallel,z,z_{\mathrm{L,R}};\epsilon)$ and $G(\mathbf{r}''_\parallel-\mathbf{r}'_\parallel,z_{\mathrm{L,R}},z';\epsilon)$ have been inserted. The unknown Fourier component of the embedding potential emerging in equation (5.10) will be calculated in the next section.
It is now possible to write down the Fourier transform of the whole equation

$$\begin{aligned}
\Bigg[-\frac{1}{2}k_\parallel^2+\frac{1}{2}\frac{\partial^2}{\partial z^2}+\epsilon-V(z)-\frac{1}{2}\delta(z-z_{\mathrm{L}})\left(\frac{\partial}{\partial\,(-z)}+2\sigma_{\mathrm{L}}(\mathbf{k}_\parallel,z_{\mathrm{L}},z_{\mathrm{L}};\epsilon)\right)\\
-\frac{1}{2}\delta(z-z_{\mathrm{R}})\left(\frac{\partial}{\partial\,(z)}+2\sigma_{\mathrm{R}}(\mathbf{k}_\parallel,z_{\mathrm{R}},z_{\mathrm{R}};\epsilon)\right)\Bigg]G(\mathbf{k}_\parallel,z,z';\epsilon)=\delta(z-z')\;.
\end{aligned} \tag{5.11}$$

In contrast to eq. (5.4) it is a one-dimensional equation in the z coordinate, where the three-dimensionality enters through the vector $\mathbf{k}_\parallel$ only.

5.3 The embedding potentials

In order to calculate the embedding potentials the solutions of the Schrödinger equations in the semi-infinite leads $V_{0,\mathrm{L}}$ and $V_{0,\mathrm{R}}$ are required. As the potential was supposed to be constant in the leads, $V(\mathbf{r})=V_{\mathrm{L}}$ on the left side for $z<z_{\mathrm{L}}$ and $V(\mathbf{r})=V_{\mathrm{R}}$ on the right side for $z>z_{\mathrm{R}}$, the wave functions are just plane waves.
At this point one can decide whether a retarded or an advanced Green function should be calculated. Incoming waves yield the embedding potential σ for advanced Green functions, thus $\psi(z)=e^{ik_zz}$, $k_z>0$ for $z<z_{\mathrm{L}}$ and $\psi(z)=e^{-ik_zz}$, $k_z>0$ for $z>z_{\mathrm{R}}$, whereas outgoing waves serve for the calculation of σ for retarded Green functions (with $\psi(z)=e^{-ik_zz}$, $k_z>0$ for $z<z_{\mathrm{L}}$ and $\psi(z)=e^{ik_zz}$, $k_z>0$ for $z>z_{\mathrm{R}}$). In the end a time-ordered Green function will be calculated. For energies with real part smaller than the chemical potential the time-ordered Green function equals the retarded one (incoming waves), for energies with bigger real part the advanced one (outgoing waves). The total wave function has to be multiplied by a plane wave in $\mathbf{r}_\parallel$ direction and results in

$$\psi(\mathbf{r})=e^{i\mathbf{k}\cdot\mathbf{r}}=e^{i\mathbf{k}_\parallel\cdot\mathbf{r}_\parallel\pm ik_zz}\;. \tag{5.12}$$

The sign of the exponent $ik_z z$ has to be chosen as explained above.
As derived in chapter 2, the embedding potential is defined by

$$\left.\frac{\partial\psi(\mathbf{r})}{\partial n_S}\right|_{\mathbf{r}=\mathbf{r}_S} = 2\int_S d^2r'_\parallel\,\sigma(\mathbf{r}_S,\mathbf{r}'_S;\epsilon)\psi(\mathbf{r}'_S)\;. \tag{5.13}$$

Exemplary, the calculation of the embedding potential of the left interface at $z = z_\mathrm{L}$ for a retarded Green function (incoming waves) will be shown. For this purpose the wave function (5.12) is inserted in equation (5.13)

$$\begin{aligned} -\left.\frac{\partial\psi(\mathbf{r})}{\partial z}\right|_{z=z_\mathrm{L}} &= -ik_z e^{i\mathbf{k}_\parallel\cdot\mathbf{r}_\parallel+ik_z z_\mathrm{L}} \\ &= 2\int_{z=z_\mathrm{L}} d^2r'_\parallel\,\sigma_\mathrm{L}\left(\mathbf{r}_\parallel-\mathbf{r}'_\parallel,z_\mathrm{L},z_\mathrm{L};\epsilon\right)e^{i\mathbf{k}_\parallel\cdot\mathbf{r}'_\parallel+ik_z z_\mathrm{L}}\;. \end{aligned} \tag{5.14}$$

Replacing $\sigma_\mathrm{L}(\mathbf{r}_\parallel-\mathbf{r}'_\parallel,z_\mathrm{L},z_\mathrm{L};\epsilon)$ by its Fourier transform

$$\sigma_\mathrm{L}(\mathbf{r}_\parallel-\mathbf{r}'_\parallel,z_\mathrm{L},z_\mathrm{L};\epsilon) = \frac{1}{(2\pi)^2}\int d^2k_\parallel\,e^{i\mathbf{k}_\parallel\cdot(\mathbf{r}_\parallel-\mathbf{r}'_\parallel)}\sigma(\mathbf{k}_\parallel,z_\mathrm{L},z_\mathrm{L};\epsilon) \tag{5.15}$$

leads to

$$-ik_z e^{i\mathbf{k}_\parallel\cdot\mathbf{r}_\parallel+ik_z z_\mathrm{L}} = 2\int_S d^2\,r'_\parallel\,\frac{1}{(2\pi)^2}\int d^2k'_\parallel\;e^{i\mathbf{k}'_\parallel\cdot(\mathbf{r}_\parallel-\mathbf{r}'_\parallel)}\sigma_\mathrm{L}(\mathbf{k}'_\parallel,z_\mathrm{L},z_\mathrm{L};\epsilon)e^{i\mathbf{k}_\parallel\cdot\mathbf{r}_\parallel+ik_z z_\mathrm{L}} \tag{5.16}$$

$$\begin{aligned} &= \frac{2}{(2\pi)^2}\int d^2k'_\parallel\;e^{i\mathbf{k}'_\parallel\cdot\mathbf{r}_\parallel}(2\pi)^2\delta(\mathbf{k}_\parallel-\mathbf{k}'_\parallel)\sigma_\mathrm{L}(\mathbf{k}'_\parallel,z_\mathrm{L},z_\mathrm{L};\epsilon)e^{ik_z z_\mathrm{L}} \\ &= 2\;\sigma_\mathrm{L}(\mathbf{k}_\parallel,z_\mathrm{L},z_\mathrm{L};\epsilon)e^{i\mathbf{k}_\parallel\cdot\mathbf{r}_\parallel+ik_z z_\mathrm{L}}\;. \end{aligned}$$

This yields

$$\sigma_\mathrm{L}(\mathbf{k}_\parallel,z_\mathrm{L},z_\mathrm{L};\epsilon) = -\frac{ik_z}{2}\;. \tag{5.17}$$

The z component of the wave vector can be expressed in terms of the energy, the constant potential V_L of the semi-infinite lead and the parallel component of the wave vector $\mathbf{k}_\parallel$

$$k_z = \sqrt{2\left(\epsilon-\frac{1}{2}\mathbf{k}_\parallel^2-V_\mathrm{L}\right)}\;. \tag{5.18}$$

Replacing k_z on the right side of equation (5.17) by the above relation results in

$$\sigma_{\mathrm{L,R}}(\mathbf{k}_\parallel,z_{\mathrm{L,R}},z_{\mathrm{L,R}};\epsilon) = -\frac{i}{2}\sqrt{2\left(\epsilon-\frac{1}{2}\mathbf{k}_\parallel^2-V_{\mathrm{L,R}}\right)}\;. \tag{5.19}$$

In this formula it is already anticipated, that the result for $\sigma_{\mathrm{R}}(\mathbf{k}_{\parallel}, z_{\mathrm{R}}, z_{\mathrm{R}}; \epsilon)$ is similar to that for $\sigma_{\mathrm{L}}(\mathbf{k}_{\parallel}, z_{\mathrm{L}}, z_{\mathrm{L}}; \epsilon)$. Even the sign of the two embedding potentials is the same, although the normal coordinate of the gradient points in the opposite direction (thus $-\frac{\partial\psi(\mathbf{r})}{\partial z}$ changes to $\frac{\partial\psi(\mathbf{r})}{\partial z}$). Indeed, the z component of the wave vector k_z changes its sign as well, in order to represent either an outgoing or an incoming wave from $-\infty$ as well as from ∞. The embedding potentials for an advanced Green function have the opposite signs of the retarded one: Since the sign of the wave function k_z changes (outgoing waves instead of incoming ones) the derivative in z direction yields the opposite sign.

5.4 Expanding the Green function in terms of plane waves

For an arbitrary potential $V(z)$ it is not possible to treat the z dependence of the Green function in the embedding region analytically. Therefore, the Green function is expanded in a convenient basis set. For the sake of simplicity the chosen basis set are plane waves

$$G(\mathbf{k}_{\parallel}, z, z'; \epsilon) = \sum_{k_z, k_z'} \frac{e^{ik_z z}}{\sqrt{d}} G_{k_z, k_z'}(\mathbf{k}_{\parallel}, \epsilon) \frac{e^{-ik_z' z'}}{\sqrt{d}} \tag{5.20}$$

or

$$G(\mathbf{r}_{\parallel}, z, z'; \epsilon) = \frac{1}{(2\pi)^2} \int d^2k_{\parallel}\, e^{i\mathbf{k}_{\parallel}\cdot\mathbf{r}_{\parallel}} \sum_{k_z, k_z'} \frac{e^{ik_z z}}{\sqrt{d}} G_{k_z, k_z'}(\mathbf{k}_{\parallel}, \epsilon) \frac{e^{-ik_z' z'}}{\sqrt{d}}\,. \tag{5.21}$$

The coefficients $G_{k_z,k_z'}(\mathbf{k}_{\parallel}, \epsilon)$ yielding the correct Green function have to be calculated numerically.
The variable d is a normalization constant which is chosen as the length of the embedding interval $d := z_{\mathrm{R}} - z_{\mathrm{L}}$. The wave vectors k_z are selected as $k_z = 2\pi n/\tilde{d}$ with $n \in [-N, N]$. The length $\tilde{d}$ is a numerical parameter which has to be larger than d, the length of the embedding interval. More details about this numerical parameter follow in chapter 5.6 about the numerical implementation. The task is now to derive a formula for the coefficients $G_{k_z,k_z'}(\mathbf{k}_{\parallel}, \epsilon)$.

5.5 Calculation of the embedding Hamiltonian

In order to calculate the expansion coefficients $G_{k_z,k_z'}(\mathbf{k}_{\parallel}, \epsilon)$ eq. (5.11) will be transformed to an equation depending on k_z, k_z' and $\mathbf{k}_{\parallel}$ instead of z, z' and $\mathbf{k}_{\parallel}$. It has to be emphasized that the coefficients do not equal the Fourier coefficients, since k_z and k_z' have to be chosen in such a way (with $k_z = 2\pi n/\tilde{d}$, $n \in [-N, N]$ with $\tilde{d} > d$) that the Green function $G(\mathbf{k}_{\parallel}, z, z'; \epsilon)$ is not periodic on the interval $[z_{\mathrm{L}}, z_{\mathrm{R}}]$ with

$z_\mathrm{R} - z_\mathrm{L} = d$. This is necessary in order that (in general different) boundary conditions at both sides might be fulfilled, i.e. that in general $G(\mathbf{k}_\parallel, z_\mathrm{L}, z') \neq G(\mathbf{k}_\parallel, z_\mathrm{R}, z')$ and $G(\mathbf{k}_\parallel, z, z_\mathrm{L}) \neq G(\mathbf{k}_\parallel, z, z_\mathrm{R})$ is valid. I choose the interval in which the basis is periodic as $[\tilde{z}_\mathrm{L}, \tilde{z}_\mathrm{R}]$ with $\tilde{z}_\mathrm{R} - \tilde{z}_\mathrm{L} = \tilde{d}$ and $[z_\mathrm{L}, z_\mathrm{R}] \subseteq [\tilde{z}_\mathrm{L}, \tilde{z}_\mathrm{R}]$. The periodicity on this interval will be used later for the treatment of the z dependent potential $V(z)$.
In the first step of the derivation, the expansion (5.20) of $G(\mathbf{k}_\parallel, z, z'; \epsilon)$ is inserted in equation (5.11). At the same time, the whole equation is multiplied by $e^{-ik_z z}$ and integrated over z on the interval $[z_\mathrm{L}, z_\mathrm{R}]$

$$\int_{z_\mathrm{L}}^{z_\mathrm{R}} dz\, e^{-ik_z z} \left[-\frac{1}{2}k_\parallel^2 + \frac{1}{2}\frac{\partial^2}{\partial z^2} + \epsilon - V(z) - \frac{1}{2}\delta(z - z_\mathrm{L}) \left(\frac{\partial}{\partial\,(-z)} + 2\sigma_\mathrm{L}(\mathbf{k}_\parallel, z_\mathrm{L}, z_\mathrm{L}; \epsilon) \right) \right.$$
$$\left. -\frac{1}{2}\delta(z - z_\mathrm{R}) \left(\frac{\partial}{\partial\,(z)} + 2\sigma_\mathrm{R}(\mathbf{k}_\parallel, z_\mathrm{R}, z_\mathrm{R}; \epsilon) \right) \right] \sum_{k_z'', k_z'} \frac{e^{ik_z'' z}}{\sqrt{d}} G_{k_z'', k_z'}(\mathbf{k}_\parallel, \epsilon) \frac{e^{-ik_z' z'}}{\sqrt{d}}$$
$$= \int_{z_\mathrm{L}}^{z_\mathrm{R}} dz\, e^{-ik_z z} \delta(z - z') \,. \quad (5.22)$$

Simplification of the right side yields

$$\int_{z_\mathrm{L}}^{z_\mathrm{R}} dz\, e^{-ik_z z} \delta(z - z') = e^{-ik_z z'} \,. \quad (5.23)$$

The only term on the left side of eq. (5.22) which could equal the z' dependence of the right side is the basis function $e^{-ik_z' z'}$. Therefore the only summand in the sum over k_z' which is allowed to contribute is $k_z' = k_z$, and equation (5.22) can be transformed to

$$\frac{1}{d} \sum_{k_z''} \int_{z_\mathrm{L}}^{z_\mathrm{R}} dz\, e^{-ik_z z} \left[-\frac{1}{2}k_\parallel^2 + \frac{1}{2}\frac{\partial^2}{\partial z^2} + \epsilon - V(z) - \frac{1}{2}\delta(z - z_\mathrm{L}) \left(\frac{\partial}{\partial\,(-z)} + 2\sigma_\mathrm{L}(\mathbf{k}_\parallel, z_\mathrm{L}, z_\mathrm{L}; \epsilon) \right) \right.$$
$$\left. -\frac{1}{2}\delta(z - z_\mathrm{R}) \left(\frac{\partial}{\partial\,(z)} + 2\sigma_\mathrm{R}(\mathbf{k}_\parallel, z_\mathrm{R}, z_\mathrm{R}; \epsilon) \right) \right] e^{ik_z'' z} G_{k_z'' k_z'}(\mathbf{k}_\parallel, \epsilon) = \delta_{k_z, k_z'} \,. \quad (5.24)$$

For the further calculation it is convenient to rewrite this equation as

$$\sum_{k_z''} \left(\epsilon S_{k_z k_z''}(\mathbf{k}_\parallel, \epsilon) - H_{k_z k_z''}(\mathbf{k}_\parallel, \epsilon) \right) G_{k_z'' k_z'}(\mathbf{k}_\parallel, \epsilon) = \delta_{k_z, k_z'} \,, \quad (5.25)$$

introducing the overlap matrix $S_{k_z k_z''}(\mathbf{k}_\parallel, \epsilon)$ defined as

$$S_{k_z k_z''}(\mathbf{k}_\parallel, \epsilon) = \frac{1}{d} \int_{z_\mathrm{L}}^{z_\mathrm{R}} dz\, e^{-ik_z z} e^{ik_z'' z} \quad (5.26)$$

and the embedding Hamiltonian

$$H_{k_z k_z''}(\mathbf{k}_\parallel, \epsilon)$$
$$= -\frac{1}{d} \int_{z_\mathrm{L}}^{z_\mathrm{R}} dz\, e^{-ik_z z} \left[-\frac{1}{2}k_\parallel^2 + \frac{1}{2}\frac{\partial^2}{\partial z^2} - V(z) - \frac{1}{2}\delta(z - z_\mathrm{L}) \left(\frac{\partial}{\partial\,(-z)} + 2\sigma_\mathrm{L}(\mathbf{k}_\parallel, z_\mathrm{L}, z_\mathrm{L}; \epsilon) \right) \right.$$
$$\left. -\frac{1}{2}\delta(z - z_\mathrm{R}) \left(\frac{\partial}{\partial\,(z)} + 2\sigma_\mathrm{R}(\mathbf{k}_\parallel, z_\mathrm{R}, z_\mathrm{R}; \epsilon) \right) \right] e^{ik_z'' z} \,. \quad (5.27)$$

The overlap matrix $S_{k_z k_z''}(\mathbf{k}_\parallel, \epsilon)$ yields

$$S_{k_z k_z''}(\mathbf{k}_\parallel, \epsilon) = \begin{cases} 1 & \text{for } k_z'' = k_z \\ \frac{1}{d}\frac{e^{i(k_z''-k_z)z_\mathrm{R}} - e^{i(k_z''-k_z)z_\mathrm{L}}}{i(k_z''-k_z)} & \text{else.} \end{cases} . \tag{5.28}$$

In order to simplify the embedding Hamiltonian in a first step all terms which contain derivatives in z direction are summed up

$$\begin{aligned} & -\frac{1}{2d}\int_{z_\mathrm{L}}^{z_\mathrm{R}} dz\, e^{-ik_z z}\left(\nabla_z^2 - \delta(z-z_\mathrm{L})\frac{\partial}{\partial(-z)} - \delta(z-z_\mathrm{R})\frac{\partial}{\partial z}\right) e^{ik_z'' z} \qquad (5.29) \\ = \;& \frac{1}{2d}\int_{z_\mathrm{L}}^{z_\mathrm{R}} dz\, \frac{\partial}{\partial z} e^{-ik_z z}\frac{\partial}{\partial z} e^{ik_z'' z} \\ = \;& \frac{1}{2d} k_z'' k_z \int_{z_\mathrm{L}}^{z_\mathrm{R}} dz\, e^{i(k_z''-k_z)z} \\ = \;& \frac{1}{2} k_z k_z'' S_{k_z k_z''}(\mathbf{k}_\parallel, \epsilon) \; . \end{aligned}$$

The integral over the z-dependent potential $V(z)$ is transformed to a Fourier transform. Therefore a modified potential $\tilde{V}(z)$ is defined on $[\tilde{z}_\mathrm{L}, \tilde{z}_\mathrm{R}]$

$$\tilde{V}(z) = V(z) \text{ for } z_\mathrm{L} \le z \le z_\mathrm{R} \text{ and 0 otherwise.} \tag{5.30}$$

With the help of $\tilde{V}(z)$ one obtains

$$\begin{aligned} \frac{1}{d}\int_{z_\mathrm{L}}^{z_\mathrm{R}} dz\, e^{-ik_z z} V(z) e^{ik_z'' z} &= \frac{1}{d}\int_{\tilde{z}_\mathrm{L}}^{\tilde{z}_\mathrm{R}} dz\, e^{-i(k_z - k_z'')z}\tilde{V}(z) \qquad (5.31) \\ &= \frac{\tilde{d}}{d} V(k_z - k_z''). \end{aligned}$$

The embedding Hamiltonian can be rewritten as

$$H_{k_z k_z''}(\mathbf{k}_\parallel, \epsilon) = \frac{1}{2}k_\parallel^2 + \frac{1}{2}k_z k_z'' + \frac{\tilde{d}}{d}V(0) + \frac{1}{d}\left[\sigma_\mathrm{L}(\mathbf{k}_\parallel, z_\mathrm{L}, z_\mathrm{L}; \epsilon) + \sigma_\mathrm{R}(\mathbf{k}_\parallel, z_\mathrm{R}, z_\mathrm{R}; \epsilon)\right] \tag{5.32}$$

for $k_z'' = k_z$ and

$$\begin{aligned} H_{k_z k_z''}(\mathbf{k}_\parallel, \epsilon) = \frac{1}{d}\Bigg[& \frac{e^{i(k_z''-k_z)z_\mathrm{R}} - e^{i(k_z''-k_z)z_\mathrm{L}}}{i(k_z''-k_z)}\left(\frac{1}{2}k_\parallel^2 + \frac{1}{2}k_z k_z''\right) + \tilde{d}\, V(k_z - k_z'') \qquad (5.33) \\ & + e^{i(k_z''-k_z)z_L}\sigma_\mathrm{L}(\mathbf{k}_\parallel, z_\mathrm{L}, z_\mathrm{L}; \epsilon) + e^{i(k_z''-k_z)z_\mathrm{R}}\sigma_\mathrm{R}(\mathbf{k}_\parallel, z_\mathrm{R}, z_\mathrm{R}; \epsilon)\Bigg] \end{aligned}$$

for $k_z'' \neq k_z$.
The coefficients $G_{k_z'' k_z'}(\mathbf{k}_\parallel, \epsilon)$ are calculated for each value of $\mathbf{k}_\parallel$ and ϵ separately. Therefore in a first step for each combination of them the matrix $\epsilon S(\mathbf{k}_\parallel, \epsilon) - H(\mathbf{k}_\parallel, \epsilon)$ has to be calculated. Then, according to eq. (5.25) this matrix will be inverted using a Lapack matrix inversion routine to obtain the coefficients $G_{k_z'' k_z'}(\mathbf{k}_\parallel, \epsilon)$ which are

the elements of the inverted matrix. The Green function $G(\mathbf{k}_\parallel, z, z'; \epsilon)$ is evaluated using eq. (5.20). Although the coefficients $G_{k''_z k'_z}(\mathbf{k}_\parallel, \epsilon)$ are only expansion coefficients and no Fourier coefficients, the summations in eq. (5.20) formally equal one-dimensional Fourier transformations. Therefore $G(\mathbf{k}_\parallel, z, z'; \epsilon)$ can be calculated using a Fast Fourier Transformation (FFT). Because of the special choice of $k_z = 2\pi n/\tilde{d}$, $n \in [-N, N]$, the Green function is obtained for $z, z' \in [\tilde{z}_\mathrm{L}, \tilde{z}_\mathrm{R}]$ with $\tilde{d} = \tilde{z}_\mathrm{R} - \tilde{z}_\mathrm{L}$, but it has only physical meaning for $z, z' \in [z_\mathrm{L}, z_\mathrm{R}]$.

5.6 Details of the implementation: The numerical parameters

The numerical calculation of the Green function $G(\mathbf{k}_\parallel, z, z'; \epsilon)$ depends on two numerical parameters:

- the number of basis functions – thus the number of wave vectors k_z – defined through N
- and the length $\tilde{d}$.

Since there are positive and negative $k_z = 2\pi n/\tilde{d}$, $n \in [-N, N]$, the number of basis functions calculates to $2N + 1$. The two numerical parameters have to be chosen carefully, because the accuracy of the calculation depends strongly on their choice. In addition, they are not independent from each other.
Let us start with the parameter $\tilde{d}$. It must be chosen bigger than the length of the embedding region d as illustrated in figure 5.3. The reason for that can be seen by

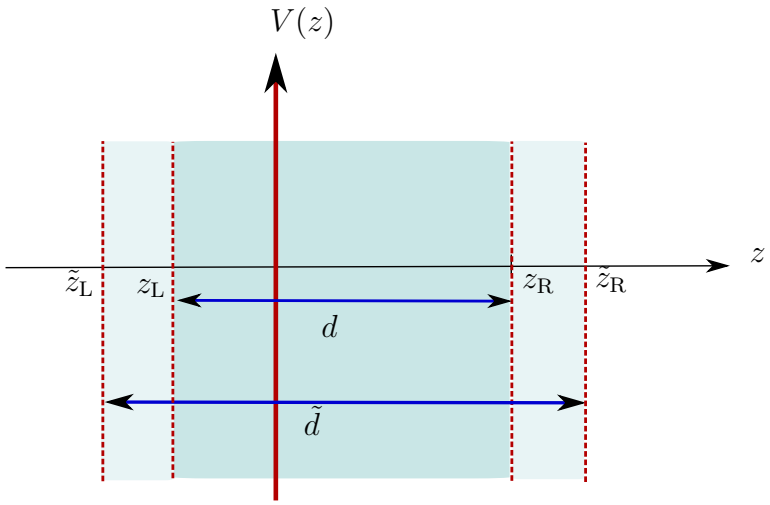

Figure 5.3: Illustration of the parameter $\tilde{d}$

having a look at the equations which define the Green function

$$(\epsilon - H_{\mathrm{emb}}(\mathbf{r}))\, G(\mathbf{r}, \mathbf{r}'; \epsilon) = \delta(\mathbf{r} - \mathbf{r}') \tag{5.34}$$

$$\sum_{k_z''} \left(\epsilon S_{k_z, k_z''} - H_{\mathrm{emb} k_z, k_z''}\left(\mathbf{k}_\parallel; \epsilon\right)\right) G_{k_z'', k_z'}(\mathbf{k}_\parallel, \epsilon) = \delta_{k_z, k_z'} \,. \tag{5.35}$$

At first glance they seem to be identical, but in fact they are not: The second equation (in Fourier space) includes periodic boundary conditions, since the basis functions in z direction are plane waves. If I chose $\tilde{d} = d$, the basis function $e^{ik_z z}$ with $k_z = 2\pi n/\tilde{d}$ with $n \in [-N, N]$ would be periodic with a period length d, and at both margins the value of the basis functions would be the same. In this case, I could not fulfill arbitrary boundary conditions different on each side, given by the embedding potentials. Choosing $\tilde{d}$ larger than d causes that the period of the basis functions is no longer d but $\tilde{d}$, and the basis function will have the same values at $\tilde{z}_\mathrm{L}$ and $\tilde{z}_\mathrm{R}$. At z_L and z_R the basis functions are free to fulfill the boundary conditions. In the intervals $[\tilde{z}_\mathrm{L}, z_\mathrm{L}]$ and $[z_\mathrm{R}, \tilde{z}_\mathrm{R}]$ the basis functions can 'close' the period. For that reason it is easy to understand that $\tilde{d}$ must not be chosen too small, because in this case the difference between d and $\tilde{d}$ is too small to ensure that arbitrary boundary conditions at z_L and z_R can be fulfilled. Additionally, the length of $\tilde{d}$ for a constant N must not be chosen too large either — increasing the value of $\tilde{d}$ entails the decrease of each wave vector k_z and thus the decrease of the maximal wave vector k_z as well. Fourier transforming the Green function back to direct space may be then not accurate because the Green function is not yet fallen to zero at maximal k_z.
For the number of wave vectors k_z there are constraints as well. Naturally, choosing N too small leads to an inaccuracy, because the number of basis functions is not enough to represent the function correctly. Furthermore, there is an upper limit for N, too. This can be explained in the following way. Using more basis function as necessary to fulfill the boundary conditions at z_L and z_R leads to an over-completeness of the basis. In this case, the overlap matrix becomes singular and the numerics fail. In other words, choosing N very large opens several possibilities to fulfill the boundary conditions and the basis representation is no longer unique. Thus, for values of N larger than a critical value N_c, the enhancement of N does not lead to a higher accuracy.
In practice, it turns out that for a given length d of the embedding region there is an optimal N and an optimal $\tilde{d}$. In order to find these optimal values for N and $\tilde{d}$ for a given d, the Green function for constant potential $V(z) = \text{const.} = V_\mathrm{L} = V_\mathrm{R}$ is calculated. This Green function equals the Green function for the homogeneous electron gas, which can be calculated analytically. The comparison of the numerical and the analytical result enables one on the one hand to check whether the method works well and whether the implementation is correct and on the other hand it serves as a tool to determine the optimal values of the two numerical parameters N and $\tilde{d}$. This is done in the next chapter.

6 Test of the Green-function embedding method

In the last chapter I have tailored the Green-function embedding method to the investigated setup and explained its numerical implementation. I will now check the method and its implementation. Therefore, in the first part of this chapter I will derive an analytical expression for the Green function of the homogeneous electron gas and of the quantum well/potential barrier which are investigated in this thesis. Since the potentials vary only in the z direction, I will start with the calculation of a one-dimensional Green function. Afterwards, the defining equation for the three-dimensional Green function $G(\mathbf{k}_\parallel, z, z'; \mu+i\omega)$ will be derived and its two-dimensional Fourier transform $G(\mathbf{r}_\parallel, z, z'; \mu + i\omega)$ will be calculated.
In the second part of this chapter, I will show and discuss the results obtained within the embedding method and compare them to the analytical ones.
In order to distinguish the Green function for an interacting system G from that for a non-interacting system without exchange and correlation effects, the latter is indexed with 0 from now on and hence written as G_0. The Green function for the homogeneous electron gas for the constant potential $V(z) = 0$ is denoted by G^{hom} or G_0^{hom}, respectively.

6.1 Analytical calculation of the Green function

6.1.1 Green function of the homogeneous electron gas

In reciprocal space, the Green function of the free electron gas for complex energies ϵ is given by

$$G_0^{\text{hom}}(\mathbf{k}_\parallel, k_z; \epsilon) = \frac{1}{\epsilon - \frac{1}{2}k_\parallel^2 - \frac{1}{2}k_z^2} \; . \tag{6.1}$$

Fourier transforming this term with respect to the z coordinate yields the representation of G as a function of $z - z'$ and $\mathbf{k}_\parallel$

$$\begin{aligned} G_0^{\mathrm{hom}}(\mathbf{k}_\parallel, z-z'; \epsilon) &= \frac{1}{2\pi}\int_{-\infty}^{\infty} dk_z\, e^{ik_z(z-z')} G_0^{\mathrm{hom}}(\mathbf{k}_\parallel, k_z, \epsilon) \\ &= \frac{1}{2\pi}\int_{-\infty}^{\infty} dk_z\, e^{ik_z(z-z')} \frac{1}{\epsilon - \frac{1}{2}k_\parallel^2 - \frac{1}{2}k_z^2} \\ &= -\frac{1}{\pi}\int_{-\infty}^{\infty} dk_z\, e^{ik_z(z-z')} \frac{1}{k_\parallel^2 + k_z^2 - 2\epsilon} \\ &= -\frac{1}{\pi}\int_{-\infty}^{\infty} dk_z\, e^{ik_z(z-z')} \frac{1}{\left(k_z - \sqrt{2\epsilon - k_\parallel^2}\right)\left(k_z + \sqrt{2\epsilon - k_\parallel^2}\right)} \,. \end{aligned} \tag{6.2}$$

The integral can be evaluated using complex analysis by closing the integral contour in the complex upper (or lower) half plane with the radius of the semicircle going to infinity. This is valid because the contribution of the upper (or lower, respectively) semicircle decays to zero if $z - z' > 0$ (or $z - z' < 0$) and thus can be added without any consequences.
For $z - z' > 0$, the function

$$e^{ik_z(z-z')} \frac{1}{\left(k_z - \sqrt{2\epsilon - k_\parallel^2}\right)\left(k_z + \sqrt{2\epsilon - k_\parallel^2}\right)} \tag{6.3}$$

has a pole in the upper half-plane at $k_z = \sqrt{2\epsilon - k_\parallel^2}$ if the imaginary part of $\sqrt{2\epsilon - k_\parallel^2}$ is positive. Since $k_\parallel^2$ is real, the condition $\mathrm{Im}\sqrt{2\epsilon - k_\parallel^2} > 0$ is equivalent to $\mathrm{Im}\,\epsilon > 0$. The integral becomes

$$G_0^{\mathrm{hom}}(\mathbf{k}_\parallel, z-z'; \epsilon) = -\frac{1}{\pi} 2\pi i \frac{e^{i\sqrt{2\epsilon - k_\parallel^2}(z-z')}}{2\sqrt{2\epsilon - k_\parallel^2}} \,. \tag{6.4}$$

If the imaginary part of $\sqrt{2\epsilon - k_\parallel^2}$ is negative, it is the other factor in the denominator which produces a pole in the upper half-plane, thus the integral yields

$$G_0^{\mathrm{hom}}(\mathbf{k}_\parallel, z-z'; \epsilon) = -\frac{1}{\pi} 2\pi i \frac{e^{-i\sqrt{2\epsilon - k_\parallel^2}(z-z')}}{-2\sqrt{2\epsilon - k_\parallel^2}} \,. \tag{6.5}$$

As already mentioned above, for z coordinates $z - z' < 0$ the integral has to be closed in the lower half-plane, so that the integral over the lower semicircle decays to zero in infinity. Equivalent to the calculations above, it has to be distinguished whether the imaginary part of $\sqrt{2\epsilon - k_\parallel^2}$ is positive or negative. If $\mathrm{Im}\sqrt{2\epsilon - k_\parallel^2} > 0$, the enclosed

pole is at $k_z = -\sqrt{2\epsilon - k_\parallel^2}$ and thus the Green function becomes

$$G_0^{\rm hom}(\mathbf{k}_\parallel, z-z';\epsilon) \;=\; -\frac{1}{\pi}\,(-2\pi i)\,\frac{e^{-i\sqrt{2\epsilon-k_\parallel^2}(z-z')}}{-2\sqrt{2\epsilon-k_\parallel^2}}\;. \tag{6.6}$$

For the second case, the relevant pole is $k_z = \sqrt{2\epsilon - k_\parallel^2}$ and thus

$$G_0^{\rm hom}(\mathbf{k}_\parallel, z-z';\epsilon) \;=\; -\frac{1}{\pi}\,(-2\pi i)\,\frac{e^{i\sqrt{2\epsilon-k_\parallel^2}(z-z')}}{2\sqrt{2\epsilon-k_\parallel^2}}\;. \tag{6.7}$$

We can now subsume the four cases in one formula

$$\begin{aligned} G_0^{\rm hom}(\mathbf{k}_\parallel, z-z';\epsilon) \;&=\; -i\;\mathrm{sgn}\left(\mathrm{Im}\,\sqrt{2\epsilon-k_\parallel^2}\right)\frac{e^{i\,\mathrm{sgn}\left(\mathrm{Im}\,\sqrt{2\epsilon-k_\parallel^2}\right)\sqrt{2\epsilon-k_\parallel^2}|z-z'|}}{\sqrt{2\epsilon-k_\parallel^2}} \\ &=\; \frac{e^{\mathrm{sgn}(\mathrm{Im}\,\epsilon)i\sqrt{2\epsilon-k_\parallel^2}|z-z'|}}{\mathrm{sgn}\,(\mathrm{Im}\,\epsilon)\,i\sqrt{2\epsilon-k_\parallel^2}}\;. \end{aligned} \tag{6.8}$$

The representation of the Green function $G_0^{\rm hom}$ as a function of z and $\mathbf{r}_\parallel$ can be calculated similarly, Fourier transforming $G_0^{\rm hom}(\mathbf{k}_\parallel, k_z;\epsilon)$ just in three dimensions. The result is

$$G_0^{\rm hom}(\mathbf{r}_\parallel, z, z';\epsilon) \;=\; -\frac{1}{2\pi}\frac{e^{\mathrm{sgn}(\mathrm{Im}\,\epsilon)i\sqrt{2\epsilon}\sqrt{r_\parallel^2+(z-z')^2}}}{\sqrt{r_\parallel^2+(z-z')^2}}\;. \tag{6.9}$$

6.1.2 One-dimensional Green function

The aim of this section is to calculate the one-dimensional Green function $G_0(z, z';\epsilon)$ for the one-dimensional problem

$$\left[\epsilon - \left(-\frac{1}{2}\frac{d^2}{dz^2} + V(z)\right)\right] G_0(z, z';\epsilon) = \delta(z-z')\;, \tag{6.10}$$

where the potential $V(z)$ is given by

$$V(z) = \begin{cases} V_{\rm L} & z < z_{\rm L} \\ \text{arbitrary} & z \in [z_{\rm L}, z_{\rm R}] \\ V_{\rm R} & z > z_{\rm R} \end{cases} \tag{6.11}$$

with constant $V_{\rm L}$ and $V_{\rm R}$. The energy ϵ is situated in the upper part of the complex plane, i.e. $\mathrm{Im}\,\epsilon > 0$. The Green function for energies with $\mathrm{Im}\,\epsilon < 0$ is obtained via the

relation $G_0(\mathbf{r},\mathbf{r}';\epsilon^*) = G_0^*(\mathbf{r},\mathbf{r}';\epsilon)$, which directly follows from the Lehmann representation of the Green function (see eq. (3.21)) and the property $G_0(\mathbf{r}',\mathbf{r};\epsilon) = G_0(\mathbf{r},\mathbf{r}';\epsilon)$. In addition to eq. (6.10), the Green function must also satisfy the asymptotic boundary condition $\lim_{|z|\to\infty} G_0(z,z';\epsilon) = 0$, which guarantees that any derived wave functions are square-integrable and thus lead to finite expectation values.
For the formal construction of the Green function I use the eigenfunctions of the Hamiltonian $\phi(z,\epsilon)$ that belong to the same given complex frequency ϵ and hence obey

$$\left[\epsilon - \left(-\frac{1}{2}\frac{d^2}{dz^2} + V(z)\right)\right]\phi(z,\epsilon) = 0\ . \tag{6.12}$$

This equation has, in general, many solutions. To satisfy the boundary conditions I select two particular solutions $\phi_\pm(z,\epsilon)$ with $\lim_{z\to\pm\infty}\phi_\pm(z,\epsilon) = 0$. The Green function is then given by

$$G_0(z,z';\epsilon) = 2\frac{\phi_-(z,\epsilon)\phi_+(z',\epsilon)\theta(z'-z) + \phi_+(z,\epsilon)\phi_-(z',\epsilon)\theta(z-z')}{W(\epsilon)}\ , \tag{6.13}$$

where $W(\epsilon)$ denotes the Wronskian

$$W(\epsilon) = \phi_-(z,\epsilon)\frac{d\phi_+(z,\epsilon)}{dz} - \frac{d\phi_-(z,\epsilon)}{dz}\phi_+(z,\epsilon)\ . \tag{6.14}$$

Green function of the potential barrier/quantum well We will now apply this formalism to a piecewise constant potential, in particular to the potential barrier/quantum well illustrated in figure 5.2 with $V(z) = V_0$ for $a > z > b$ and $V(z) = 0$ otherwise (i.e. $V_\mathrm{L} = V_\mathrm{R} = 0$). In each of the three regions the solutions of the Schrödinger equation are (damped) plane waves; the total wave functions are constructed by matching these piecewise solutions

$$\phi(z,\epsilon) = \begin{cases} Ae^{i\sqrt{2\epsilon}z} + Be^{-i\sqrt{2\epsilon}z} & \text{if} \quad z \le a \\ Ce^{i\sqrt{2(\epsilon-V_0)}z} + De^{-i\sqrt{2(\epsilon-V_0)}z} & \text{if} \quad a \le z \le b \\ Ee^{i\sqrt{2\epsilon}z} + Fe^{-i\sqrt{2\epsilon}z} & \text{if} \quad z \ge b \end{cases} \tag{6.15}$$

and ensuring that the wave functions as well as their derivatives are continuous at the boundaries of the regions.
As ϵ lies in the upper part of the complex frequency plane, the imaginary part of the complex root is positive and $\sqrt{2\epsilon} > 0$. The particular solution that goes to zero for large negative z is given by $\phi_-(z,\epsilon) = e^{-i\sqrt{2\epsilon}z}$ for $z \le a$; the coefficients C_-, D_-, E_- and F_- in the other regions are then determined by the four continuity equations at the boundaries of the region. The particular solution that goes to zero for large positive z is given by $\phi_+(z,\epsilon) = e^{i\sqrt{2\epsilon}z}$ for $z \ge b$, while the coefficients A_+, B_+, C_+ and D_+ again follow from the continuity conditions. All the resulting equations can

in fact be solved explicitly and yield the formulas

$$C_- = \frac{1}{2}\left(1 - \frac{\sqrt{\epsilon}}{\sqrt{\epsilon - V_0}}\right)\frac{e^{-i\sqrt{2\epsilon}a}}{e^{i\sqrt{2(\epsilon-V_0)}a}} \tag{6.16}$$

$$D_- = \frac{1}{2}\left(1 + \frac{\sqrt{\epsilon}}{\sqrt{\epsilon - V_0}}\right)\frac{e^{-i\sqrt{2\epsilon}a}}{e^{-i\sqrt{2(\epsilon-V_0)}a}} \tag{6.17}$$

$$E_- = \frac{1}{2}\left[\left(1 + \frac{\sqrt{\epsilon - V_0}}{\sqrt{\epsilon}}\right)C_-\frac{e^{i\sqrt{2(\epsilon-V_0)}b}}{e^{i\sqrt{2\epsilon}b}} + \left(1 - \frac{\sqrt{\epsilon - V_0}}{\sqrt{\epsilon}}\right)D_-\frac{e^{-i\sqrt{2(\epsilon-V_0)}b}}{e^{i\sqrt{2\epsilon}b}}\right] \tag{6.18}$$

$$F_- = \frac{1}{2}\left[\left(1 - \frac{\sqrt{\epsilon - V_0}}{\sqrt{\epsilon}}\right)C_-\frac{e^{i\sqrt{2(\epsilon-V_0)}b}}{e^{-i\sqrt{2\epsilon}b}} + \left(1 + \frac{\sqrt{\epsilon - V_0}}{\sqrt{\epsilon}}\right)D_-\frac{e^{-i\sqrt{2(\epsilon-V_0)}b}}{e^{-i\sqrt{2\epsilon}b}}\right] \tag{6.19}$$

as well as

$$A_+ = \frac{1}{2}\left[\left(1 + \frac{\sqrt{\epsilon - V_0}}{\sqrt{\epsilon}}\right)C_+\frac{e^{i\sqrt{2(\epsilon-V_0)}a}}{e^{i\sqrt{2\epsilon}a}} + \left(1 - \frac{\sqrt{\epsilon - V_0}}{\sqrt{\epsilon}}\right)D_+\frac{e^{-i\sqrt{2(\epsilon-V_0)}a}}{e^{i\sqrt{2\epsilon}a}}\right] \tag{6.20}$$

$$B_+ = \frac{1}{2}\left[\left(1 - \frac{\sqrt{\epsilon - V_0}}{\sqrt{\epsilon}}\right)C_+\frac{e^{i\sqrt{2(\epsilon-V_0)}a}}{e^{-i\sqrt{2\epsilon}a}} + \left(1 + \frac{\sqrt{\epsilon - V_0}}{\sqrt{\epsilon}}\right)D_+\frac{e^{-i\sqrt{2(\epsilon-V_0)}a}}{e^{-i\sqrt{2\epsilon}a}}\right] \tag{6.21}$$

$$C_+ = \frac{1}{2}\left(1 + \frac{\sqrt{\epsilon}}{\sqrt{\epsilon - V_0}}\right)\frac{e^{i\sqrt{2\epsilon}b}}{e^{i\sqrt{2(\epsilon-V_0)}b}} \tag{6.22}$$

$$D_+ = \frac{1}{2}\left(1 - \frac{\sqrt{\epsilon}}{\sqrt{\epsilon - V_0}}\right)\frac{e^{i\sqrt{2\epsilon}b}}{e^{-i\sqrt{2(\epsilon-V_0)}b}} \tag{6.23}$$

The Wronskian does not vary along the z axis and can hence be calculated once at a convenient location, for example in the central scattering region. The result

$$W(\epsilon) = \frac{i\sqrt{\epsilon - V_0}}{\sqrt{2}}\left[\left(1 + \frac{\sqrt{\epsilon}}{\sqrt{\epsilon - V_0}}\right)^2\frac{e^{i\sqrt{2\epsilon}(b-a)}}{e^{i\sqrt{2(\epsilon-V_0)}(b-a)}} - \left(1 - \frac{\sqrt{\epsilon}}{\sqrt{\epsilon - V_0}}\right)^2\frac{e^{i\sqrt{2\epsilon}(b-a)}}{e^{-i\sqrt{2(\epsilon-V_0)}(b-a)}}\right] \tag{6.24}$$

reduces to $W(\epsilon) = 2i\sqrt{2\epsilon}$ in the homogeneous limit $V_0 = 0$. In this limit, the coefficients C_-, E_-, B_+ and D_+ becomes 0 and the remaining coefficients D_-, F_-, A_+ and C_- simplify to 1. Therefore the wave functions reduce to the two solutions

$$\phi_\pm(z, \epsilon) = e^{\pm i\sqrt{2\epsilon}z} \, . \tag{6.25}$$

Inserting the simplified wave functions and the Wronskian into eq. (6.13) yields

$$G_0(z,z';\epsilon) = 2\frac{e^{-i\sqrt{2\epsilon}z}e^{i\sqrt{2\epsilon}z'}\theta(z'-z) + e^{i\sqrt{2\epsilon}z}e^{-i\sqrt{2\epsilon}z'}\theta(z-z')}{2i\sqrt{2\epsilon}} = \frac{e^{i\sqrt{2\epsilon}|z-z'|}}{i\sqrt{2\epsilon}} \tag{6.26}$$

which equals the result eq. (6.8) with $\operatorname{Im}\epsilon > 0$ and $\mathbf{k}_\parallel = 0$ calculated in the previous section.

Arbitrary potentials If the potential is not piecewise constant, the procedure discussed here can still be used, but it is necessary to integrate the Schrödinger equation numerically to obtain the wave functions $\phi_-(z,\epsilon)$ for $z < a$ and $\phi_+(z,\epsilon)$ for $z < b$.

6.1.3 Relation between the one-dimensional and the three-dimensional Green function

Transformation of $G_0(z,z';\epsilon)$ to $G_0(\mathbf{k}_\parallel,z,z';\epsilon)$ In the previous section the one-dimensional Green function $G_0(z,z';\epsilon)$ was calculated. Here, I will generalize it to a Green function for a three-dimensional system with a potential $V(z)$, which varies only in the z direction and corresponds to the potential described in the last section. The defining equation for the Green function of the three-dimensional system can be written as

$$\left[\epsilon - \left(-\frac{1}{2}\left(\nabla^2_{\mathbf{r}_\parallel} + \frac{d^2}{dz^2}\right) + V(z)\right)\right] G_0(\mathbf{r}_\parallel,z,z';\epsilon) = \delta(\mathbf{r}_\parallel)\delta(z-z') \; . \tag{6.27}$$

Compared to eq. (6.10), it contains only one additional term $-\frac{1}{2}\nabla^2_{\mathbf{r}_\parallel}$, corresponding to the kinetic energy for the additional degrees of freedom. The Hamiltonian is separable in the $\mathbf{r}_\parallel$ and z directions. The Fourier transformation of eq. (6.27) leads to

$$\left[\epsilon - \frac{1}{2}k_\parallel^2 - \left(-\frac{1}{2}\frac{d^2}{dz^2} + V(z)\right)\right] G_0(\mathbf{k}_\parallel,z,z';\epsilon) = \delta(z-z') \; . \tag{6.28}$$

This equation equals eq. (6.10) with a reduced energy $\tilde{\epsilon} = \epsilon - \frac{1}{2}k_\parallel^2$. Therefore the three-dimensional Green function $G_0(\mathbf{k}_\parallel,z,z';\epsilon)$ equals the one-dimensional Green function $G_0(z,z';\tilde{\epsilon})$.

Two-dimensional Fourier transformation of $G_0(\mathbf{k}_\parallel,z,z';\epsilon)$ to $G_0(\mathbf{r}_\parallel,z,z';\epsilon)$ In order to obtain the three-dimensional Green function in real space, $G_0(\mathbf{k}_\parallel,z,z';\epsilon)$ has to be Fourier transformed in two directions. This two-dimensional Fourier transformation can be partly performed analytically, since the Green function depends only on the absolute value of $\mathbf{k}_\parallel$, i.e. $k_\parallel^2$. Therefore, $G_0(\mathbf{r}_\parallel,z,z';\epsilon)$ may be simplified

according to

$$\begin{aligned} G_0(\mathbf{r}_\parallel, z, z'; \epsilon) &= \frac{1}{(2\pi)^2} \int_{-\infty}^{\infty} d^2k_\parallel \, e^{i\mathbf{k}_\parallel \cdot \mathbf{r}_\parallel} G_0(\mathbf{k}_\parallel, z, z'; \epsilon) \\ &= \frac{1}{(2\pi)^2} \int_0^{\infty} k_\parallel dk_\parallel \, G_0(k_\parallel, z, z'; \epsilon) \int_0^{2\pi} d\phi \, e^{ik_\parallel r_\parallel \cos\phi} \\ &= \frac{1}{2\pi} \int_0^{\infty} k_\parallel dk_\parallel \, G_0(k_\parallel, z, z'; \epsilon) J_0(k_\parallel r_\parallel) \, , \end{aligned} \tag{6.29}$$

where $J_0(k_\parallel r_\parallel)$ is the Bessel function of zeroth order. The remaining integral has to be calculated numerically. For the numerical calculation Simpson's rule is used, which is based on a quadratic interpolation of the integrand. The Green function results in

$$\begin{aligned} G_0(\mathbf{r}_\parallel, z, z'; \epsilon) \approx \frac{1}{2\pi} \frac{\Delta k_\parallel}{3} \Bigg[& 2 \sum_{j=1}^{\frac{n_{k_\parallel \max}}{2}-1} (2j\Delta k_\parallel) G_0(2j\Delta k_\parallel, z, z'; \epsilon) J_0(2j\Delta k_\parallel r_\parallel) \\ & + 4 \sum_{j=0}^{\frac{n_{k_\parallel \max}}{2}-1} ((2j+1)\Delta k_\parallel) G_0((2j+1)\Delta k_\parallel, z, z'; \epsilon) J_0((2j+1)\Delta k_\parallel r_\parallel) \\ & + k_{\parallel \max} G_0(k_{\parallel \max}, z, z'; \epsilon) J_0(k_{\parallel \max} r_\parallel) \Big] \end{aligned} \tag{6.30}$$

with $k_{\parallel \max} = n_{k_\parallel \max} \Delta k_\parallel$, $n_{k_\parallel \max}$ even.
$\Delta k_\parallel$ and $k_{\parallel \max}$ (or $n_{k_\parallel \max}$, respectively,) are numerical parameters, which have to be chosen such that the sum converges. Their numerical values chosen for the calculations in this thesis will be presented in section 6.2.3.

6.2 Determination of the numerical convergence parameters

6.2.1 Comparison to the Green function of the homogeneous electron gas

The comparison of the three-dimensional Green function $G_0(\mathbf{k}_\parallel, z, z'; \epsilon) = G_0(z, z'; \epsilon - \frac{1}{2}k_\parallel^2)$ for constant potential $V(z) = 0$ and energies $\epsilon + i\delta$, where $\delta > 0$ and infinitesimally small, with the analytical result

$$G_0^{\text{hom}}(\mathbf{k}_\parallel, z, z'; \epsilon) = \frac{e^{i\sqrt{2\epsilon - \mathbf{k}_\parallel^2}|z-z'|}}{i\sqrt{2\epsilon - \mathbf{k}_\parallel^2}}$$

for the homogeneous electron gas derived in section 6.1.1 serves as a first check of the embedding method. Additionally, it enables one to determine the two numerical

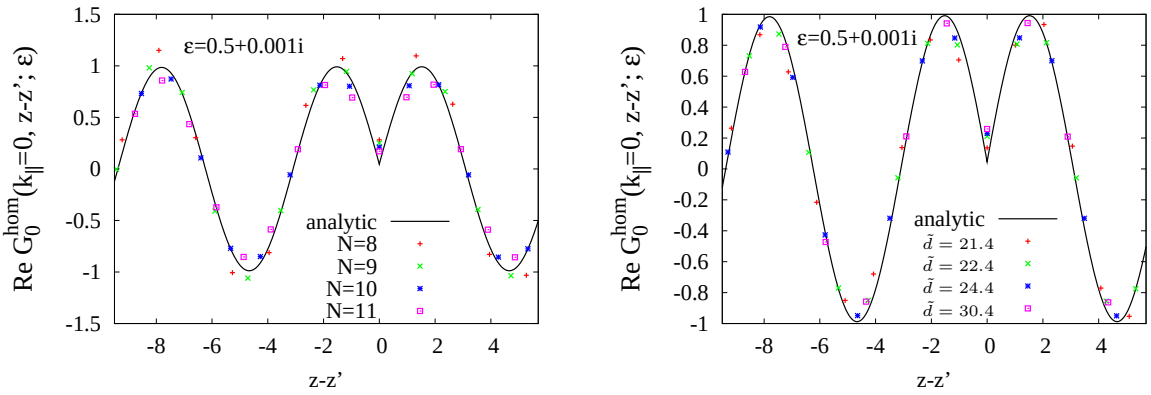

Figure 6.1: Real part of the Green function $\mathrm{Re}\, G_0^{\mathrm{hom}}(\mathbf{k}_\parallel = 0, z - z'; \epsilon)$ for the homogeneous electron gas. The results calculated with the embedding method (symbols) for $V(z) = 0$ and different values of the convergence parameters are compared to the analytical ones at the energy $\epsilon = 0.5 + 0.001i$. *Left:* The parameter N is varied for constant $\tilde{d} = 22.4$. *Right:* Whereas the number of basis functions $2N+1$ is set to 21 (N fixed to the constant value $N = 10$), the length $\tilde{d}$ is varied. In practice, one z coordinate was hold at a constant value approximately in the center of the embedding region (e.g. $z = \mathrm{const}$), and the other z coordinate z' was varied. Since the z grid depends on the choice of the basis functions, the value of z is not the same for the different curves. It is chosen as $z' = -10{+}9\Delta z$ with $\Delta z = \tilde{d}/(2N + 1)$ and therefore it varies between $z' = -1.23$ for $N = 11$ and $z' = 1.86$ for $N = 8$ (*left*) and $z' = -0.03$ for $\tilde{d} = 21.4$ and $z' = 3.03$ for $\tilde{d} = 30.4$.

parameters N and $\tilde{d}$ for the chosen embedding region $[z_{\mathrm{L}} = -10, z_{\mathrm{R}} = 10]$. Since the insertion of $\mathbf{k}_\parallel \neq 0$ leads to a shift along the real energy axis only, it suffices to compare the Green functions for $\mathbf{k}_\parallel = 0$.

For the considered system with $d = 20$, the Green function for $V(z) = 0$ calculated with the embedding method is shown in figure 6.1 for different values of the convergence parameters N and $\tilde{d}$ at the energy $\epsilon = 0.5 + 0.001i$. For a fixed value of $\tilde{d} = 22.4$, the best agreement of the Green function calculated with the embedding method and the analytical result is achieved for $N = 9$ or $N = 10$ (see the left plot of figure 6.1). For further calculations, $N = 10$ (i.e. 21 basis functions) is chosen because a higher number of basis functions leads to a better resolution in z, since Δz is given through $\Delta z = \tilde{d}/(2N + 1)$.

In the right plot of figure 6.1 the length $\tilde{d}$ is varied between $\tilde{d} = 21.4$ and $\tilde{d} = 30.4$. As one can see, the difference between the points and the analytical curve does not vary much for different values of the parameter $\tilde{d}$. Although at $z - z' = 0$ the best agreement to the analytical curve is achieved for $\tilde{d} = 21.4$, the average deviation for this choice of $\tilde{d}$ with the analytical curve is the biggest among the presented curves. I choose $\tilde{d} = 22.4$ for the same reason as I chose $N = 10$ instead of $N = 9$: The

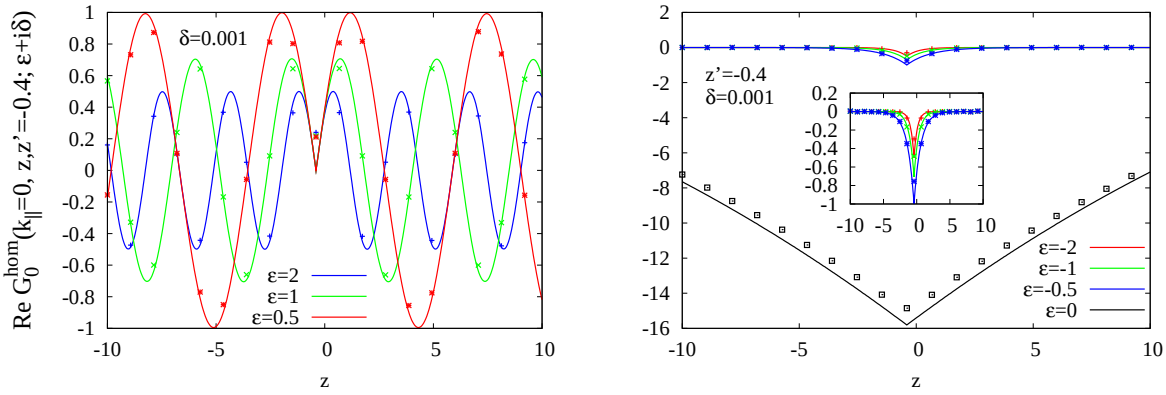

Figure 6.2: Real part of the Green function $\mathrm{Re}\, G_0^{\mathrm{hom}}(\mathbf{k}_\parallel = 0, z - z'; \epsilon + i\delta)$ for the homogeneous electron gas at $z' = -0.4$ for varying z. The results calculated with the embedding method (symbols) for $V(z) = 0$ and the parameters $N = 10$ and $\tilde{d} = 22.4$ are in good agreement with the analytical results (lines) for positive energies (*left*) as well as for negative energies (*right*). To all energies ϵ a small imaginary part $i\delta = 0.001i$ was added.

difference Δz between two points on the z grid increases linearly with the length $\tilde{d}$, thus the resolution in z direction increases for decreasing $\tilde{d}$.

For the chosen parameters $N = 10$ and $\tilde{d} = 22.4$ the Green function for homogeneous electron gas for different real energies is displayed in figure 6.2. As expected, for constant energy ϵ the Green function depends only on the difference $|z - z'|$ and not on z, z', respectively. For positive energies it oscillates with increasing $|z - z'|$, whereas for negative energies it decays exponentially.

The biggest deviations of the analytical results from the Green function calculated with the embedding method can be observed for small $|z - z'|$, especially for $z = z'$. This was expected, since the implementation of the Green-function embedding method uses a plane-wave basis, which is not suitable for the representation of a sharp kink or an exponential decay.

Another limit of the Green-function embedding method can be observed in figure 6.3. Here, the Green function is plotted for constant distances $z - z'$ but varying energy ϵ. As one can see, the analytical and the numerical values agree only up to energies of approximately 3.5. In order to reproduce the Green function for higher energies, one has to increase the number of basis functions. Then, in order to ensure the accuracy, the other parameters d and $\tilde{d}$ has to be determined anew. However, this limitation on the real frequency axis does not pose a problem. Since, as I will show in the next chapter, the Green function is only required on the imaginary frequency axis for a constant real part much smaller than 3.5.

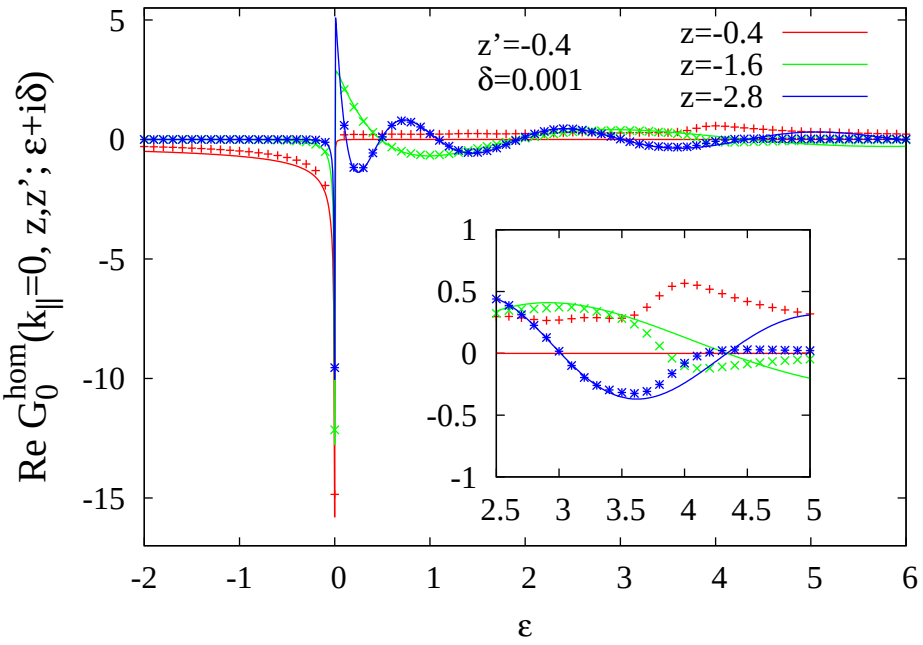

Figure 6.3: Real part of the Green function $\mathrm{Re}\, G_0^{\mathrm{hom}}(\mathbf{k}_{\parallel} = 0, z, z'; \epsilon)$ for the homogeneous electron gas for constant distance $z - z'$ and varying energy ϵ. The comparison of the embedding method (points) to the analytical result(lines) shows that the chosen basis set reproduces the analytically calculated Green function only up to energies of approximately 3.5.

6.2.2 Simple one-dimensional potential problems

Real energies

In the last section the embedding method with a constant potential was checked and the two numerical parameters N and $\tilde{d}$ were determined. In the next step, the embedding method will be applied to simple one-dimensional potentials in order to check whether it works for these problems as well. I assume that the best choice of the numerical parameters does not depend on the chosen potential. Therefore I reuse the same convergence parameters, i.e. ($N = 10$ and $\tilde{d} = 22.4$) as for the homogeneous electron gas.
The quantum well with $V = -0.1$ and the potential barrier with $V = 0.15$ are the two potentials with the largest positive and negative values investigated in this thesis. Therefore I determine the convergence parameters for these two extreme cases only, supposing that they require the 'highest' convergence parameters. For reasons of simplicity, the two potentials with these values are denoted simply as the quantum well and the potential barrier from now on. Thus, every time I speak of the quantum well (potential barrier), the one with $V = -0.1$ ($V = 0.15$) is meant. As presented in chapter 5, the chemical potential is set to $\mu = 0.1$ and the width of the potential

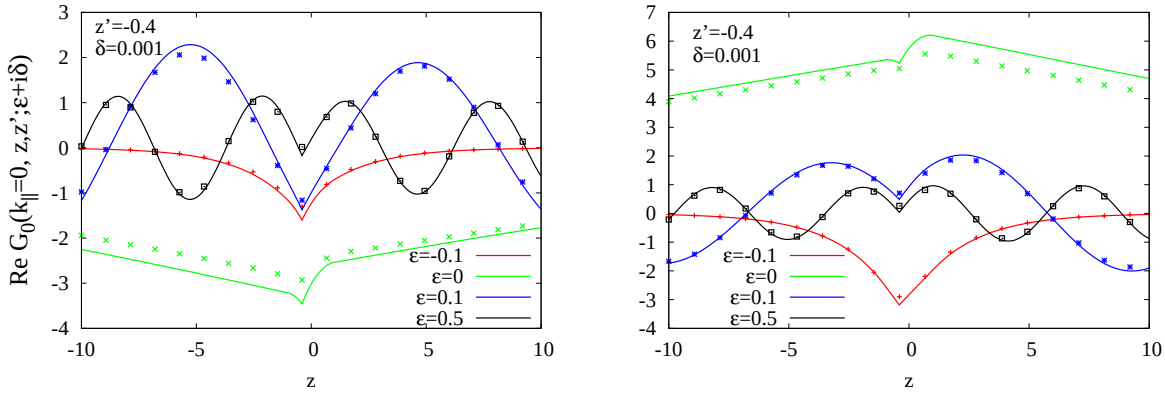

Figure 6.4: Real part of the Green function $\mathrm{Re}\, G_0(\mathbf{k}_{\parallel} = 0, z, z'; \epsilon + i\delta)$ for the potential barrier (*left*) and the quantum well (*right*) with $V(z) = 0.15$ or $V(z) = -0.1$, respectively, for $-1 \leq z \leq 1$ and $V(z) = 0$ otherwise. For the energy $\epsilon = 0.5$ the difference between the Green functions of the two potentials is much less pronounced than for energies which are in the range of the barrier and the well.

(not of the embedding region!) to $d_{\mathrm{V}} = 2$.
In figure 6.4, the Green functions for the quantum well and the potential barrier are displayed for different (real) energies. The deviations of the Green function for $V(z) \neq 0$ calculated with the embedding method from the analytical result calculated according to section 6.1.2 have approximately the same order of magnitude as those with the potential $V(z) = 0$.

The comparison of the curves in figure 6.4 corresponding to different energies shows the expected behavior: The three curves for the energies $\epsilon = -0.1$, $\epsilon = 0$ and $\epsilon = 0.1$ which are in the range of the two potentials differ from the Green function of the homogeneous electron gas and are distinct for the quantum well and the potential barrier. In contrast, the Green function for $\epsilon = 0.5$, which is much larger than the potentials with $V = -0.1$ and $V(z) = 0.15$, respectively, is barely affected by the potentials.

Complex frequencies

For further calculations the Green function on the complex frequency axis at $\epsilon = \mu + i\omega$ is required, because it is less structured and decays faster on the imaginary-frequency than on the real-energy axis[1]. Therefore from here on all comparisons will be done for energies $\epsilon = \mu + i\omega$, where the real part μ of the energy ϵ denotes the chemical potential of the considered system.
Furthermore, all calculations will not be performed with the Green function itself but with the difference ΔG_0 of the Green function G_0 for $V(z) \neq 0$ and the Green

[1]More details will follow in chapter 7.

function G_0^{hom} of the homogeneous electron gas of the leads (i.e. $V(z) = 0$). As I will show in chapter 7, this decomposition of the Green function is essential for the calculation of the polarization function — given as a convolution of two Green functions in frequency space — because for small distances $r = (r_\parallel^2 + (z - z')^2)^{1/2}$ the Green function decays very slowly for increasing complex frequency[2]. Although this decomposition of the Green function in $G_0 = G_0^{\text{hom}} + \Delta G_0$ is not essential until the calculation of the polarization function, it is convenient to split it from here on: In the next step (see next section), the Green function $G_0(\mathbf{k}_\parallel, z, z'; \mu + i\omega)$ (or $\Delta G_0(\mathbf{k}_\parallel, z, z'; \mu + i\omega)$) is Fourier transformed numerically to $G_0(\mathbf{r}_\parallel, z, z'; \mu + i\omega)$. Since

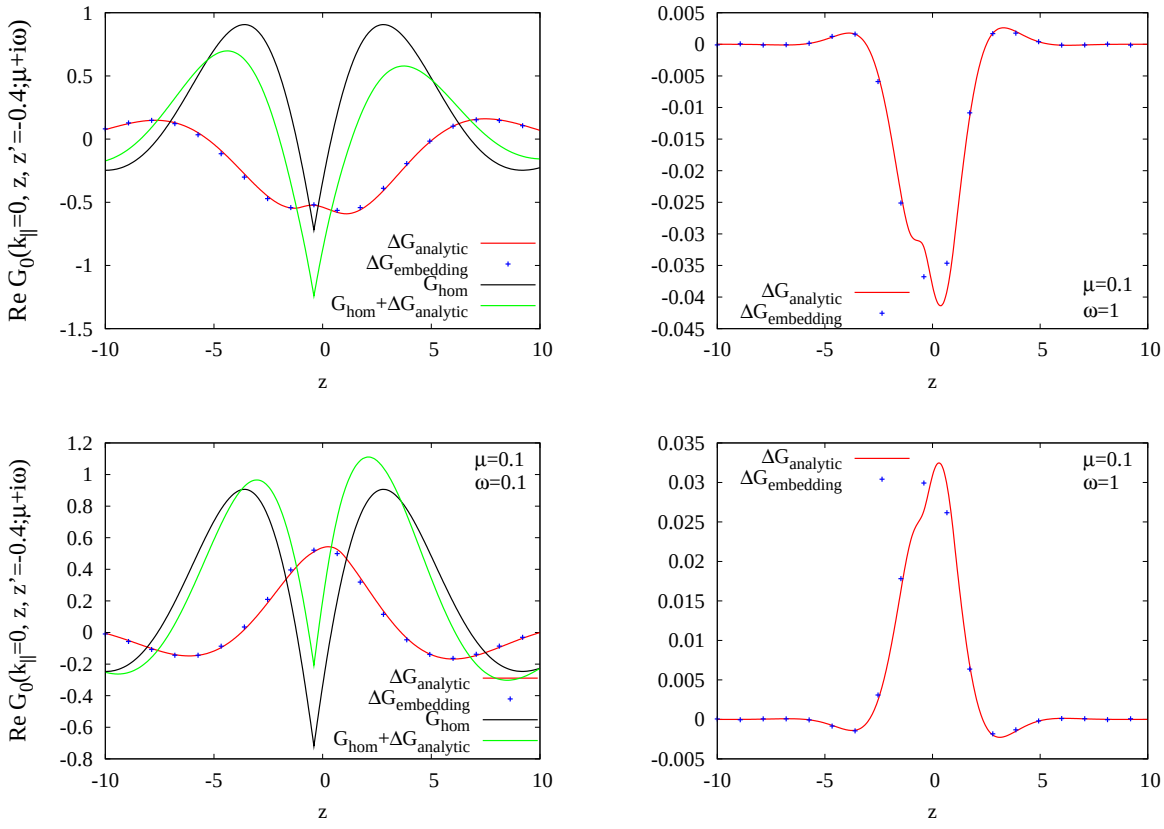

Figure 6.5: Real part of the Green function $\mathrm{Re}\, G_0(\mathbf{k}_\parallel = 0, z, z'; \mu + i\omega)$ for the potential barrier (*top*) and the quantum well potential (*bottom*). At the left side the Green functions with $V(z) \neq 0$ as well as the Green functions of the homogeneous leads and their differences are shown for $\omega = 0.1$. At the right side only the differences ΔG_0 for $\omega = 1$ are plotted. In all figures the differences ΔG_0 calculated with the Green-function embedding method (points) are compared to the analytical results (lines).

[2]The same decomposition of G_0 for the numerical calculation of the polarization P_0 was made by Fratesi [FBM04].

$\Delta G_0(\mathbf{k}_\parallel, z, z'; \mu + i\omega)$ has much smaller absolute values and decays much faster than $G_0(\mathbf{k}_\parallel, z, z'; \mu + i\omega)$, the numerical effort for the numerical treatment is significantly reduced compared to the Fourier transformation of $G_0(\mathbf{k}_\parallel, z, z'; \mu + i\omega)$ itself. This faster decay of $\Delta G_0(\mathbf{k}_\parallel, z, z'; \mu + i\omega)$ for increasing $k_\parallel$ can be easily understood. As already explained, the insertion of $\mathbf{k}_\parallel \neq 0$ leads only to a shift along the real energy axis, more precisely the enhancement of $k_\parallel$ entails the decrease of the energy. For energies much smaller than the potential, the corresponding Green functions converges to the Green function of the homogeneous electron gas, which leads to $\Delta G_0 \to 0$.
The complete Green function $G_0(\mathbf{r}_\parallel, z, z'; \mu + i\omega)$ is obtained by the addition of $G_0^{\text{hom}}(\mathbf{r}_\parallel, z, z'; \mu + i\omega)$ calculated analytically according to eq. (6.9). The real part of the Green function $G_0(\mathbf{k}_\parallel = 0, z, z'; \mu + i\omega)$ as well as of $G_0^{\text{hom}}(\mathbf{k}_\parallel = 0, z, z'; \mu + i\omega)$ and $\Delta G_0(\mathbf{k}_\parallel = 0, z, z'; \mu + i\omega)$ for complex energies are shown in figure 6.5. Looking at the spatial behavior of the Green functions, one observes that the basis of the embedding method does not contain enough points for a good resolution of the important features. For small $z - z'$ the description of the analytical curve with the points of the embedding method is very poor, especially for frequencies with a higher imaginary part $i\omega$, since the width of the peak around $z - z'$ decreases with increasing imaginary frequency.

6.2.3 Three-dimensional Green function

Two-dimensional Fourier transformation As already mentioned in the last section, the three-dimensional Green function $G_0(\mathbf{r}_\parallel, z, z'; \mu + i\omega)$ is obtained via a two-dimensional numerical Fourier transformation (see section 6.1.3) of $\Delta G_0(\mathbf{k}_\parallel, z, z'; \mu + i\omega)$ and the addition of the Green function $G_0^{\text{hom}}(\mathbf{r}_\parallel, z, z'; \mu + i\omega)$ (see eq. (6.9)) of the homogeneous electron gas of the leads.

The numerical calculation of $\Delta G_0(\mathbf{r}_\parallel, z, z'; \mu + i\omega)$ according to eq. (6.30) involves two parameters $\Delta k_\parallel$ and $k_{\parallel\max}$. In the upper plots of figure 6.6 the result for the analytical curve for the potential barrier is presented for varying parameter $\Delta k_\parallel$ and $k_{\parallel\max} = 10$. As expected, the convergence for $\omega = 0.1$ (plot on the right side) is much faster than for $\omega = 0.01$ (left side), since the oscillations of the Green function for frequencies with larger imaginary part are more damped than for frequencies close to the real energy axis. Thus, for ω approaching 0 the integrand becomes more-structured and a higher resolution (i.e. a smaller $\Delta k_\parallel$) is required. Nevertheless, for both values of ω an adequate convergence is reached for $\Delta k_\parallel = 0.025$.

For the chosen value of $\Delta k_\parallel = 0.025$, the maximal $k_{\parallel\max}$ is varied (see lower plots of figure 6.6). In contrast to the parameter $\Delta k_\parallel$, the investigation of $k_{\parallel\max}$ for different frequencies (i.e. $\omega = 0.5$ and $\omega = 0.01$) leads to the same result. This is reasonable since the increase of $k_\parallel$ implies the decrease of the energy (see previous section) and therefore the addition of a (small) imaginary part does not carry weight. As one can see, most $k_\parallel$ are required for points with small $|z - z'|$. It does not matter whether the point $z = z'$ itself is converged or not, since it will extrapolated in a later step anyway. This is due to the fact that the convolution of the two Green functions for the calculation of the polarization requires very high frequencies (in the range

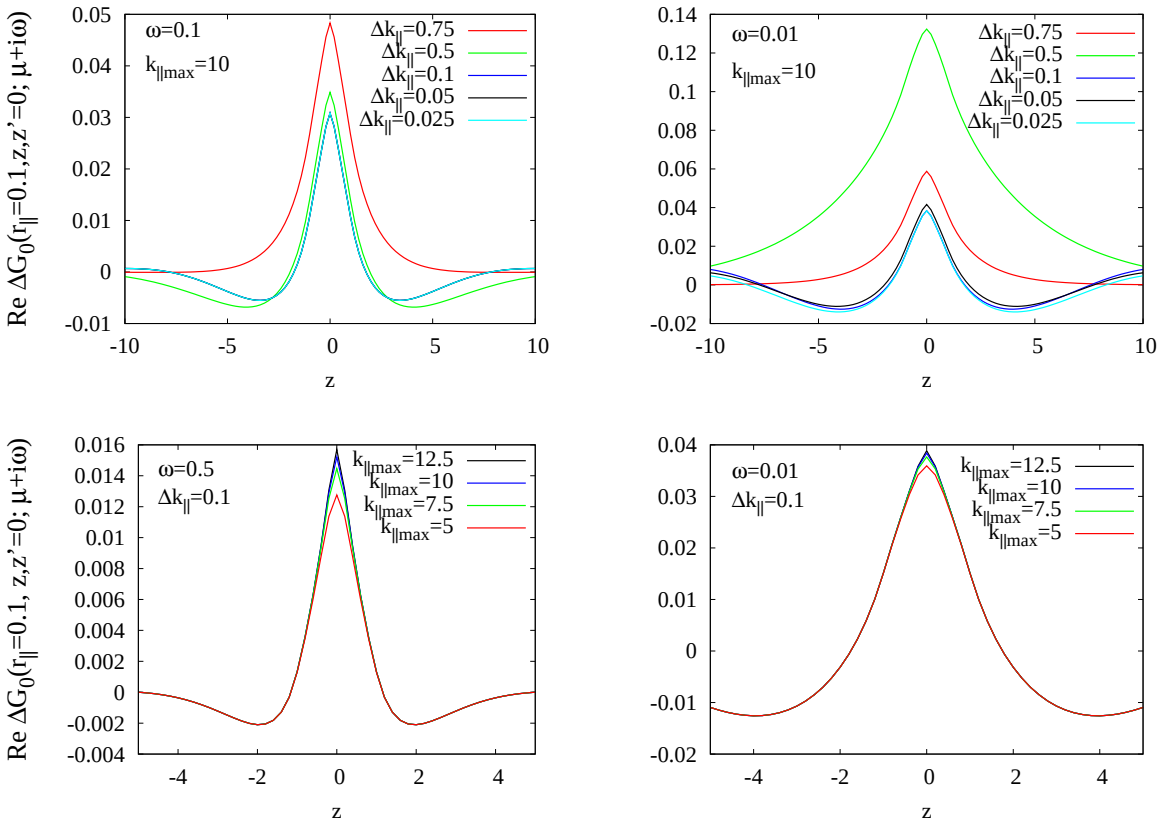

Figure 6.6: Determination of the convergence parameter $\Delta k_{\parallel}$ (*top*) and $k_{\parallel\max}$ (*bottom*) for the potential barrier. *Top*: The result of the numerical Fourier transformation $\mathrm{Re}\,\Delta G_0(\mathbf{r}_{\parallel}, z, z'; \mu + i\omega)$ is displayed for different values of $\Delta k_{\parallel}$ for constant $k_{\parallel\max} = 10$ and for $\omega = 0.01$ (*left*) and $\omega = 0.1$ (*right*). The curves are converged for $\Delta k_{\parallel} = 0.025$. *Bottom*: For the constant value $\Delta k_{\parallel} = 0.025$ the maximal value of $k_{\parallel}$ is varied. The different curves both for $\omega = 0.5$ (*left*) and for $\omega = 0.01$ (*right*) shows that an adequate convergence is reached for $k_{\parallel\max} = 10$.

of $\omega \approx 100$) for the convergence of the point $z = z'$, much more than for all other points $z \neq z'$. Details will be demonstrated in chapter 7. For further calculations, $k_{\parallel\max} = 10$ is chosen since both curves (for $\omega = 0.01$ as well as for $\omega = 0.5$) for this value of $k_{\parallel\max}$ and $z \neq z'$ are in good agreement with the curves with $k_{\parallel\max} = 12.5$. For the quantum well, the same parameters have been determined. The results are shown in figure 6.7. Whereas the required maximal value of $k_{\parallel}$ does not differ from that of the potential barrier, $\Delta k_{\parallel} = 0.025$ does not suffice for convergence. Therefore, I will choose a smaller $\Delta k_{\parallel} = 0.01$, for which an adequate convergence is achieved.

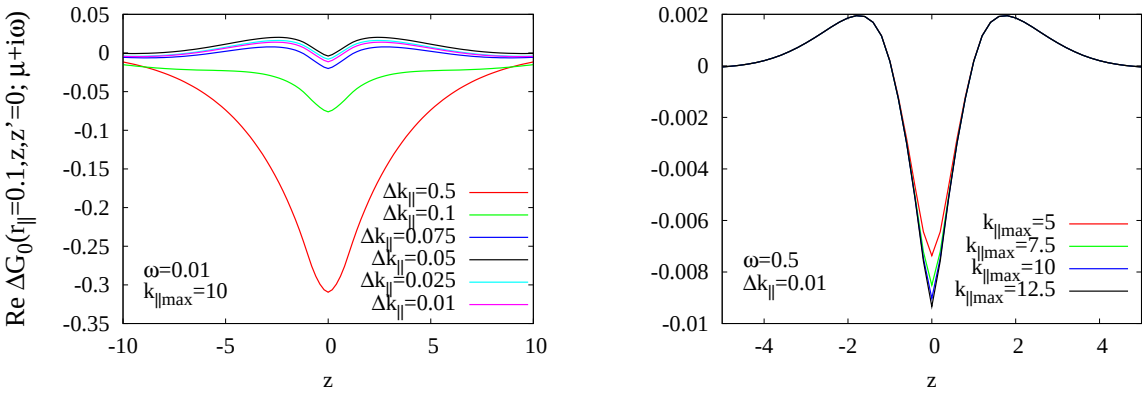

Figure 6.7: Determination of the convergence parameters $\Delta k_{\parallel}$ (*left*) and $k_{\parallel\max}$ (*right*) for the quantum well. The check of the parameter $\Delta k_{\parallel}$ was made for a very small frequency, since the investigations for the quantum barrier have shown that the convergence is worst for frequencies close to the real energy axis. For further calculations, the values $k_{\parallel\max} = 10$ and $\Delta k_{\parallel} = 0.01$ are chosen.

Comparison of the analytical and the numerical results We will now compare the results obtained by the one-dimensional analytical Green function to the numerical ones calculated with the embedding method. The results are shown in figure 6.8. The two figures at the top show both Green functions as a function of z for constant $r_{\parallel}$, z' and ω. Again, the largest deviations can be observed for $z \approx z'$, where ΔG_0 is most structured.

In order to investigate the deviations of the embedding method from the results obtained with the analytical one-dimensional Green function, in the two figures at the bottom of figure 6.8 the Green function for the quantum well is displayed for $z = z' = -0.4$ and constant $r_{\parallel}$ on the complex frequency axis. The relative deviations of the curve obtained with the Green-function embedding method from the analytical curve are larger for $r_{\parallel} = 0.1$ than for $r_{\parallel} = 1$. This could be expected, since the $1/r$ behavior of the Green function (see eq. (6.9) for the homogeneous electron gas) is not well represented in the plane-wave basis. Though, even for $r_{\parallel} = 1$ the two curves do not agree well. Since the corresponding curves for the quantum barrier do not lead to new insights, they are not shown here. I have to stress, that although the deviations of the Green function obtained with the embedding method to the analytical results are quite large, they might not be significant for the final results for the conductance. First, as already explained, the case $z = z'$ is difficult to describe in a plane-wave basis set, and therefore it is the case with the worst agreement. Secondly, the point $z = z'$ does not enter in the final calculation of the conductance, since it is extrapolated anyway. Furthermore, tests of the convergence of Δz show (see the inversion of the renormalization function in section 7.6) that even the sparsity of the z grid might not play a role.

Nevertheless, I will abandon the Green-function embedding method here in order

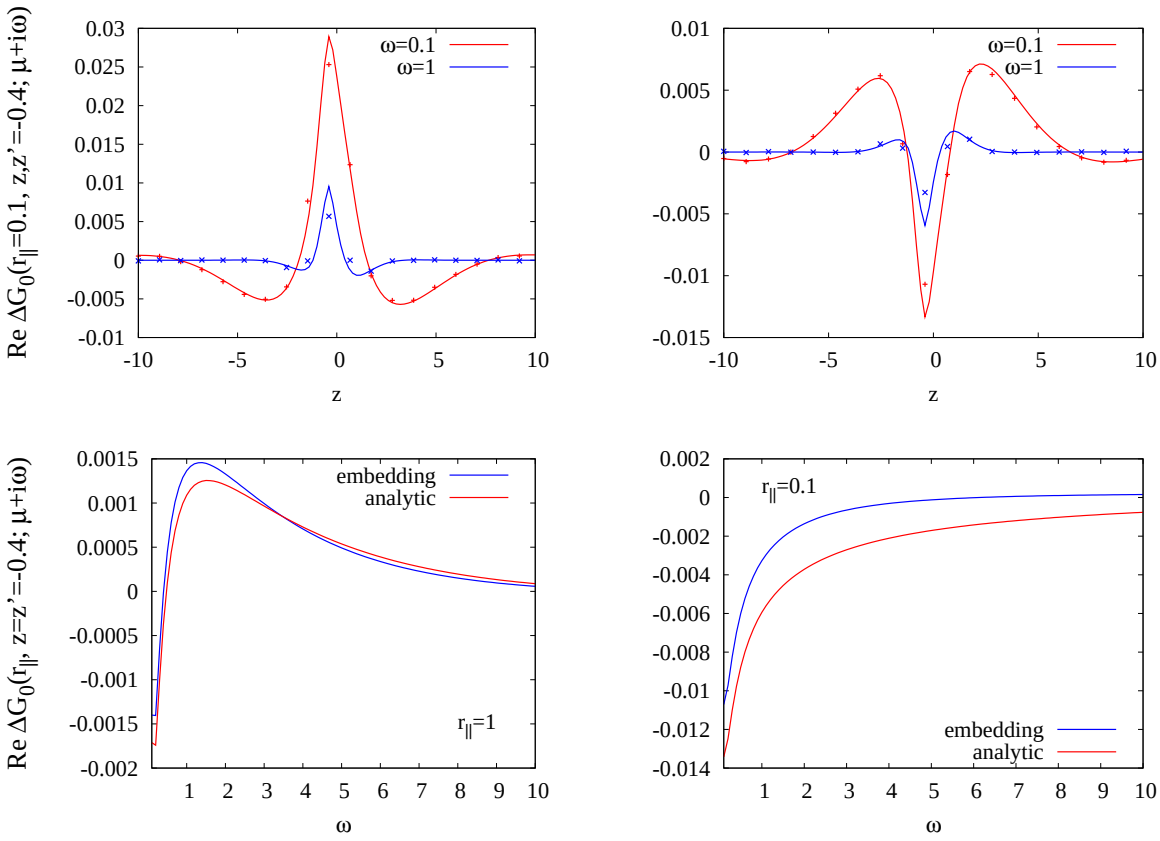

Figure 6.8: *Top:* Comparison of the Green function obtained with the Green-function embedding method (symbols) to the Green functions calculated from the analytical one-dimensional Green functions (lines) for the quantum well (*left*) and the potential barrier (*right*). The deviations are largest for $z = z'$. *Bottom:* In contrast to the previous figures, the Green function for the quantum well obtained with the embedding method (blue lines) is compared to analytical result (red lines) as a function of the complex frequency ω for constant values $z = z'$ and $r_\parallel = 0.1$ (*right*) (or $r_\parallel = 1$ (*left*), respectively,).

to obtain more accurate results. It has to checked in future whether the results for the conductance obtained with the Green-function embedding method are in good agreement with the results calculated in this diploma thesis or not.

Decay of the Green function Before closing this chapter I will compare the decay of ΔG_0 on the complex frequency axis to that of G_0 itself in order to justify the decomposition of the Green function in a homogeneous part G_0^{hom} and a remainder ΔG_0. The three functions G_0, G_0^{hom} and ΔG_0 are shown in figure 6.9 as a function of ω for constant $z = z' = -0.4$ and $r_\parallel = 0.1$ (or $r_\parallel = 1$, respectively,). As expected, the difference ΔG_0 of the two Green functions decays much faster than G_0 itself.

Additionally, it is several orders of magnitude smaller and represents only a small correction to the Green function of the homogeneous electron gas G_0^{hom}. It is obvious that the numerical integration over the difference ΔG_0 on the complex frequency axis is much cheaper than that over G_0 itself.
Comparing the two plots of figure 6.9 for $r_\parallel = 0.1$ (left) and $r_\parallel = 1$ (right), one can observe that the value of G_0 is much higher for small values of $r_\parallel$ than for large ones. This is simply a consequence of the divergence of the three-dimensional Green in the limit $r_\parallel \to 0$. For the homogeneous electron gas, this behavior agrees with the analytical result (6.9).

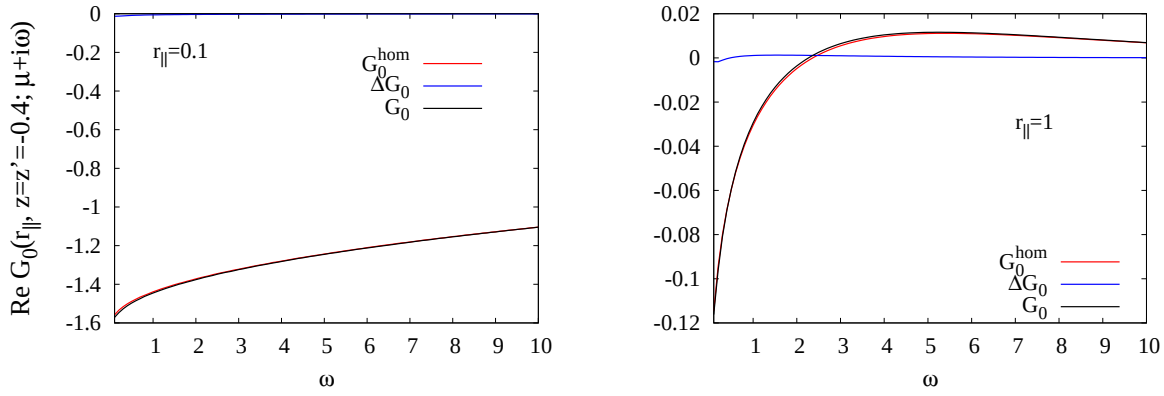

Figure 6.9: Comparison of the decay on the complex frequency axis for G_0, G_0^{hom} and ΔG_0 for the quantum well for constant $z = z' = -0.4$ and different values of $r_\parallel$. The difference ΔG_0 is several orders of magnitude smaller and decays much faster than the Green function G_0 itself. (For a better resolution of ΔG_0 see figure 6.8.) Furthermore, the decay of ΔG_0 and especially of G_0 for large values of $r_\parallel$ (*left*) is much faster than for small values of $r_\parallel$ (*right*).

7 Polarization function

In this chapter I present the calculation of the irreducible polarization function. Whereas in the first part the polarization P_0 for an effective potential is evaluated, in the second part exchange and correlation effects are included and the irreducible polarization function is calculated.
The first part itself is structured as follows: At the beginning, I explain the procedure how to calculate the polarization and introduce the applied equations. Afterwards, the involved numerical parameters are investigated and the results for the polarization function for an effective potential are presented. The second part of the chapter starts with the numerical calculation of the electron density which is required for the evaluation of the exchange-correlation kernel. Finally, I present the calculation of the irreducible polarization function including electronic exchange and correlation.

7.1 Polarization function in the complex frequency plane

As demonstrated in section 3.9 the polarization function (see eq. (3.46)) depending on time and space coordinates is given as a product of two Green functions

$$P_0(1,2) = -iG^{(0)}(1,2)G^{(0)}(2,1) \; .$$

The upper index (0) denotes that the Green function is the initial Green function of Hedin's equations. It will be dropped in the following derivation. Instead, as already introduced in the last chapter, the Green function and the polarization function for non-interacting particles are indexed with 0. Since the potential neither depends on time nor on the x or y coordinates, the Green function $G(1,2)$ depends only on the differences $\tau = t_1 - t_2$ and $\mathbf{r}_\parallel = \mathbf{r}_{\parallel,1} - \mathbf{r}_{\parallel,2}$ as well as on the spins σ_1 and σ_2. Therefore eq. (3.46) simplifies to

$$P_0(\mathbf{r}_\parallel, z_1, z_2; \tau; \sigma_1, \sigma_2) = -iG_0(\mathbf{r}_\parallel, z_1, z_2; \tau; \sigma_1, \sigma_2)G_0(-\mathbf{r}_\parallel, z_2, z_1; -\tau; \sigma_2, \sigma_1) \; . \quad (7.1)$$

In the following, the two space coordinates z_1 and z_2 are again denoted by z and z' in order to stay consistent with the notation chosen in chapter 5. Furthermore, I consider non-magnetic systems only. In this case, the Green function is diagonal in the spin coordinates and and can be written as

$$G_0(\mathbf{r}_\parallel, z_1, z_2; \tau; \sigma_1, \sigma_2) = G_0(\mathbf{r}_\parallel, z_1, z_2; \tau)\delta_{\sigma_1\sigma_2} \; . \quad (7.2)$$

The same applies to P_0 as defined by Hedin. The integration to obtain the screened interaction W (see eq. (3.42)) leads in this case to an additional factor 2. Often, this factor 2 is already included in the polarization. I follow this convention and redefine

$$P_0(\mathbf{r}_\parallel, z, z'; \tau) = -2iG_0(\mathbf{r}_\parallel, z, z'; \tau)G_0(-\mathbf{r}_\parallel, z', z; -\tau) \; . \tag{7.3}$$

In frequency space the product between $G_0(\mathbf{r}_\parallel, z, z'; \tau)$ and $G_0(-\mathbf{r}_\parallel, z', z; -\tau)$ becomes a convolution, i.e.

$$\begin{aligned} P_0(\mathbf{r}_\parallel, z, z'; \epsilon) &= \int_{-\infty}^{\infty} d\tau e^{i\epsilon\tau} P_0(\mathbf{r}_\parallel, z, z'; \tau) \\ &= -2i \int_{-\infty}^{\infty} d\tau e^{i\epsilon\tau} \frac{1}{2\pi} \int_{-\infty}^{\infty} d\epsilon'' e^{-i\epsilon''\tau} G_0(\mathbf{r}_\parallel, z, z'; \epsilon'') \frac{1}{2\pi} \int_{-\infty}^{\infty} d\epsilon' e^{i\epsilon'\tau} G_0(-\mathbf{r}_\parallel, z', z; \epsilon') \\ &= \frac{-2i}{(2\pi)^2} \int_{-\infty}^{\infty} d\epsilon'' \int_{-\infty}^{\infty} d\epsilon' 2\pi\delta(\epsilon - \epsilon'' + \epsilon') G_0(\mathbf{r}_\parallel, z, z'; \epsilon'') G_0(-\mathbf{r}_\parallel, z', z; \epsilon') \\ &= -\frac{2i}{2\pi} \int_{-\infty}^{\infty} G_0(\mathbf{r}_\parallel, z, z'; \epsilon + \epsilon') G_0(-\mathbf{r}_\parallel, z', z; \epsilon') \, d\epsilon' \; . \end{aligned} \tag{7.4}$$

The convolution is an integral over the real energy axis. Its evaluation is quite complicated since the Green function (see section 3.4) has poles very close to the real energy axis. To avoid numerical difficulties, one can define the analytic continuation of P_0 to complex frequencies — where the Green function has less structure — and calculate $P_0(i\omega)$ instead of $P_0(\epsilon)$.

Since the Green function and therefore the whole integrand of eq. (7.4) decays to zero for infinite energies I can add the integral along the upper semi-circle (whose result is zero) and carry out the integration along a closed contour. According to the theorem of residues it has the same value as the sum over the enclosed poles. The time-ordered Green function has poles in the upper half-plane only for $\epsilon < \mu$ and below the real energy axis only for $\epsilon > \mu$. Therefore, for purely imaginary frequencies $i\omega$ the integration contour can be rotated counter-clockwise to the shifted complex frequency axis, so that it forms a closed integral over the left half-plane (see figure 7.1). Even the poles of the Green function $G_0(\epsilon + \epsilon')$ are inside the contour, since for purely imaginary frequencies $\epsilon = i\omega$, the poles of the Green function are shifted only perpendicular to the real frequency axis, whereas the real part of the frequency does not change.

Finally, using the same argument as at the beginning, the contour integral over the left semi-circle can be neglected, and the polarization on the imaginary frequency axis may be written as

$$\begin{aligned} P_0(\mathbf{r}_\parallel, z, z'; i\omega) &= -2\frac{i}{2\pi} \int_{\mu - i\infty}^{\mu + i\infty} G_0(\mathbf{r}_\parallel, z, z'; \epsilon' + i\omega) G_0(-\mathbf{r}_\parallel, z', z; \epsilon') \, d\epsilon' \\ &= \frac{1}{\pi} \int_{-\infty}^{\infty} G_0(\mathbf{r}_\parallel, z, z'; \mu + i\omega + i\omega') G_0(\mathbf{r}_\parallel, z, z'; \mu + i\omega') \, d\omega' \; . \end{aligned} \tag{7.5}$$

In the last step, the spatial arguments of the second Green function are permuted, since it does not change under exchange of the two coordinates, and I used the substitution $\epsilon' = \mu + i\omega'$ which implies $d\epsilon' = id\omega'$.

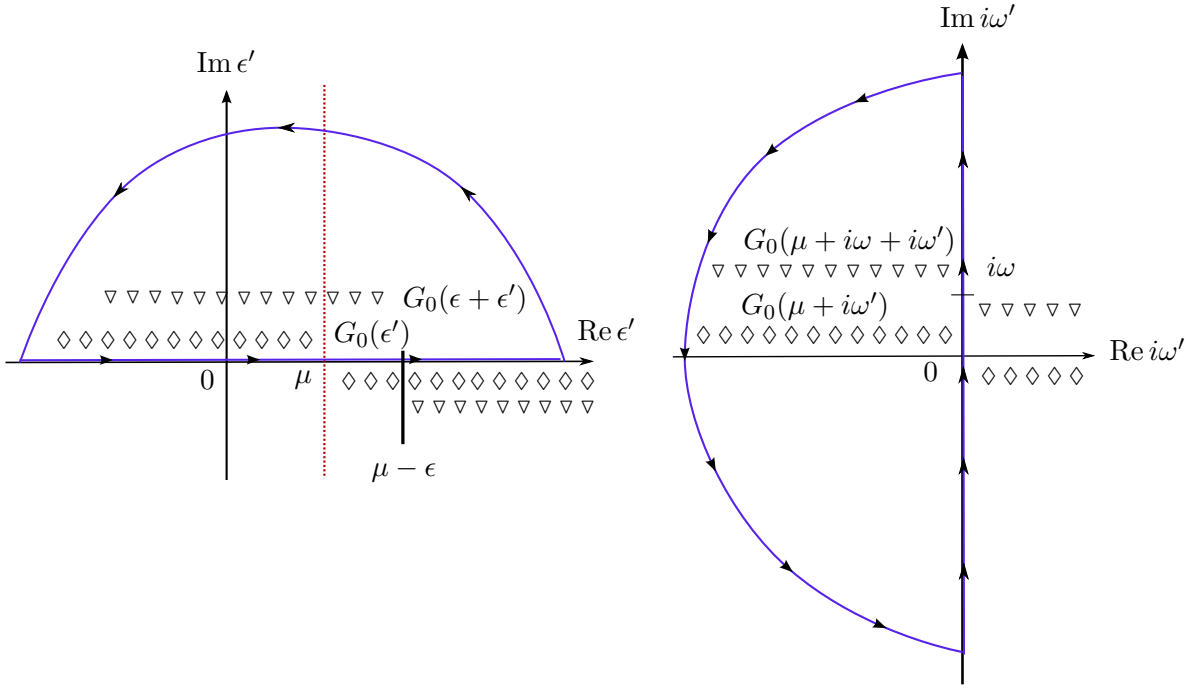

Figure 7.1: *Left:* The poles of the time-ordered Green function $G_0(\epsilon')$ (represented as lozenges), ϵ' real, are situated close to the real frequency axis. They are in the upper half-plane for $\epsilon' < \mu$ and in the lower half-plane otherwise. The addition of a real energy ϵ to ϵ' leads to a translation of the poles along the real energy axis, such that the sign of the poles changes at $\mu - \epsilon$ instead of μ. Nevertheless, both the poles of $G_0(\epsilon')$ as well as of $G_0(\epsilon + \epsilon')$ (displayed as triangles) are in the upper half-plane and therefore inside the integration contour. *Right:* Whereas the addition of a real frequency ϵ (left) has led to a translation of the poles along the real energy axis, the addition of a purely imaginary frequency $i\omega$ leads to a shift of the poles along the imaginary frequency axis. Therefore the integration contour can be rotated to the left half-plane without neglecting any of the poles included in the original integration contour on the left side.

As the Green function decays to zero for very large positive and negative frequencies, the integrand does so as well. Therefore it is sufficient to approximate the integral over the complex frequency axis by a sum over a finite interval of frequencies. Unfortunately, as I have shown in the last chapter (compare figure 6.9), the decay of the Green function (and of the integrand, respectively,) is very slow whenever $r = (r_\parallel^2 + (z - z')^2)^{1/2}$ becomes very small. For that reason one has to include a wide range of frequencies, which makes the calculation very time-consuming. As already mentioned, one possibility to deal with this problem is to split the Green function into two terms

$$G_0(\mathbf{r}_\parallel, z, z'; \mu + i\omega') = \tilde{G}_0(\mathbf{r}_\parallel, z, z'; \mu + i\omega') + \Delta G_0(\mathbf{r}_\parallel, z, z'; \mu + i\omega') \; . \tag{7.6}$$

Inserting this partition in eq. (3.40) for the polarization function leads to an integral over four terms

$$\begin{aligned} P_0(\mathbf{r}_\parallel, z, z'; i\omega) = \frac{1}{\pi}\int_{-\infty}^{\infty} \tilde{G}_0(\mathbf{r}_\parallel, z, z'; \mu + i\omega + i\omega')\tilde{G}_0(\mathbf{r}_\parallel, z, z'; \mu + i\omega')\, d\omega' \\ +\frac{1}{\pi}\int_{-\infty}^{\infty} \Big[\tilde{G}_0(\mathbf{r}_\parallel, z, z'; \mu + i\omega + i\omega')\Delta G_0(\mathbf{r}_\parallel, z, z'; \mu + i\omega') \\ +\Delta G_0(\mathbf{r}_\parallel, z, z'; \mu + i\omega + i\omega')\tilde{G}_0(\mathbf{r}_\parallel, z, z'; \mu + i\omega') \\ +\Delta G_0(\mathbf{r}_\parallel, z, z'; \mu + i\omega + i\omega')\Delta G_0(\mathbf{r}_\parallel, z, z'; \mu + i\omega')\Big]\, d\omega' \,. \end{aligned} \tag{7.7}$$

Denoting the first term as

$$\tilde{P}_0(\mathbf{r}_\parallel, z, z'; i\omega) := \frac{1}{\pi}\int_{-\infty}^{\infty} \tilde{G}_0(\mathbf{r}_\parallel, z, z'; \mu + i\omega + i\omega')\tilde{G}_0(\mathbf{r}_\parallel, z, z'; \mu + i\omega')\, d\omega' \tag{7.8}$$

and the second integral containing all terms with ΔG_0 by

$$\begin{aligned} \Delta P_0(\mathbf{r}_\parallel, z, z'; i\omega) := \frac{1}{\pi}\int_{-\infty}^{\infty} \Big[\tilde{G}_0(\mathbf{r}_\parallel, z, z'; \mu + i\omega + i\omega')\Delta G_0(\mathbf{r}_\parallel, z, z'; \mu + i\omega') \\ +\Delta G_0(\mathbf{r}_\parallel, z, z'; \mu + i\omega + i\omega')\tilde{G}(\mathbf{r}_\parallel, z, z'; \mu + i\omega') \\ +\Delta G_0(\mathbf{r}_\parallel, z, z'; \mu + i\omega + i\omega')\Delta G_0(\mathbf{r}_\parallel, z, z'; \mu + i\omega')\Big]\, d\omega' \,, \end{aligned} \tag{7.9}$$

the equation for the complete polarization function can be rewritten as

$$P_0(\mathbf{r}_\parallel, z, z'; i\omega) = \tilde{P}_0(\mathbf{r}_\parallel, z, z'; i\omega) + \Delta P_0(\mathbf{r}_\parallel, z, z'; i\omega) \,. \tag{7.10}$$

The artifice is to choose the Green function $\tilde{G}_0(\mu + i\omega)$ such that it fulfills two conditions: First, it must be possible to calculate $\tilde{P}_0(\mathbf{r}_\parallel, z, z'; i\omega)$ given by eq. (7.8) in another way than by numerical integration over the frequency axis (for example analytically or numerically using another method). Secondly, $\tilde{G}_0(\mu + i\omega)$ must show the same convergence behavior for imaginary frequencies with a large absolute value ω as the whole Green function $G_0(\mu + i\omega)$, so that $\Delta G_0(\mu + i\omega)$ decays much faster to zero than $G_0(\mu + i\omega)$. In this case the integral leading to $\Delta P_0(\mathbf{r}_\parallel, z, z'; i\omega)$ given by eq. (7.9) over the three terms containing $\Delta G_0(\mu + i\omega)$ converges much faster than the original one in eq. (3.40) and can therefore be evaluated numerically.
The question is how to choose the Green function $\tilde{G}_0(\mathbf{r}_\parallel, z, z'; \mu + i\omega)$ best. The easiest Green function which one can imagine is the Green function of the homogeneous electron gas, denoted by $G_0^{\text{hom}}(\mathbf{r}_\parallel, z, z'; \mu + i\omega)$, whose derivation yields (6.9). In this case, both conditions are fulfilled: First, the polarization function of the homogeneous electron gas is known analytically. Secondly, as I have already shown in the last chapter (see figure 6.9), the difference of the Green function with $V(z) \neq 0$ and the Green function of the homogeneous electron gas decays much faster than the Green function itself (at least for the systems under consideration).

7.2 Polarization function of the homogeneous electron gas

An analytical derivation of the polarization function for the homogeneous electron gas in reciprocal space yields

$$P_0^{\text{hom}}(\mathbf{k}; i\omega) = -\frac{k_\text{F}}{2\pi^2}\left(1 + \frac{1}{2k_\text{F}k^3}\left[4\mu\epsilon_k - (\epsilon_k + i\omega)^2\right]\ln\left[\frac{\epsilon_k + kk_\text{F} + i\omega}{\epsilon_k - kk_\text{F} + i\omega}\right]\right. \\ \left. + \frac{1}{2k_\text{F}k^3}\left[4\mu\epsilon_k - (\epsilon_k - i\omega)^2\right]\ln\left[\frac{\epsilon_k + kk_\text{F} - i\omega}{\epsilon_k - kk_\text{F} - i\omega}\right]\right) \tag{7.11}$$

with $\epsilon_k = \frac{k^2}{2}$ and $\mu = \frac{k_\text{F}^2}{2}$. Although in this representation the polarization function $P_0^{\text{hom}}(\mathbf{k}; i\omega)$ seems to be a complex number, it turns out to be a real function of $\mathbf{k}$ and ω

$$P_0^{\text{hom}}(\mathbf{k}; i\omega) = -\frac{k_\text{F}}{2\pi^2}\left(1 + \frac{1}{2k_\text{F}k^3}\left[4\mu\epsilon_k - \epsilon_k^2 + \omega^2\right]\ln\left[\frac{(\epsilon_k + kk_\text{F})^2 + \omega^2}{(\epsilon_k - kk_\text{F})^2 + \omega^2}\right]\right. \\ \left. + \frac{\omega}{kk_\text{F}}\left[\arctan\left(\frac{\omega}{\epsilon_k + kk_\text{F}}\right) - \arctan\left(\frac{\omega}{\epsilon_k - kk_\text{F}}\right)\right]\right) . \tag{7.12}$$

Furthermore, $P_0^{\text{hom}}(\mathbf{k}; i\omega)$ depends on the absolute value of $\mathbf{k}$ only, i.e. on $k = (k_\parallel^2 + k_z^2)^{1/2}$. A derivation of eq. (7.11) can be found in [Mah90].
For further calculations the polarization function P_0 and P_0^{hom}, respectively, have to be of the form $P_0(\mathbf{k}_\parallel, z, z'; i\omega)$. This representation is obtained from eq. (7.11) as the one-dimensional Fourier transform of $P_0^{\text{hom}}(\mathbf{k}; i\omega)$

$$P_0^{\text{hom}}(\mathbf{k}_\parallel, z, z'; i\omega) = \int_{-\infty}^{\infty} dk_z e^{ik_z|z-z'|} P_0^{\text{hom}}(\mathbf{k}_\parallel, k_z; i\omega) . \tag{7.13}$$

Eq. (7.13) is evaluated numerically using a Fast Fourier Transformation (FFT). Since the system is invariant under spatial translations, P_0^{hom} depends on the difference of the two z coordinates only and can hence be written as $P_0^{\text{hom}}(\mathbf{k}_\parallel, z, z'; i\omega) = P_0^{\text{hom}}(\mathbf{k}_\parallel, |z - z'|; i\omega)$. Moreover, the polarization function is needed for $\mathbf{k}_\parallel = \mathbf{0}$ only, since it serves for the calculation of the conductance which is obtained from the irreducible polarization $P(\mathbf{k}_\parallel)$ at $\mathbf{k}_\parallel = \mathbf{0}$ according to eq. (4.36). Unfortunately, $P_0^{\text{hom}}(\mathbf{k}; i\omega)$ contains terms which diverge for $\mathbf{k} = \mathbf{0}$ and therefore a straightforward numerical evaluation fails. This problem can be solved by calculating the limit $k \to 0$ of $P_0^{\text{hom}}(k; i\omega)$ analytically

$$\lim_{k\to 0} P_0^{\text{hom}}(k; i\omega) \approx \frac{k_\text{F}}{2\pi^2}\left[1 + \frac{2}{3}\left(\frac{kk_\text{F}}{i\omega}\right)^2 + \cdots\right] \\ \approx \frac{k_\text{F}}{2\pi^2} . \tag{7.14}$$

Setting $P_0^{\text{hom}}(\mathbf{k}_\parallel = \mathbf{0}, k_z; i\omega)$ for $k_z = 0$ to the constant value $P_0^{\text{hom}}(\mathbf{k}_\parallel = \mathbf{0}, 0; i\omega) = \frac{k_\text{F}}{2\pi^2}$, the FFT of $P_0^{\text{hom}}(\mathbf{k}_\parallel = \mathbf{0}, k_z; i\omega)$ yields $P_0^{\text{hom}}(\mathbf{k}_\parallel = \mathbf{0}, |z - z'|; i\omega)$ as presented in figure 7.2.
The two convergence parameters Δk_z and $k_{z,\text{max}} = -k_{z,\text{min}}$ involved in the FFT are tested for frequencies very close to the real frequency axis (i.e. at $\omega = 0.01$), since the function $P_0^{\text{hom}}(\mathbf{k}_\parallel = \mathbf{0}, k_z; i\omega)$ has higher absolute values for small complex frequencies than for large ones and hence a higher resolution might be required. This can be observed at the top of figure 7.2, where the function $P_0^{\text{hom}}(\mathbf{k}_\parallel = \mathbf{0}, k_z; i\omega)$ is displayed for the three different frequencies $\omega = 0.1$, $\omega = 0.05$ and $\omega = 0.01$. An adequate convergence is achieved for $\Delta k_z = 0.01$ and $k_{z,\text{max}} = 6.2$.

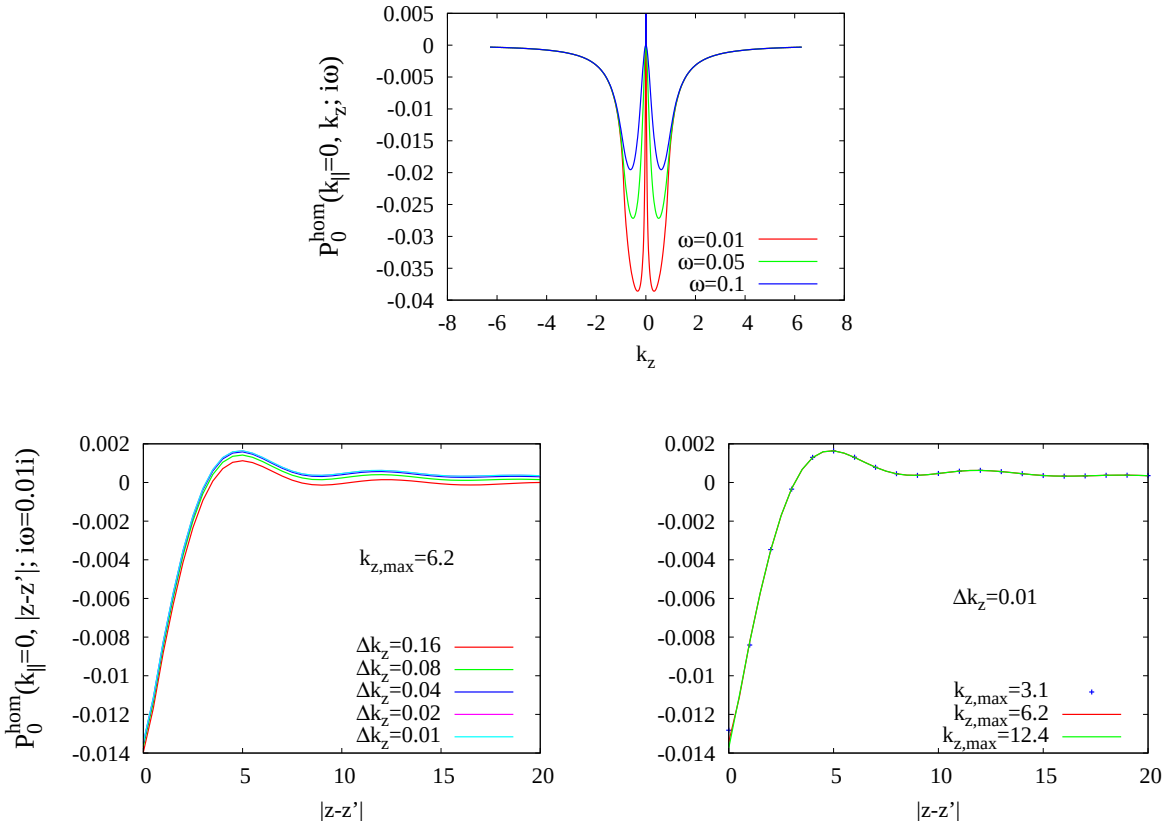

Figure 7.2: Polarization function of the homogeneous electron gas $P_0^{\text{hom}}(\mathbf{k}_\parallel = \mathbf{0}, k_z; i\omega)$ (*top*) and its Fourier transform $P_0(\mathbf{k}_\parallel = \mathbf{0}, |z - z'|; i\omega)$ (*bottom*). Since the one-dimensional Fourier transformation is carried out with the help of a FFT, the resulting function $P_0^{\text{hom}}(\mathbf{k}_\parallel = \mathbf{0}, |z - z'|; i\omega)$ is shown here for different convergence parameters Δk_z (*bottom left*) and $k_{z,\text{max}}$ (*bottom right*). An adequate convergence is reached for $\Delta k_z = 0.01$ and $k_{z,\text{max}} = 6.2$.

7.3 Numerical calculation of $\Delta P_0(\mathbf{k}_\parallel, z, z'; i\omega)$

This section deals with the numerical calculation of the remainder $\Delta P_0(\mathbf{k}_\parallel, z, z'; i\omega)$. Whereas in the first part details about the concrete numerical procedure are given, in the second part the numerical convergence parameters are investigated.

7.3.1 Convolution on the complex frequency axis

In a first step, I need to calculate the polarization function ΔP_0 in the representation $\Delta P_0(\mathbf{r}_\parallel, z, z'; i\omega)$, which according to eq. (7.9) calculates as a numerical convolution over the complex frequency axis

$$\begin{aligned}\Delta P_0(\mathbf{r}_\parallel, z, z'; i\omega) := \frac{1}{\pi}\int_{-\infty}^{\infty} \big[& G_0^{\mathrm{hom}}(\mathbf{r}_\parallel, z, z'; \mu + i\omega + i\omega')\Delta G_0(\mathbf{r}_\parallel, z, z'; \mu + i\omega') \\ & + \Delta G_0(\mathbf{r}_\parallel, z, z'; \mu + i\omega + i\omega') G_0^{\mathrm{hom}}(\mathbf{r}_\parallel, z, z'; \mu + i\omega') \\ & + \Delta G_0(\mathbf{r}_\parallel, z, z'; \mu + i\omega + i\omega')\Delta G_0(\mathbf{r}_\parallel, z, z'; \mu + i\omega') \big]\, d\omega' \,.\end{aligned}$$

I consider the three summands separately. The first summand is approximated as

$$\begin{aligned}&\frac{1}{\pi}\int_{-\infty}^{\infty} G_0^{\mathrm{hom}}(\mathbf{r}_\parallel, z, z'; \mu + i\omega + i\omega')\Delta G_0(\mathbf{r}_\parallel, z, z'; \mu + i\omega') d\omega' \\ &\approx \frac{1}{\pi}\int_{-\omega_{\max}}^{\omega_{\max}} G_0^{\mathrm{hom}}(\mathbf{r}_\parallel, z, z'; \mu + i\omega + i\omega')\Delta G_0(\mathbf{r}_\parallel, z, z'; \mu + i\omega') d\omega' \\ &\approx \frac{1}{\pi}\frac{\Delta\omega}{3}\Bigg[2 \sum_{j=-\left(\frac{n_{\omega\max}}{2}-1\right)}^{\frac{n_{\omega\max}}{2}-1} G_0^{\mathrm{hom}}(\mu + i\omega + i2j\Delta\omega)\Delta G_0(\mu + i2j\Delta\omega) \\ &\qquad + 4 \sum_{j=-\left(\frac{n_{\omega\max}}{2}-1\right)}^{\frac{n_{\omega\max}}{2}-1} G_0^{\mathrm{hom}}(\mu + i\omega + i(2j+1)\Delta\omega)\Delta G_0(\mu + i(2j+1)\Delta\omega) \\ &\qquad\qquad + G_0^{\mathrm{hom}}(\mu + i\omega + i\omega_{\max})\Delta G_0(\mu + i\omega_{\max})\Big] \,, \quad (7.15)\end{aligned}$$

where I have introduced the three numerical parameters $\omega_{\max}$, $n_{\omega\max}$ and $\Delta\omega$, which are related through $\omega_{\max} = n_{\omega\max}\Delta\omega$. In the last step Simpson's rule was used. The difference ΔG_0 is thus calculated for frequencies in the interval $[-\omega_{\max}, \omega_{\max}]$ only, for larger and smaller frequencies it is assumed to be zero. In contrast, the Green function of the homogeneous electron gas is needed for frequencies $\omega \in [-\omega_{\max} + \omega, \omega_{\max} + \omega]$. This choice of the integration limits is quite reasonable, since G_0^{hom} decays much more slowly than ΔG_0 and therefore even for frequencies not in the vicinity of zero it might contribute at $\omega_{\max} + \omega$, although $\Delta G_0(\omega_{\max}) \approx 0$ might be valid. Of course, the maximal frequency $\omega_{\max}$ (or the minimal frequency $\omega_{\min} = -\omega_{\max}$, respectively,) as well as the step size $\Delta\omega$ are numerical parameters which have to be determined. For the potential barrier as well as for the quantum well this will be done in the next section.

Since ΔG_0 is assumed to be nonzero for frequencies $\omega \in [-\omega_{\max}, \omega_{\max}]$ only, in the second summand the variable ω' is transformed to $\omega'' = \omega' + \omega$ and the numerical integration limit can be chosen equivalently to that of the first summand

$$\begin{aligned}
&\frac{1}{\pi}\int_{-\infty}^{\infty} \Delta G_0(\mathbf{r}_\parallel, z, z'; \mu + i\omega + i\omega') G_0^{\mathrm{hom}}(\mathbf{r}_\parallel, z, z'; \mu + i\omega') d\omega' \\
&= \frac{1}{\pi}\int_{-\infty}^{\infty} \Delta G_0(\mathbf{r}_\parallel, z, z'; \mu + i\omega') G_0^{\mathrm{hom}}(\mathbf{r}_\parallel, z, z'; \mu + i\omega' - i\omega) d\omega' \\
&\approx \frac{1}{\pi}\int_{-\omega_{\max}}^{\omega_{\max}} \Delta G_0(\mathbf{r}_\parallel, z, z'; \mu + i\omega') G_0^{\mathrm{hom}}(\mathbf{r}_\parallel, z, z'; \mu + i\omega' - i\omega) d\omega' \,. \qquad (7.16)
\end{aligned}$$

This time, the Green function of the homogeneous electron gas is needed for frequencies $\omega \in [-\omega_{\max} - \omega, \omega_{\max} - \omega]$. The integral is evaluated equivalently to the first summand with Simpson's rule.
The third summand will be split into two terms. One of them is treated equally to the first summand, whereas in the second one the integration variable is transformed as in the second summand. Hence, for positive frequencies ω the third summand is given by

$$\begin{aligned}
&\frac{1}{\pi}\int_{-\infty}^{\infty} \Delta G_0(\mathbf{r}_\parallel, z, z'; \mu + i\omega + i\omega') \Delta G_0(\mathbf{r}_\parallel, z, z'; \mu + i\omega') d\omega' \\
&\approx \frac{1}{\pi}\left[\frac{1}{2}\int_{-\omega_{\max}}^{\omega_{\max}-\omega} \Delta G_0(\mathbf{r}_\parallel, z, z'; \mu + i\omega + i\omega') \Delta G_0(\mathbf{r}_\parallel, z, z'; \mu + i\omega') d\omega' \right. \\
&\qquad \left. \frac{1}{2}\int_{-\omega_{\max}+\omega}^{\omega_{\max}} \Delta G_0(\mathbf{r}_\parallel, z, z'; \mu - i\omega + i\omega') \Delta G_0(\mathbf{r}_\parallel, z, z'; \mu + i\omega') d\omega'\right] . \qquad (7.17)
\end{aligned}$$

The decomposition of the third term was made in order to keep the result symmetric for positive and negative frequencies ω, i.e., to ensure that $\Delta P_0(i\omega) = \Delta P_0(-i\omega)$ is valid. This expression can be obtained by inserting the frequency $-i\omega$ in the third summand and by taking into account ΔG_0 is assumed to be zero for frequencies $|\omega| > \omega_{\max}$. Equivalent to the first and the second summand, the two integrals are discretized and calculated using Simpson's rule.
All three numerical integrations include the Green function (or G_0^{hom} and ΔG_0, respectively,) on the real frequency axis, i.e. $G(\mu)$. Intrinsically, the Green function is not defined for real frequencies, and therefore in general a (positive or negative) infinitesimally imaginary part is added. However, I can define the Green function on the real frequency axis as the average of the two limits $\delta \to 0^+$ and $\delta \to 0^-$ of $G(\epsilon + i\delta)$, where ϵ and δ are real numbers. Since the Green function obeys the relation $G(\mu - i\omega) = G^*(\mu + i\omega)$, the real parts of the two Green functions which have to be averaged are the same, whereas the imaginary parts have just the opposite sign (but the same absolute values) and therefore its sum cancels out. Consequently, at the real energy μ it suffices to take either the real part of the Green function for positive frequencies or for negative frequencies and set the imaginary part to zero.

7.3.2 Two-dimensional Fourier transformation

So far I have presented the calculation of the difference ΔP_0 as a function of $\mathbf{r}_\parallel, z, z'$ and $i\omega$. Since for further calculations the polarization function as a function of $\mathbf{k}_\parallel$, z, z' and $i\omega$ is required, $\Delta P_0(\mathbf{r}_\parallel, z, z'; i\omega)$ — the result of the numerical convolution following eq. (7.9) — has to be Fourier transformed. The two-dimensional Fourier transform of $\Delta P_0(\mathbf{r}_\parallel, z, z'; i\omega)$ is calculated equivalently to the two-dimensional (inverse) Fourier transform of ΔG_0

$$\begin{aligned}\Delta P_0(\mathbf{k}_\parallel, z, z'; i\omega) &= \int d^2 r_\parallel e^{-i\mathbf{k}_\parallel \cdot \mathbf{r}_\parallel} \Delta P_0(\mathbf{r}_\parallel, z, z'; i\omega) \\ &= \int_0^\infty r_\parallel dr_\parallel \Delta P_0(r_\parallel, z, z'; i\omega) \int_0^{2\pi} d\phi\, e^{-ik_\parallel r_\parallel \cos\phi} \\ &= 2\pi \int_0^\infty r_\parallel \Delta P_0(r_\parallel, z, z'; i\omega) J_0(k_\parallel r_\parallel)\, dr_\parallel \ .\end{aligned} \tag{7.18}$$

This integral involves again $J_0(k_\parallel r_\parallel)$, the Bessel function of zeroth order and is evaluated numerically using Simpson's rule

$$\begin{aligned}\Delta P_0(\mathbf{k}_\parallel, z, z'; i\omega) \approx \frac{\Delta r_\parallel}{3} \Bigg[& 2 \sum_{j=1}^{\frac{n_{r_\parallel \max}}{2}-1} (2j\Delta r_\parallel) \Delta P_0(2j\Delta r_\parallel, z, z'; i\omega) J_0(2j\Delta r_\parallel k_\parallel) \\ & + 4 \sum_{j=0}^{\frac{n_{r_\parallel \max}}{2}-1} ((2j+1)\Delta r_\parallel) \Delta P_0((2j+1)\Delta r_\parallel, z, z'; i\omega) J_0((2j+1)\Delta r_\parallel k_\parallel) \\ & + r_{\parallel \max} \Delta P_0(r_{\parallel \max}, z, z'; i\omega) J_0(r_{\parallel \max} k_\parallel) \Big] \ .\end{aligned} \tag{7.19}$$

It involves the two convergence parameter $r_{\parallel \max}$ and $\Delta r_\parallel$, which will be determined in the next section.

7.3.3 Convergence parameters

The numerical evaluation of $\Delta P_0(\mathbf{k}_\parallel, z, z'; i\omega)$ involves several convergence parameters: First, the convolution over the complex frequency axis, i.e. the evaluation of (7.15), (7.16) and (7.17) includes the grid size $\Delta\omega$ as well as the maximal frequency $\omega_{\max}$. Secondly, for the numerical Fourier transformation (see eq. (7.18)) from $\Delta P_0(\mathbf{r}_\parallel)$ to $\Delta P_0(\mathbf{k}_\parallel)$ the sufficient maximal values for $r_\parallel$ and for the step size $\Delta r_\parallel$ have to be tested. Similarly to the determination of the numerical parameters for the Fourier transformation of the Green function (see chapter 6), all parameters will be investigated for the potential barrier and the quantum well with the largest positive ($V(z) = 0.15$) and negative ($V(z) = -0.1$) values of the potential.

Parameters involved in the convolution over the complex frequency axis The polarization function $\Delta P_0(\mathbf{r}_\parallel, z, z'; i\omega)$ for the potential barrier is displayed in figure

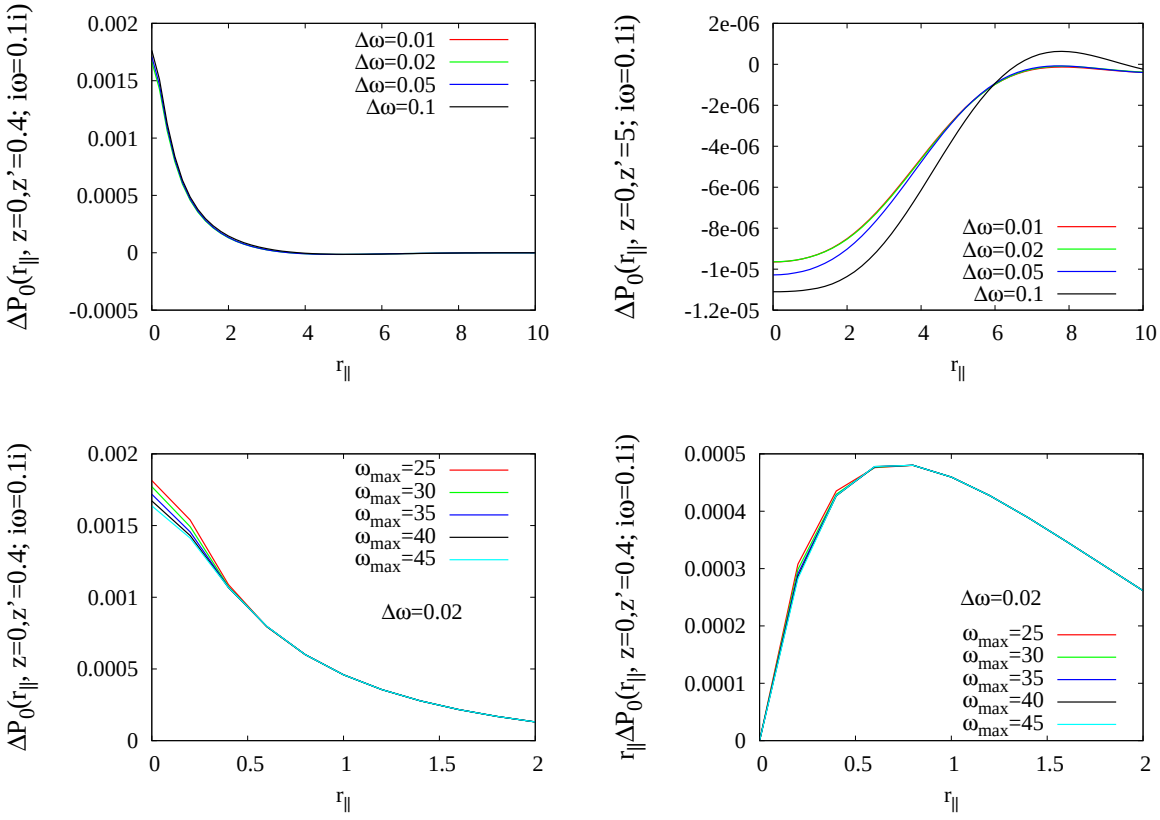

Figure 7.3: *Top:* $\Delta P_0(\mathbf{r}_\parallel, z, z'; i\omega)$ is shown as a function of $r_\parallel$ for different grid sizes $\Delta\omega$ and constant maximal frequency $\omega_{\max}$. Whereas z is situated in the center of the potential, the second spatial coordinate is set to $z' = 0.4$ (*left*) or $z' = 5.0$ (*right*). Although the absolute values of the curves for large distances $|z - z'|$ (*right*) are much smaller than for small ones (*left*), a higher resolution, i.e. a smaller $\Delta\omega$ is required. For $z' = 0.4$ only a marginal deviation of the curves for different values of $\Delta\omega$ can be observed. Thus, for both positions of z' an adequate choice is $\Delta\omega = 0.02$. *Bottom:* For the constant parameter $\Delta\omega = 0.02$ the maximal frequency $\omega_{\max}$ is varied between $\omega_{\max} = 25$ and $\omega_{\max} = 45$. Although the five curves for ΔP_0 (*left*) differ from each other for small values of $r_\parallel$, the multiplication with $r_\parallel$ (*right*) leads to a reduction of the difference of the curves. Since in the next step $r_\parallel \Delta P(r_\parallel)$ will be integrated to obtain $\Delta P_0(\mathbf{k}_\parallel = \mathbf{0})$, the maximal frequency $\omega = 40$ suffices for an adequate convergence.

7.3 as a function of $r_\parallel$ for different values of $\Delta\omega$ and $\omega_{\max}$. As one can see, an adequate convergence is achieved for $\Delta\omega = 0.02$ and $\omega_{\max} = 40$. The curves corresponding to different parameters $\Delta\omega$ (see the two upper plots in figure 7.3) are compared for the constant frequency $\omega = 0.1$ which is the lowest common multiple of the chosen values of $\Delta\omega$. In the limit of small frequencies ω (i.e. for frequencies much smaller

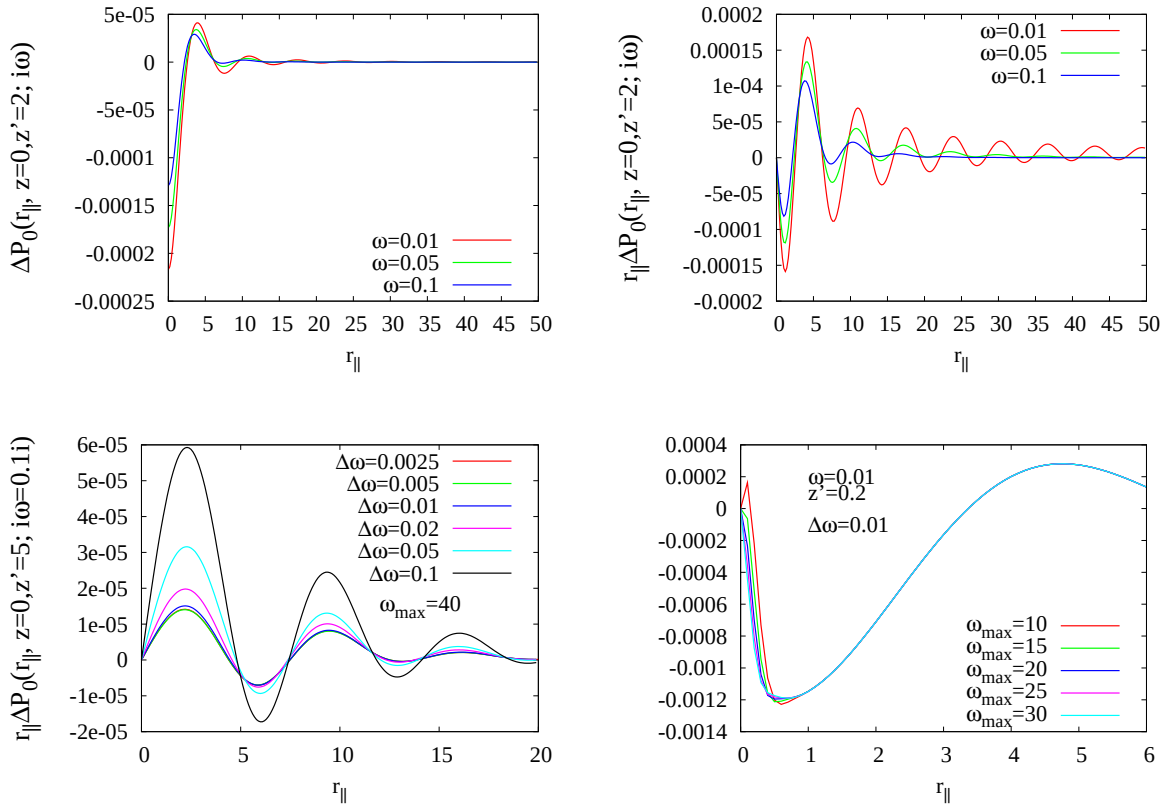

Figure 7.4: *Top:* $\Delta P_0(\mathbf{r}_\parallel)$ and $r_\parallel \Delta P_0(\mathbf{r}_\parallel)$, the integrand of the two-dimensional Fourier transformation, for the quantum well for different values of ω. For frequencies in the vicinity of 0, $\Delta P_0(\mathbf{r}_\parallel)$ (or $r_\parallel \Delta P_0(\mathbf{r}_\parallel)$, respectively,) oscillate strongly and decay much slower to zero than for higher frequencies. *Bottom:* Determination of the convergence parameters $\Delta\omega$ (*left*) and $\omega_{\max}$ (*right*) for the convolution on the complex frequency for the quantum well. Compared to the potential barrier, the parameter $\Delta\omega$ has to be chosen much smaller, i.e. $\Delta\omega = 0.005$ (instead of $\Delta\omega = 0.02$ for the potential barrier). As far as the parameter $\omega_{\max}$ is concerned, an adequate convergence is reached for $\omega_{\max} \approx 30$.

than $\omega_{\max}$) the required convergence parameters $\Delta\omega$ and $\omega_{\max}$ merely depend on the frequency at which ΔP_0 is compared, since the frequency ω shifts only the limits of the Green function G_0^{hom} (see section 7.1).
In the plot on the right side of the bottom of figure 7.3 the polarization function ΔP_0 is multiplied with $r_\parallel$. This multiplication was made having in mind already the next step, which is the two-dimensional Fourier transformation of ΔP_0 to reciprocal space. According to eq. (7.18), ΔP_0 is multiplied with $r_\parallel$ and the Bessel function $J_0(r_\parallel k_\parallel)$. Since I am interested in $\Delta P_0(\mathbf{k}_\parallel = \mathbf{0})$ only, the Bessel function simplifies to 1 and the Fourier transformation reduces to an integration over the function $r_\parallel \Delta P_0(r_\parallel)$. The function $r_\parallel \Delta P_0(r_\parallel)$ decays much slower to 0 than $\Delta P_0(r_\parallel)$ itself and reveals

the oscillating behavior of $\Delta P_0(r_\parallel)$ as a function of $r_\parallel$. Of course, this oscillating behavior depends strongly on the complex frequency at which ΔP_0 (or $r_\parallel \Delta P_0(r_\parallel)$, respectively,) is considered. This can be observed in the two plots at the top of figure 7.4, where $\Delta P_0(r_\parallel)$ and $r_\parallel \Delta P_0(r_\parallel)$ are shown for different frequencies for the quantum well. For the calculations I have used the convergence parameters $\Delta\omega$ and $\omega_{\max}$ for the quantum well which are tested in the two plots at the bottom of figure 7.4. There, $r_\parallel \Delta P(r_\parallel)$ is displayed for different parameters $\Delta\omega$ (left side) and $\omega_{\max}$ (right side) as a function of $r_\parallel$. As the comparison for the potential barrier has revealed that the convergence is worse for larger $|z - z'|$ (see figure 7.3), one of the z coordinates was chosen to be in the center of the potential $z = 10$ and the other at $z' = 5$. Whereas in the case of the potential barrier an adequate convergence is reached for $\Delta\omega = 0.02$, for the quantum well a smaller step size is required. Although the reduction of $\Delta\omega$ is very expensive, for all further calculations for the quantum well $\Delta\omega = 0.005$ is used. In contrast, the maximal frequency $\omega_{\max}$ can be reduced to $\omega_{\max} \approx 30$, which is much smaller than the maximal frequency for the potential barrier $\omega_{\max} \approx 40$.

Convergence parameters of the two-dimensional Fourier transformation The two-dimensional Fourier transformation of the polarization function $\Delta P_0(r_\parallel, z, z'; i\omega)$ to the representation $\Delta P_0(\mathbf{k}_\parallel = \mathbf{0}, z, z'; i\omega)$ is evaluated numerically using Simpson's rule according to eq. (7.19). It involves again two numerical parameters, $\Delta r_\parallel$ and $r_{\parallel\max}$ which are determined in the following. As one can recognize in figure 7.4, it is very important at which frequency the check of the parameters is done: The integrand of the numerical integration $r_\parallel \Delta P_0(r_\parallel)$ is most structured and has the slowest decay for frequencies close to the real frequency axis. Since in my implementation I can calculate $\Delta P_0(\mathbf{k}_\parallel = \mathbf{0}, z, z'; i\omega)$ only for frequencies on a grid which is determined by the choice of $\Delta\omega$ of the convolution on the complex frequency axis, the smallest possible frequency amounts to $\omega = 0.02$ for the potential barrier and to $\omega = 0.005$ for the quantum well. In order to treat both potentials similarly, I will test the convergence for the lowest common multiple $\omega = 0.02$. (Though possible for the quantum well, from now on I will not regard $\Delta P_0(\mathbf{k}_\parallel = \mathbf{0}, z, z'; i\omega)$ for frequencies smaller than $\omega = 0.02$.) The results of $\Delta P_0(\mathbf{k}_\parallel = \mathbf{0}, z, z'; i\omega)$ as a function of z with z' centered in the potential are presented in figure 7.5 for different parameters $\Delta r_\parallel$ and $r_{\parallel\max}$. For the determination of the parameters I ignore the point at which the two z coordinates are the same, i.e. $z = z' = 0$. As I will demonstrate in section 7.3.4, it is very difficult to achieve convergence at this special point and therefore it will be treated in a different way. For all other z coordinates an adequate convergence concerning $\Delta r_\parallel$ is reached both for the potential barrier and the quantum well for $\Delta r_\parallel = 0.2$. In contrast, the maximal $r_{\parallel\max}$ has to be chosen differently for the two potentials. Whereas for the quantum barrier convergence is reached for $r_{\parallel\max} \approx 40$, for the quantum well a higher $r_{\parallel\max} \approx 50$ is required.

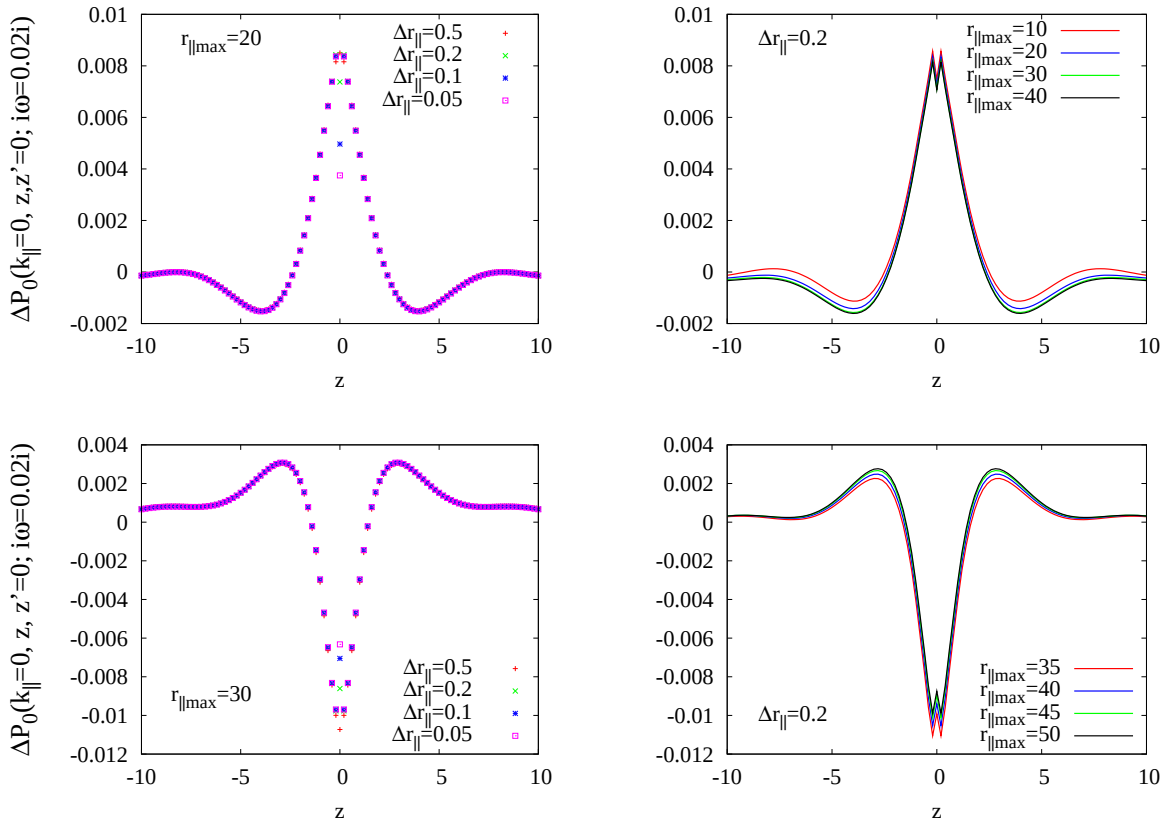

Figure 7.5: Determination of the convergence parameters $\Delta r_\parallel$ and $r_{\parallel\max}$ for the potential barrier (*top*) and the quantum well (*bottom*). In all four figures the polarization function $\Delta P_0(\mathbf{k}_\parallel = \mathbf{0}, z, z' = 0; i\omega)$ is presented as a function of z for constant $z' = 0$. On the left side, the parameter $\Delta r_\parallel$ is varied. An adequate convergence is reached both for the potential barrier and the quantum well for $\Delta r_\parallel = 0.2$. In contrast, the maximal $r_\parallel$ (*right*) has to be chosen differently for the two potentials: Whereas $r_{\parallel\max} \approx 40$ suffices for the potential barrier, for the quantum well convergence is reached not until $r_{\parallel\max} \approx 50$.

7.3.4 Extrapolation to $z = z'$

I will now consider the point $z = z'$ which was neglected so far. As one can observe in figure 7.5, the enhancement of the number of $r_\parallel$ does not lead to a better convergence — in contrast, both the enhancement of $r_{\parallel\max}$ for constant $\Delta r_\parallel$ and the downsizing of $\Delta r_\parallel$ at constant $r_{\parallel\max}$ changes the result for the worse. Furthermore, since the Green function $\Delta G_0(\mathbf{r}_\parallel, z, z'; \mu + i\omega)$ for the parameter $k_{\parallel,\max} = 10$ is almost converged at $z = z'$ (see figure 6.6 and 6.7), I conclude that in order to obtain convergence the parameters of the numerical convolution on the complex frequency axis have to be enhanced. 7.3.3. This assumption can be verified easily by calculating the polarization function for parameters $\omega_{\max}$ much larger than the maximal

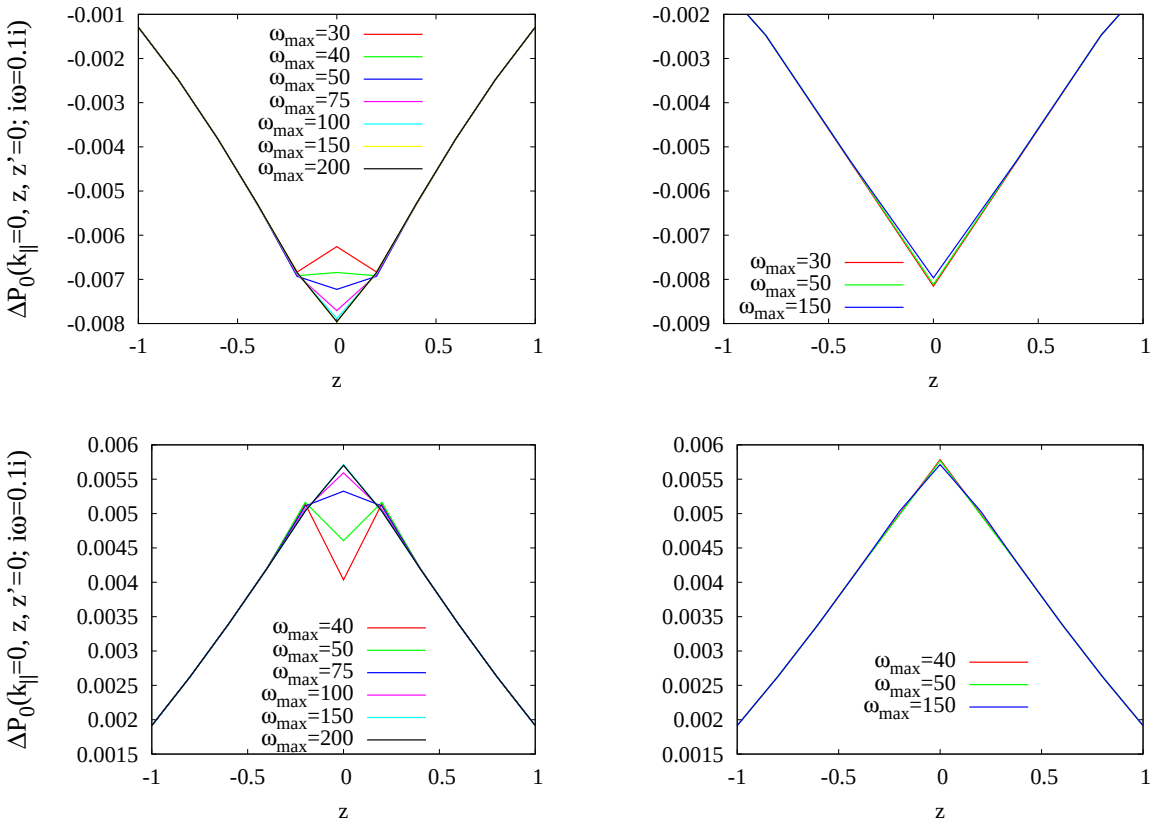

Figure 7.6: Polarization function ΔP_0 for the quantum well (*top*) and the potential barrier (*bottom*). On the left side, ΔP_0 is shown for different parameters $\omega_{\max}$ of the convolution of the complex frequency axis, whereas on the right side the extrapolated points are compared to the converged results. *Top right:* The extrapolated points from the results obtained for the parameters $\omega_{\max} = 30$ and $\omega_{\max} = 50$ are slightly too small in comparison to the converged result for $\omega_{\max} = 150$. *Bottom right:* For the potential barrier, the agreement of the extrapolated points ($\omega_{\max} = 40$ and $\omega_{\max} = 50$) with the converged result ($\omega_{\max} = 150$) is even better than for the quantum well.

frequency $\omega_{\max} = 30$ determined in section 7.3.3. In figure 7.6 the polarization function $\Delta P_0(\mathbf{k}_\parallel = \mathbf{0}, z, z'; i\omega)$ is displayed as a function of z for different values of $\omega_{\max}$, starting from $\omega_{\max} = 30$ for the quantum well and $\omega_{\max} = 40$ for the potential barrier, respectively. Although convergence is reached for $\omega_{\max} \approx 150$, it is not a practical solution to deal with these high maximal values $\omega_{\max}$ since it makes the calculations very expensive. Thus, another way was found to deal with the point $z = z'$ exploiting the fact that the gradient close to $z = z'$ is approximately linear. I will extrapolate the point $z = z'$ from its neighboring points, i.e.

$$\Delta P_0(\mathbf{k}_\parallel, z, z; i\omega) \approx 2\Delta P_0(\mathbf{k}_\parallel, z, z - \Delta z; i\omega) - \Delta P_0(\mathbf{k}_\parallel, z, z - 2\Delta z; i\omega) \; . \qquad (7.20)$$

For the final calculation the grid size Δz will be chosen larger than it was the case in the calculations presented until here, where it amounted to $\Delta z = 0.2$. Extrapolation of $\Delta P(z, z)$ at $z = 0$ for $\Delta z = 0.4$ from the two values $\Delta P(0, -0.4)$ and $\Delta P_0(0, -0.2)$ for $\omega_{\max} = 50$ and $\omega_{\max} = 30$ for the quantum well (or $\omega_{\max} = 40$ for the potential barrier) yields

$\Delta P(z, z)$	$\omega_{\max} = 150$	$\omega_{\max} = 50$	$\omega_{\max} = 30(40)$
quantum well	$-0.7966 \cdot 10^{-2}$	$-0.8114 \cdot 10^{-2}$	$-0.8154 \cdot 10^{-2}$
potential barrier	$0.5714 \cdot 10^{-2}$	$0.5768 \cdot 10^{-2}$	$0.5784 \cdot 10^{-2}$

In the second column the converged (and not extrapolated) results obtained with $\omega_{\max} = 150$ are presented. The results of the extrapolation are compared graphically to the converged results on the right side of figure 7.6. As one can recognize in the table as well as in figure 7.6, the extrapolated values slightly differ from the converged result. Although the relative deviation amounts to approximately two percent for the quantum well and one percent for the potential barrier it is accepted in favor of a significantly shorter calculation time. Having now all ingredients together, the total polarization function can be calculated.

7.4 Total polarization function

According to eq. (7.10), the total polarization function $P_0(\mathbf{k}_\parallel, z, z'; i\omega)$ is given as the sum

$$P_0(\mathbf{k}_\parallel, z, z'; i\omega) = P_0^{\text{hom}}(\mathbf{k}_\parallel, z, z'; i\omega) + \Delta P_0(\mathbf{k}_\parallel, z, z'; i\omega) \; . \tag{7.21}$$

In figure 7.7, P_0 is presented together with its two constituents $P_0^{\text{hom}}(\mathbf{k}_\parallel, z, z'; i\omega)$ and $\Delta P_0(\mathbf{k}_\parallel, z, z'; i\omega)$ both for the potential barrier and the quantum well. Whereas for

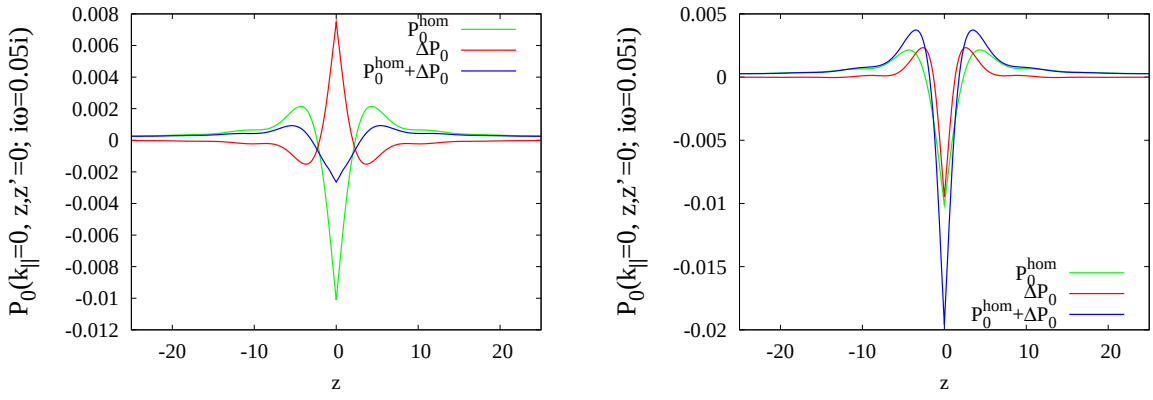

Figure 7.7: The polarization function P_0 and its two compounds ΔP_0 and P_0^{hom} for the potential barrier (*left*) and the quantum well (*right*).

the quantum well the polarization is enhanced compared to the polarization function of the homogeneous electron gas, in the case of the potential barrier ΔP_0 has the opposite sign of P_0^{hom} and the total polarization is reduced. This is quite reasonable, since the density in the quantum well is expected to behave equivalently: Classically the electrons are not allowed to be located in the region of the potential barrier, whereas the probability for the electrons to be in the region of the quantum well is classically expected to be larger than in the leads. The density of the two potentials is discussed in the following section.
In figure 7.8 the total polarization function P_0 as well as the remainder ΔP_0 is shown for all potentials presented in section 5.1. It can be observed that the diminution of the potential from positive potentials (potential barriers) as well as from negative potentials (quantum wells) results in the approach of the polarization function to that of the homogeneous electron gas with $V = 0$.
Compared to previous calculations, I have extended the investigated region in order

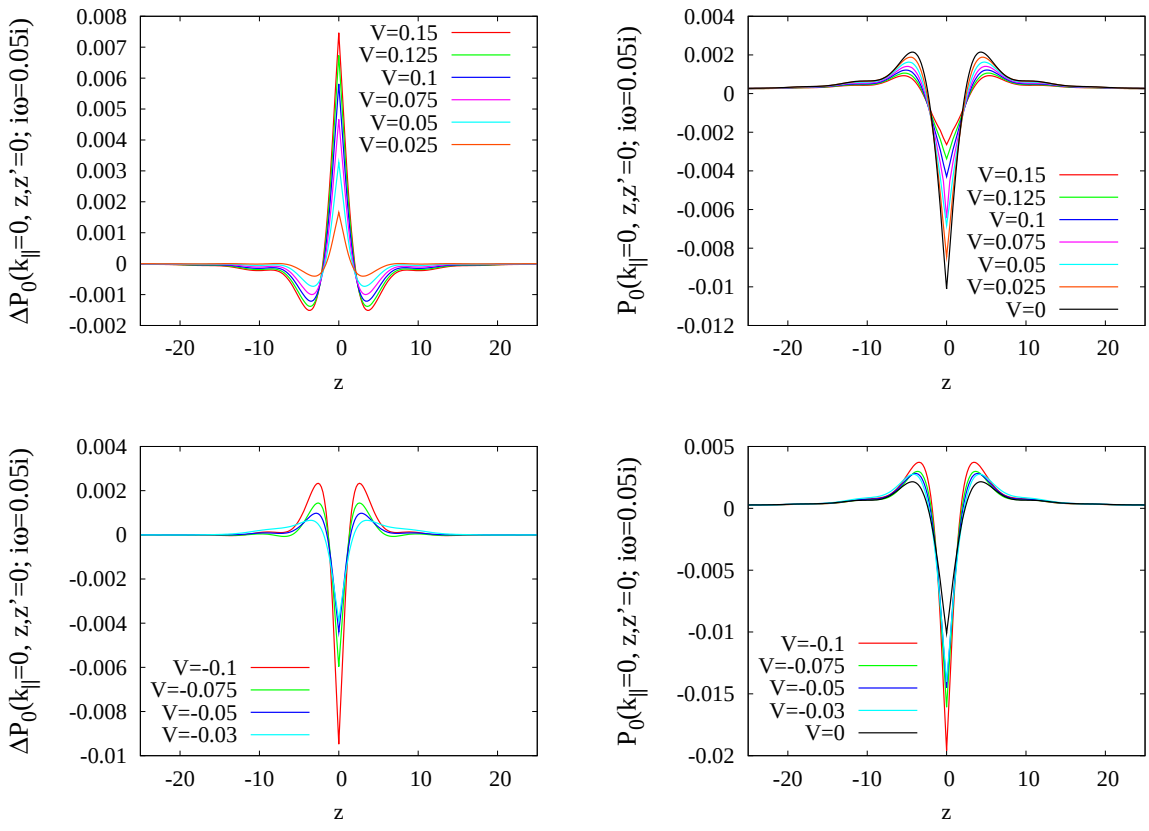

Figure 7.8: Polarization function ΔP_0 (*left*) and P_0 (*right*) for the potentials presented in section 5.1. In the two plots at the top, the potential has the nature of a potential barrier, (thus $V \geq 0$) whereas in the bottom the polarization function for different quantum wells ($V \leq 0$) is presented.

to observe the decay of $\Delta P_0(z)$ as a function of z and to estimate the interval in which $\Delta P_0(z)$ differs from zero. This is important to know, since the calculations both of the conductance and the irreducible polarization include integrations over the z axis. One can already see, that $\Delta P_0(z)$ decays slower for the potential barriers than for the quantum wells and therefore for the former broader intervals are needed. While the exact length of the required intervals will be tested in chapter 8, it seems that the interval chosen in figure 7.8 is sufficient. Furthermore, it can be observed that $\Delta P_0(z)$ decays much faster on the z axis than $P_0(z)$ itself.

7.5 Density

The aim of this chapter is the calculation of the irreducible polarization. As presented in section 3.10 it depends on the exchange-correlation kernel, which is a function of the electron density. Hence, I need to calculate the density, which will be the subject of this section.
The density of a system can be calculated with the help of the imaginary part of the retarded Green function $G_0(\mathbf{r}_\parallel = 0, z, z; \epsilon)$, which is proportional to the energy-dependent density of states

$$n(z;\epsilon) = -2\frac{1}{\pi}\,\mathrm{Im}\,G_0(\mathbf{r}_\parallel = 0, z, z; \epsilon)\ . \tag{7.22}$$

The density of states is then obtained by integrating $n(z;\epsilon)$ over the real frequency axis up to to the chemical potential μ

$$n(z) = \int_{-\infty}^{\mu} n(z;\epsilon)d\epsilon\ . \tag{7.23}$$

In order to prove the relation (7.22) I write the Green function in the Lehmann representation (compare eq. (3.21))

$$G_0(\mathbf{r}_\parallel, z, z'; \epsilon) = \sum_j \frac{\psi_j(\mathbf{r}_{\parallel,1}, z)\psi_j^*(\mathbf{r}_{\parallel,2}, z')}{\epsilon - \epsilon_j + i\eta}$$

with $\mathbf{r}_\parallel = \mathbf{r}_{\parallel,1} - \mathbf{r}_{\parallel,2}$. The wave functions $\psi_j(\mathbf{r}_\parallel, z)$ are eigenfunctions with the corresponding eigenvalues ϵ_j. Using the Dirac identity

$$\lim_{\eta\to 0^+}\frac{1}{x \mp i\eta} = P\left(\frac{1}{x}\right) \pm i\pi\delta(x)\ , \tag{7.24}$$

where P denotes the principal value, one can rewrite the imaginary part of the diagonal elements of $G_0(\mathbf{r}_\parallel = \mathbf{0}, z, z; \epsilon)$ as

$$\begin{aligned}\mathrm{Im}\,G_0(\mathbf{r}_\parallel = \mathbf{0}, z, z; \epsilon) &= \sum_j \left|\psi_j(\mathbf{r}_\parallel, z)\right|^2 \mathrm{Im}\lim_{\eta\to+0}\frac{1}{\epsilon - \epsilon_j + i\eta}\\ &= -\pi\sum_j \left|\psi_j(\mathbf{r}_\parallel, z)\right|^2 \delta(\epsilon - \epsilon_j)\\ &= -\frac{\pi}{2}n(z;\epsilon)\ .\end{aligned} \tag{7.25}$$

Since the validity of eq. (7.22) is proved I can insert it in eq. (7.23) and obtain the electron density

$$\begin{aligned} n(z) &= \int_{-\infty}^{\mu} n(z,\epsilon) d\epsilon \\ &= -\frac{2}{\pi} \int_{-\infty}^{\mu} \operatorname{Im} G_0(\mathbf{r}_\parallel = \mathbf{0}, z, z; \epsilon) d\epsilon \\ &= -\frac{2}{\pi} \int_{-\infty}^{\mu} \left(\frac{1}{2\pi} \int_0^{\infty} \operatorname{Im} G_0(\mathbf{k}_\parallel, z, z; \epsilon) k_\parallel dk_\parallel \right) d\epsilon \ . \end{aligned} \tag{7.26}$$

In the last step I have inserted the two-dimensional Fourier representation of $G_0(\mathbf{r}_\parallel = \mathbf{0}, z, z; \epsilon)$ as derived in eq. (6.29) and exploited the fact that the Bessel function reduces to 1 for $r_\parallel = \mathbf{0}$. Interchanging the order of the two integrations $n(z)$ results in

$$n(z) = -\frac{1}{\pi^2} \int_0^{\infty} \left(\int_{-\infty}^{\mu} \operatorname{Im} G_0(\mathbf{k}_\parallel, z, z; \epsilon) d\epsilon \right) k_\parallel dk_\parallel \ . \tag{7.27}$$

Although the integral over the real frequency axis has the lower limit $-\infty$, it suffices (for all potentials) to integrate from -0.1 to the chemical potential 0.1, since for lower energies there are no allowed states and therefore the imaginary part of the Green function is zero. However, the integration over the real energy axis is not easy to perform because the poles are situated close to the real frequency axis at energies $\epsilon - i\eta$. For $\operatorname{Re}\epsilon < \mu$, the Green function has no poles in the upper half-plane and therefore each closed integral results in 0. This fact can be exploited for the calculation of the integral choosing an integration contour as shown in figure 7.9. Since the total integral along the contour amounts to zero, the contribution of the upper semicircle must have the same absolute value and the opposite sign of the integral over the real

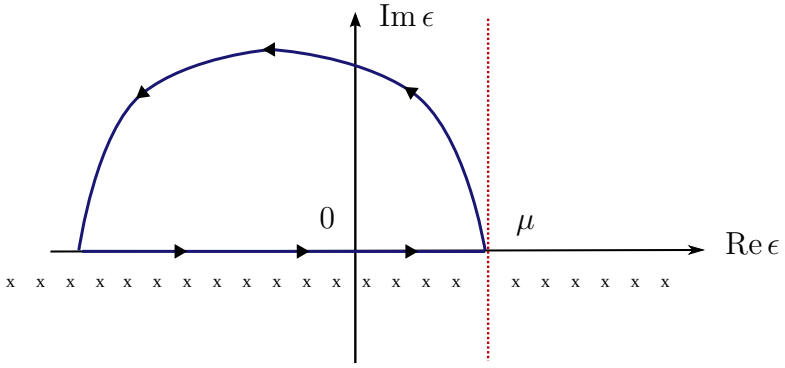

Figure 7.9: Integration contour for the calculation of the density together with the poles of the retarded Green function. The integral over the real frequency axis is the negative of the integral of the semi-circle, since there are no poles inside the contour and therefore the integral must amount to zero.

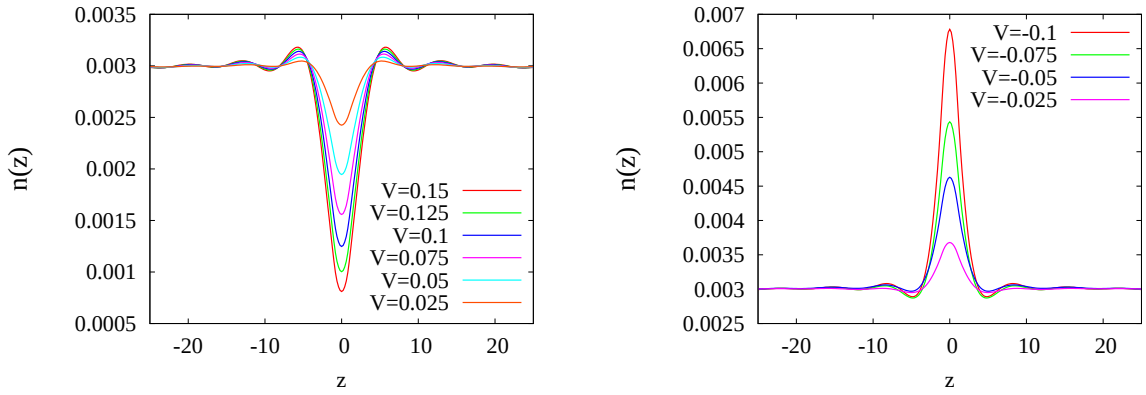

Figure 7.10: Electronic density of the potential barrier (*left*) and the quantum well (*right*) for different strengths of the potential as a function of z. For z coordinates far away from the center of the potential, the densities of all potentials approach the density of the homogeneous electron gas $n = (2\mu)^{3/2}/(3\pi^2) = 0.0030$ for the chemical potential $\mu = 0.1$. Whereas the density of the quantum wells in the vicinity of the center of the potential ($z = 0$) is enhanced compared to the density in the leads, it is reduced for the quantum barriers.

frequency axis. The integral along the semi-circle can be easily parametrized and the density is obtained by calculating the negative of the contribution of the upper semi-circle. For the numerical calculation it is sufficient to take 31 points on the integration contour, since the Green function – which now is evaluated at points which are not close to poles – has not much structure. Moreover, the Fourier transform was calculated numerically with the same convergence parameters as determined for the Fourier transformation of $\Delta G_0(\mathbf{k}_\parallel, z, z'; \mu + i\omega)$ to $\Delta G_0(\mathbf{r}_\parallel, z, z'; \mu + i\omega)$.
The resulting densities for the quantum well and the potential barrier for different values of V are displayed in figure 7.10. As one can observe for z coordinates far away from the potential the density of all potentials converge to a constant value which is the density of the homogeneous electron gas of the leads. Its value is determined by the chemical potential μ, since the number of particles N in a volume V is related to the radius of the Fermi sphere according to

$$N = 2\frac{V}{(2\pi)^3}\frac{4}{3}\pi k_\mathrm{F}^3 \; . \tag{7.28}$$

The factor two arises because each state can be occupied by two electrons (with different spin). Since $\mu = \frac{1}{2}k_\mathrm{F}^2$, the density of the homogeneous electron gas results in

$$n = \frac{N}{V} = \frac{(2\mu)^{3/2}}{3\pi^2} \; . \tag{7.29}$$

7.6 Irreducible polarization function

I have now all ingredients to calculate the irreducible polarization function which includes exchange and correlation effects via the exchange-correlation kernel. Therefore in the first part details of the numerical calculation are presented, followed by the determination of the involved convergence parameters (for the homogeneous electron gas). Finally, the numerical results for the potential barrier and the quantum well are presented.

7.6.1 Numerical calculation

In chapter 3 the Dyson-type equation (3.49), which relates the irreducible polarization P to the polarization P_0 was presented

$$P(\mathbf{r},\mathbf{r}';\omega) = P_0(\mathbf{r},\mathbf{r}';\omega) + \int d^3r'' \int d^3r''' P_0(\mathbf{r},\mathbf{r}'';\omega) f_{\mathrm{xc}}(\mathbf{r}'',\mathbf{r}''';\omega) P(\mathbf{r}''',\mathbf{r}';\omega) \; .$$

I will calculate now the former (P) with the exchange-correlation kernel $f_{\mathrm{xc}}^{\mathrm{ALDA}}(\mathbf{r},\mathbf{r}';\omega)$ in the ALDA. Since eq. (3.49) is not very convenient for practical implementation, I define a renormalization function

$$\varepsilon(\mathbf{k}_\parallel, z, z'; i\omega) = \delta(z-z') - \int_{-\infty}^{\infty} f_{\mathrm{xc}}(\mathbf{k}_\parallel, z, z'', i\omega) P_0(\mathbf{k}_\parallel, z'', z'; i\omega)\, dz'' \; . \tag{7.30}$$

With its inverse $\varepsilon^{-1}(\mathbf{k}_\parallel, z, z'; i\omega)$ given by

$$\int_{-\infty}^{\infty} \varepsilon(\mathbf{k}_\parallel, z, z''; i\omega) \varepsilon^{-1}(\mathbf{k}_\parallel, z'', z'; i\omega)\, dz'' = \delta(z-z') \; , \tag{7.31}$$

the irreducible polarization can be rewritten as

$$P(\mathbf{k}_\parallel, z, z'; i\omega) = \int_{-\infty}^{\infty} P_0(\mathbf{k}_\parallel, z, z''; i\omega) \varepsilon^{-1}(\mathbf{k}_\parallel, z'', z'; i\omega)\, dz'' \; . \tag{7.32}$$

In the ALDA, the exchange-correlation kernel $f_{\mathrm{xc}}(\mathbf{k}_\parallel, z, z'; i\omega)$ is local, i.e., it depends on z via the electron density $n(z)$ only. Thus, introducing the approximation

$$f_{\mathrm{xc}}(\mathbf{k}_\parallel, z, z'; i\omega) \approx f_{\mathrm{xc}}^{\mathrm{ALDA}}(n(z)) \delta(z-z') \tag{7.33}$$

in eq. (7.30), the integral can be solved analytically and the calculation of the renormalization function reduces to a simple product

$$\varepsilon(\mathbf{k}_\parallel, z, z'; i\omega) = \delta(z-z') - f_{\mathrm{xc}}^{\mathrm{ALDA}}(n(z)) P_0(\mathbf{k}_\parallel, z, z'; i\omega) \; . \tag{7.34}$$

The inversion of $\varepsilon(\mathbf{k}_\parallel, z, z'; i\omega)$ involves an integration over the whole z axis. However, the integration can be restricted to a finite interval since the inverse of the renormalization function is required in a finite volume only and the renormalization

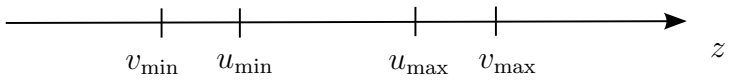

Figure 7.11: Demonstration of the intervals which are important for the inversion of the renormalization function. Whereas the inverse is calculated in the outer interval $[v_{\min}, v_{\max}]$, finite-size effects cause that the inverse is correct in the inner interval $[u_{\min}, u_{\max}]$ only. The differences $v_{\max} - u_{\max}$ and $u_{\min} - v_{\min}$ have to be chosen big enough that the renormalization function is zero when one z argument is located in the inner interval and the other argument is outside the outer window.

function decays to zero for increasing distances $|z - z'|$. In the following I denote the interval in which I want to calculate $\varepsilon^{-1}(\mathbf{k}_\parallel, z, z'; i\omega)$ with $[u_{\min}, u_{\max}]$. Furthermore I define an interval $[v_{\min}, v_{\max}]$ with $[u_{\min}, u_{\max}] \subset [v_{\min}, v_{\max}]$, which has to be chosen such that $\varepsilon(\mathbf{k}_\parallel, z, z'; i\omega) = 0$ for all $z \in [u_{\min}, u_{\max}]$ and z' outside of $[v_{\min}, v_{\max}]$ (see figure 7.11). Under this condition it can be proved [FBM04] that the inverse of $\varepsilon(\mathbf{k}_\parallel, z, z'; i\omega)$ calculated in the interval $[v_{\min}, v_{\max}]$ equals the 'correct' inverse (inverted in the infinite interval) in the subset $[u_{\min}, u_{\max}]$. The extent of the interval $[v_{\min}, v_{\max}]$ is a numerical parameter, which will be determined in the next section. The calculation of the inverse $\varepsilon^{-1}(\mathbf{k}_\parallel, z, z'; i\omega)$ following eq. (7.31) can be simplified in another way, too, exploiting that $\varepsilon(\mathbf{k}_\parallel, z, z'; i\omega)$ is composed of a delta function and a remainder — therefore, I can assume that its inverse is composed equivalently, thus

$$\varepsilon^{-1}(\mathbf{k}_\parallel, z, z'; i\omega) = \delta(z - z') + \Delta\varepsilon^{-1}(\mathbf{k}_\parallel, z, z'; i\omega)\,. \tag{7.35}$$

In this case the integral on the left-hand side of eq. (7.31) can be rewritten as

$$\begin{aligned}
&\int_{-\infty}^{\infty} \left[\delta(z - z'') - f_{\mathrm{xc}}^{\mathrm{ALDA}}(n(z)) P_0(\mathbf{k}_\parallel, z, z''; i\omega)\right] \left[\delta(z'' - z') + \Delta\varepsilon^{-1}(\mathbf{k}_\parallel, z'', z'; i\omega)\right] dz'' \\
&= \delta(z - z') - f_{\mathrm{xc}}^{\mathrm{ALDA}}(n(z)) P_0(\mathbf{k}_\parallel, z, z'; i\omega) + \Delta\varepsilon^{-1}(\mathbf{k}_\parallel, z, z'; i\omega) \\
&\qquad - \int_{-\infty}^{\infty} f_{\mathrm{xc}}^{\mathrm{ALDA}}(n(z)) P_0(\mathbf{k}_\parallel, z, z''; i\omega) \Delta\varepsilon^{-1}(\mathbf{k}_\parallel, z'', z'; i\omega)\, dz''
\end{aligned} \tag{7.36}$$

and eq. (7.31) simplifies to

$$\begin{aligned}
\Delta\varepsilon^{-1}(\mathbf{k}_\parallel, z, z'; i\omega) - \int_{-\infty}^{\infty} f_{\mathrm{xc}}^{\mathrm{ALDA}}(n(z)) P_0(\mathbf{k}_\parallel, z, z''; i\omega) \Delta\varepsilon^{-1}(\mathbf{k}_\parallel, z'', z'; i\omega)\, dz'' \\
= f_{\mathrm{xc}}^{\mathrm{ALDA}}(n(z)) P_0(\mathbf{k}_\parallel, z, z'; i\omega)\,.
\end{aligned} \tag{7.37}$$

For constant $\mathbf{k}_\parallel$ and constant $i\omega$, the remaining integral can be approximated by a sum over an equidistant discrete mesh. The expression on the left-hand side can then be written in the form of a matrix multiplication, which yields

$$\left[1 - \Delta z f_{\mathrm{xc}}^{\mathrm{ALDA}} P_0(\mathbf{k}_\parallel; i\omega)\right] \Delta\varepsilon^{-1}(\mathbf{k}_\parallel; i\omega) = f_{\mathrm{xc}}^{\mathrm{ALDA}} P_0(\mathbf{k}_\parallel; i\omega)\,. \tag{7.38}$$

Hence, $\Delta\varepsilon^{-1}(\mathbf{k}_\parallel; i\omega)$ is given as the solution of a system of linear equations.
The decomposition of ε^{-1} in a delta function and a remainder $\Delta\varepsilon^{-1}$ can also be used for the following calculation of the irreducible polarization according to eq. (7.32)

$$P(\mathbf{k}_\parallel, z, z'; i\omega) = P_0(\mathbf{k}_\parallel, z, z'; i\omega) + \int_{-\infty}^{\infty} P_0(\mathbf{k}_\parallel, z, z''; i\omega)\Delta\varepsilon^{-1}(\mathbf{k}_\parallel, z'', z'; i\omega)\, dz'' \,. \tag{7.39}$$

The last integral can be evaluated (for constant $\mathbf{k}_\parallel$ and $i\omega$) as a matrix multiplication of $P_0(\mathbf{k}_\parallel; i\omega)$ and $\varepsilon^{-1}(\mathbf{k}_\parallel; i\omega)$ multiplied by the step size Δz

$$P(\mathbf{k}_\parallel; i\omega) = P_0(\mathbf{k}_\parallel; i\omega) + \Delta z P_0(\mathbf{k}_\parallel; i\omega)\Delta\varepsilon^{-1}(\mathbf{k}_\parallel; i\omega) \,. \tag{7.40}$$

Similarly to the integration (or inversion, respectively,) for the calculation of $\varepsilon^{-1}(\mathbf{k}_\parallel, z, z'; i\omega)$ I have restricted the integration over the z axis to a finite interval. This restriction can be justified regarding the fact that the irreducible polarization is needed in a finite volume only. Nevertheless, in order to avoid effects which are due to the finite size of the integration interval, it has to be chosen larger than the interval in which the irreducible polarization has to be calculated. Again, the size of the integration interval is a numerical parameter which has to be chosen appropriately.

7.6.2 Homogeneous electron gas

I will now present the renormalization function, its inverse and the irreducible polarization of the homogeneous electron gas. Furthermore, I determine the involved convergence parameters. Although these parameters are obtained for the homogeneous electron gas, they will be used for the calculations of the corresponding functions for all investigated potentials. Thus, I assume that they do not change for the different potentials. This assumption can be justified by looking at the polarization functions presented in figure 7.8: They differ in a finite region only, and they decay in the same way for large $|z - z'|$.

Renormalization function For the homogeneous electron gas with $V = \text{const.}$ both the density and the exchange-correlation kernel are constant everywhere. The latter amounts to $f_{\text{xc}}^{\text{ALDA}} = -19.10$ for the chemical potential $\mu = 0.1$. As expected, the exchange part $f_{\text{x}}^{\text{ALDA}} = -15.71$ yields a larger contribution than the correlation part with $f_{\text{c}}^{\text{ALDA}} = -3.39$. The renormalization function is simply given as the sum of the delta function $\delta(z - z')$ and the polarization function of the homogeneous electron gas multiplied by the constant $-f_{\text{xc}}^{\text{ALDA}}$ (see eq. (7.34)). $\Delta\varepsilon(\mathbf{k}_\parallel, z, z'; i\omega) = -f_{\text{xc}}^{\text{ALDA}} P(\mathbf{k}_\parallel, z, z'; i\omega)$ is depicted in figure 7.12.

Inverse renormalization function The inversion of the renormalization function involves two numerical parameters. In addition to the grid size Δz, I need to determine the size of the interval used to integrate $\Delta\varepsilon(\mathbf{k}_\parallel, z, z'; i\omega)$. Since all other functions like the polarization and the renormalization function were calculated in

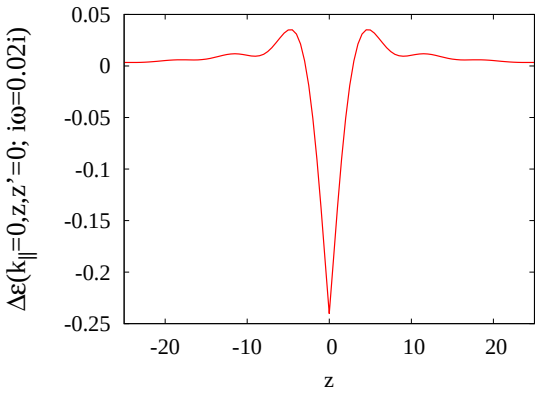

Figure 7.12: Renormalization function (or $\Delta\varepsilon(\mathbf{k}_\parallel, z, z'; i\omega) = \varepsilon(\mathbf{k}_\parallel, z, z'; i\omega) - \delta(z - z')$, respectively,) for the homogeneous electron gas with $\mu = 0.1$.

the interval $[-25, 25]$, I want to calculate $\varepsilon^{-1}(\mathbf{k}_\parallel, z, z'; i\omega)$ in this interval as well. Therefore I have to evaluate all functions calculated previously in a larger interval $[-25 - d_{\text{inv}}, 25 + d_{\text{inv}}]$ since the region in which $\varepsilon(\mathbf{k}_\parallel, z, z'; i\omega)$ is inverted is larger than the interval in which it leads to a correct result for $\varepsilon^{-1}(\mathbf{k}_\parallel, z, z'; i\omega)$. On the left side of figure 7.13 $\Delta\varepsilon^{-1}(\mathbf{k}_\parallel, z, z'; i\omega)$ is displayed for $z \in [-25, -15]$ calculated for different parameters d_{inv}. One can see that it is sufficient to choose $d_{\text{inv}} = 10$. As far as the step size is concerned, the figure on the right side of 7.13 shows that $\Delta z = 0.75$ leads to an adequate convergence.

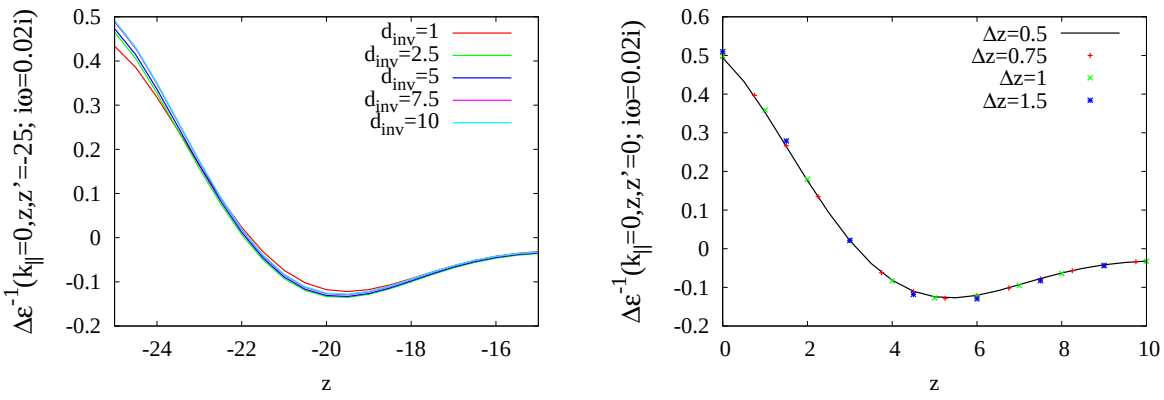

Figure 7.13: Determination of the convergence parameters for the inversion of the renormalization function. Whereas on the right side the inverse of the renormalization function $\Delta\varepsilon(\mathbf{k}_\parallel, z, z'; i\omega)$ is shown for different Δz, on the left side the integration limit is varied. An adequate convergence is reached for $\Delta z = 0.75$ and $d_{\text{inv}} = 10$.

Irreducible polarization In the next step, the irreducible polarization according to eq. (7.39) is evaluated. In order to determine the necessary size of the integration limits I have calculated the irreducible polarization function for varying integration limits $z_{\min} = -25 - d_{\text{pol}}$ and $z_{\max} = 25 + d_{\text{pol}}$. On the left side of figure 7.14 the irreducible polarization as a function of z and different values of d_{pol} is displayed with one z coordinate fixed at the lower limit of the interval, thus at $z' = -25$. The two curves with $d_{\text{pol}} = 2.5$ and $d_{\text{pol}} = 5$ agree very well, therefore in each case $d_{\text{pol}} = 5$ should be sufficient.
It is quite interesting to compare the irreducible polarization function in the ALDA with the non-interacting polarization function P_0^{hom} (see the right side of figure 7.14). The inclusion of exchange and correlation effects leads to an increase of the polarization, whose magnitude might not have been expected. The discussion of this enhancement is postponed to the following chapter, where I will show that as a consequence, the conductance increases, too.

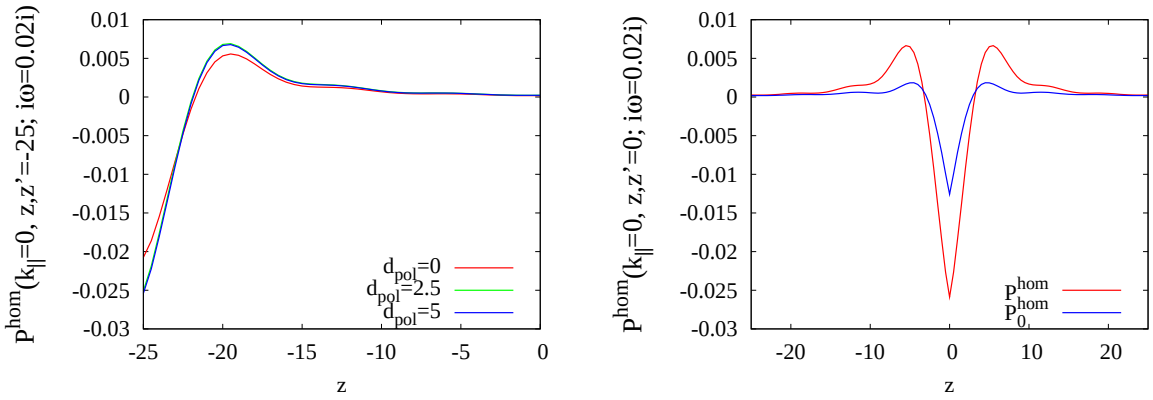

Figure 7.14: *Left:* Irreducible polarization function of the homogeneous electron gas for different convergence parameters d_{pol}. Convergence is reached already for $d_{\text{pol}} = 5$. *Right:* Comparison of the polarization function of the homogeneous electron gas with and without exchange and correlation effects. The former has much larger absolute values.

7.6.3 Potential barrier and quantum well

With the convergence parameters determined in the last subsection the irreducible polarization of the potential barrier and the quantum well can be calculated. The results are displayed in figure 7.15. Equivalently to the irreducible polarization of the homogeneous electron gas, the inclusion of exchange and correlation effects in the ALDA leads to a strong enhancement of the polarization. As expected, for the potential barriers the irreducible polarization is reduced compared to that of the homogeneous electron gas, and it decreases for increasing barriers. In contrast, an enhancement of the irreducible polarization can be observed for the quantum well

potentials.
However, in this work the irreducible polarization on the imaginary frequency axis is just a tool to calculate the conductance of the system, which will be the subject of the next chapter.

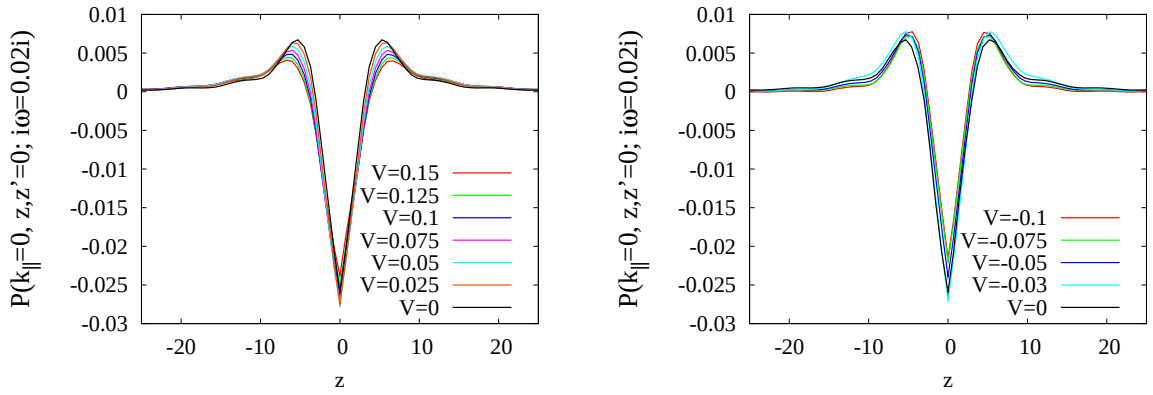

Figure 7.15: Irreducible polarization for the potential barrier (*left*) and the quantum well (*right*). The inclusion of exchange and correlation effects leads to an enhanced polarization but does not influence the qualitative dependence on the potential V.

8 Conductance

This chapter deals with the calculation of the conductance Γ both for non-interacting electrons and systems including electron-electron interaction in linear response. In the first case, the result equals the conductance obtained within the single-particle picture of the Landauer approach (see chapter 4), which from now on is denoted by 'Landauer conductance'.
In the second part of this chapter exchange and correlation effects are taken into account, and the conductance is calculated using the irreducible polarization presented in the last chapter. Finally, I analyze the results and discuss the effects of electron-electron interaction on the conductance. I perform all calculations both for the homogeneous electron gas and the different potentials presented in section 5.1.

8.1 Landauer conductance

As presented in chapter 4, the conductance is related to the polarization following eq. (4.36)

$$\Gamma = \frac{2\pi}{\mu} \lim_{\omega \to 0^+} \omega \int_0^\infty dz \int_{-\infty}^0 dz' P(\mathbf{k}_\parallel = \mathbf{0}, z, z'; i\omega) \; .$$

In order to calculate the Landauer conductance for non-interacting electrons the polarization P_0 is inserted instead of the irreducible polarization. Again, for the numerical calculation the integrals have to be discretized and are calculated using Simpson's rule. The integrations over the half z axis can be limited to finite intervals since the irreducible polarization swiftly decays to zero for large distances $|z - z'|$. The size of these intervals is investigated in the next section whereas the step size of the numerical integrations can be chosen equally large to the grid size of the inversion and the numerical integration of the irreducible polarization investigated in the last chapter.
Furthermore, I will calculate $\Gamma(\omega)$ for finite values of ω and extrapolate to the real frequency axis, i.e. I take the limit $\omega \to 0$ to obtain the conductance. The calculation at $\omega = 0$ itself does not make any sense, since the result of the integral in eq. (4.36) must be infinite in order to obtain a finite conductance. It has to be emphasized that although $\Gamma(\omega)$ is displayed for finite values of ω, only the value of $\Gamma(\omega)$ extrapolated to $\omega = 0$ has physical meaning and represents the conductance.

8.1.1 Homogeneous electron gas

The conductance within the non-interacting single-particle picture can be calculated with the Landauer formula (4.10)

$$\Gamma = \frac{1}{\pi} \sum_{i,j} |t_{ij}|^2 \ .$$

Compared to eq. (4.10) I have added a factor two to take the spin degeneracy into account, since this factor is included in the polarization function, too. For the case of the homogeneous electron gas ($\sum_{i,j} |t_{ij}|^2 = 1$) I expect the conductance $\Gamma_0^{\mathrm{hom}} = \frac{1}{\pi}$. From now on all results for the conductance will be normalized to the conductance of the homogeneous electron gas in the single-particle picture $\Gamma_0^{\mathrm{hom}} = \frac{1}{\pi}$.
The polarization function for the effective potential of the homogeneous electron gas $P_0^{\mathrm{hom}}(\mathbf{k}_\parallel = \mathbf{0}, z, z'; i\omega)$ is calculated in section 7.2. Inserting it in eq. (4.36), it turns out that for small frequencies, the integral is not yet converged in the interval $[-25, 25]$, in which I have calculated the polarization function so far. In order to achieve convergence the total interval in which the irreducible polarization is calculated is enlarged to $[-25 - d_\mathrm{c}, 25 + d_\mathrm{c}]$ and therefore the lower integration limit of z becomes $-25 - d_\mathrm{c}$ whereas the upper limit of the integration over z' increases to $25 + d_\mathrm{c}$. On the left side of figure 8.1, $\Gamma_0^{\mathrm{hom}}(\omega)/\Gamma_0^{\mathrm{hom}}$ is presented for different values of d_c. One can observe that for decreasing imaginary frequency a larger d_c is re-

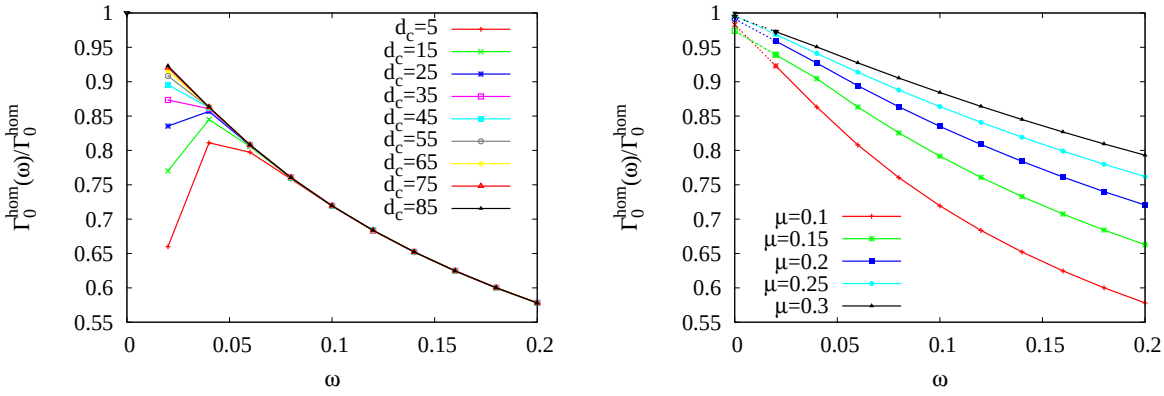

Figure 8.1: $\Gamma_0^{\mathrm{hom}}(\omega)/\Gamma_0^{\mathrm{hom}}$ in the non-interacting single-electron picture for the homogeneous electron gas. *Left:* Check of the integration limits for the calculation of Γ for the chemical potential $\mu = 0.1$. Convergence is reached for $d_\mathrm{c} = 85$. *Right:* Linear extrapolation of the conductance for different values of the chemical potential (comparable to corresponding values for metals). Evaluation of the extrapolated curves yields the conductance $\Gamma_0^{\mathrm{hom}}(\omega)/\Gamma_0^{\mathrm{hom}} = 1$. As expected, in the single-particle picture the conductance does not depend on the chemical potential and has the finite value $\Gamma = \frac{1}{\pi}$ calculated with the Landauer formula.

quired. This is quite reasonable, since the imaginary part of the frequency dampens the oscillations and causes a faster decay. For all frequencies displayed in figure 8.1 convergence is reached for $d_c = 85$. The deviation of the curves $\Gamma_0^{\text{hom}}(\omega)$ for small values of ω towards $\Gamma = 0$ is a finite size effect, which is due to the restriction of the infinite integration limits to finite values. In the limit $\omega \to 0$, this restriction is no longer valid, and the integrations in eq. (4.36) have to be performed over the semi-infinite axes.
According to the Landauer formula, the conductance of the homogeneous electron gas for non-interacting electrons is expected not to depend on the chemical potential μ. This is verified on the right side of figure 8.1. A linear extrapolation from the two smallest frequencies shows that all curves for different values of μ in the limit $\omega \to 0$ yields the conductance $\Gamma_0^{\text{hom}}(\omega = 0) \approx \frac{1}{\pi}$. Since the curves are convex, linear extrapolation slightly underestimates the correct value. However, I can conclude, that the results agree very well with the Landauer formula.

8.1.2 Potential problems

The calculation of the conductance for potentials $V \neq$ const. proceeds similarly to the calculation of the conductance of the homogeneous electron gas. In particular, starting from the polarization function for an effective potential all numerical parameters can be assumed to be the same. This includes the interval $[-110, 110]$, in which the polarization has to be evaluated in order to reach convergence for Γ (see figure 8.1). However, there is no need to calculate ΔP_0 in this large interval as well, since for increasing $|z - z'|$ it decays much faster to zero than P_0 itself. In order to investigate the required length l of the interval $[-\frac{l}{2}, \frac{l}{2}] \subseteq [-110, 110]$, in which ΔP_0 has to be evaluated, the conductance $\Gamma_0(\omega)$ for the potential barrier $V = 0.15$ and the quantum well $V = -0.1$ (with the chemical potential $\mu = 0.1$) for different values of l is evaluated. Obviously, for varying l the potential is always kept in the center

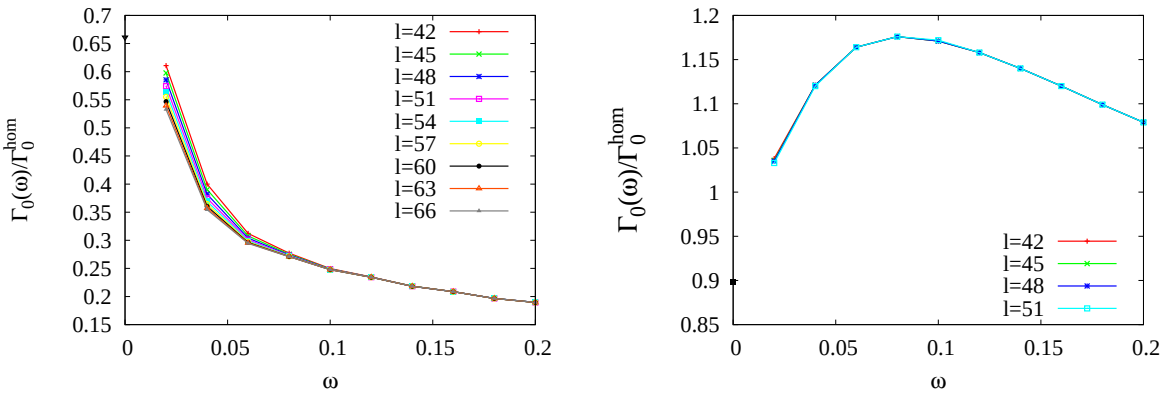

Figure 8.2: Conductance for the potential barrier (*left*) and the quantum well (*right*) for different lengths of the interval in which the difference ΔP_0 is calculated.

of the interval at $z = 0$ and the width of the potential is not changed. Figure 8.2 shows that for the potential barrier a broader interval than for the quantum well is required. For the potential barrier, convergence is reached not until $l \approx 54$, whereas for the quantum well $l = 48$ suffices.
For these simple potentials the theoretical value of the conductance can be calculated analytically. The transmission coefficient for the potential barrier/quantum well $T(\mu) = |t(\mu)|^2$ at the chemical potential μ has to be inserted in the Landauer formula eq. (4.10). $t(\epsilon)$ can be calculated analytically by wave-function matching and yields

$$t(\epsilon) = \frac{4ik\kappa e^{-i\kappa d}}{(ik+\kappa)^2 + (k+i\kappa)^2 e^{\kappa d}} \tag{8.1}$$

with $k = \sqrt{2\epsilon}$ and $\kappa = \sqrt{2V - k^2}$. Formula (8.1) is valid for both, positive and negative potentials. The length d is the width of the potential barrier/quantum well, which in the investigated systems amounts to $d = 2$. In figure 8.3 the analytical values of the conductance for the different potential barriers are shown at $\omega = 0$. Linear extrapolation of $\Gamma_0(\omega)$ to $\omega = 0$ leads to a relatively good agreement with the analytical result. Whereas for the highest barrier ($V = 0.15$) the conductance

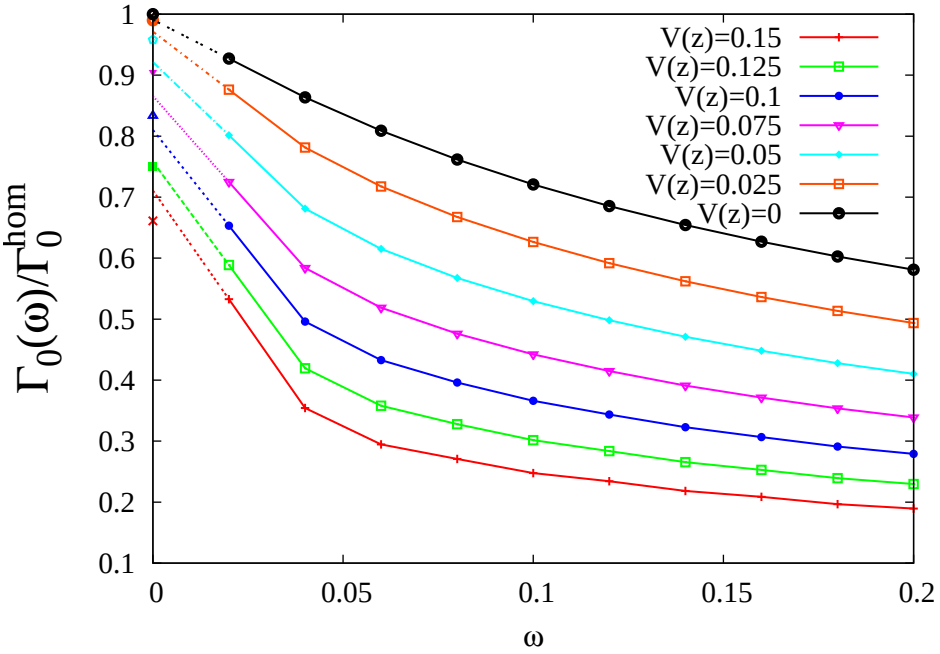

Figure 8.3: Conductance of the potential barrier for different values of V divided by $\Gamma_0^{\text{hom}} = \frac{1}{\pi}$. At $\omega = 0$, the analytically calculated values obtained with the Landauer formula are shown. Linear extrapolation of the curves $\Gamma(\omega)$ from the two lowest frequencies $\omega = 0.02$ and $\omega = 0.04$ leads to a relatively good agreement with the analytical results.

is slightly overestimated, for small barriers ($V = 0.05$, $V = 0.025$) the extrapolated values are too small. In contrast, for the quantum wells displayed in figure 8.4, a linear extrapolation of $\Gamma_0(\omega)$ to $\omega = 0$ is not sufficient. Especially for very flat quantum wells ($V = -0.03$ and $V = -0.05$), a linear extrapolation would lead to a conductance higher than that of the homogeneous electron gas. In order to improve the result a better curve for fitting has to be found. That is not easy, since even in the case of the homogeneous electron gas the frequency-dependence $\Gamma_0^{\mathrm{hom}}(\omega)$ is not known analytically and therefore cannot be used for fitting purposes. On the other hand, an improvement of the extrapolation can already be reached by a parabolic fit taking the three lowest frequencies into account.
Of course, a more accurate conductance could be obtained by calculating $\Gamma_0(\omega)$ at lower frequencies. However, this would drastically increase the computation time, since much higher convergence parameter would be required. It has to be said that for the quantum wells even $\Gamma_0(\omega)$ shown here might not be fully converged for small values of ω.

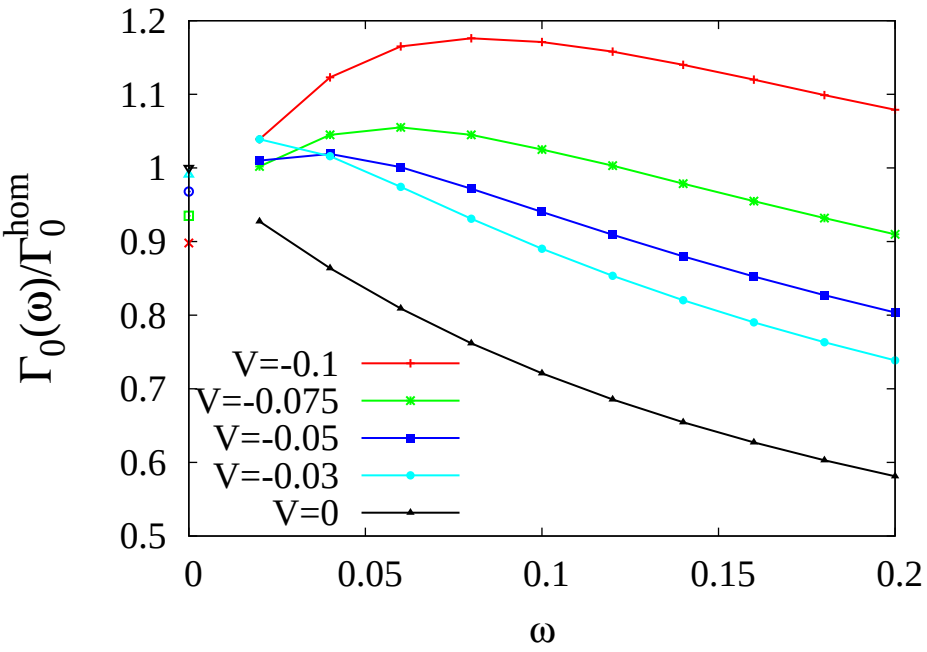

Figure 8.4: Conductance of the quantum well for different values of V and $\mu = 0.1$. At $\omega = 0$, the analytically calculated values obtained with the Landauer formula are shown. In contrast to the potential barriers (see figure 8.3), linear extrapolation of the curves $\Gamma(\omega)$ is not sufficient in the case of the quantum wells. For the curves of very flat wells ($V = -0.03$ and $V = -0.05$) linear extrapolation leads to an unphysical conductance larger than that of the homogeneous electron gas.

8.2 Inclusion of exchange and correlation effects

In the following section I will investigate the influence of electron-electron interaction on the conductance. Therefore I evaluate eq. (4.36) for the irreducible polarization calculated in section 7.6 instead of the polarization for non-interacting electrons.

8.2.1 Homogeneous electron gas

The numerical results $\Gamma^{\mathrm{hom}}(\omega)$ for the homogeneous electron gas for different chemical potentials are displayed in figure 8.5. Compared to the Landauer conductance (see figure 8.1), one observes a systematic increase in the conductance. Furthermore, in contrast to the conductance in the non-interacting single-particle picture, the absolute value of the full conductance within the adiabatic local-density approximation (ALDA) strongly depends on the chemical potential μ: The effects of exchange and correlation increase with decreasing chemical potential (i.e. decreasing density). However, although the dependence of the conductance on the chemical potential is reasonable, the quantity of the influence of exchange and correlation in general is not expected. The extrapolated values for Γ^{hom} are very large. For example, for $\mu = 0.1$ I obtain $\Gamma^{\mathrm{hom}}/\Gamma_0^{\mathrm{hom}} \approx 1.77$. They are equal to the numerical results calculated by P. Bokes *et al.* [BJG06] presented in the following table.

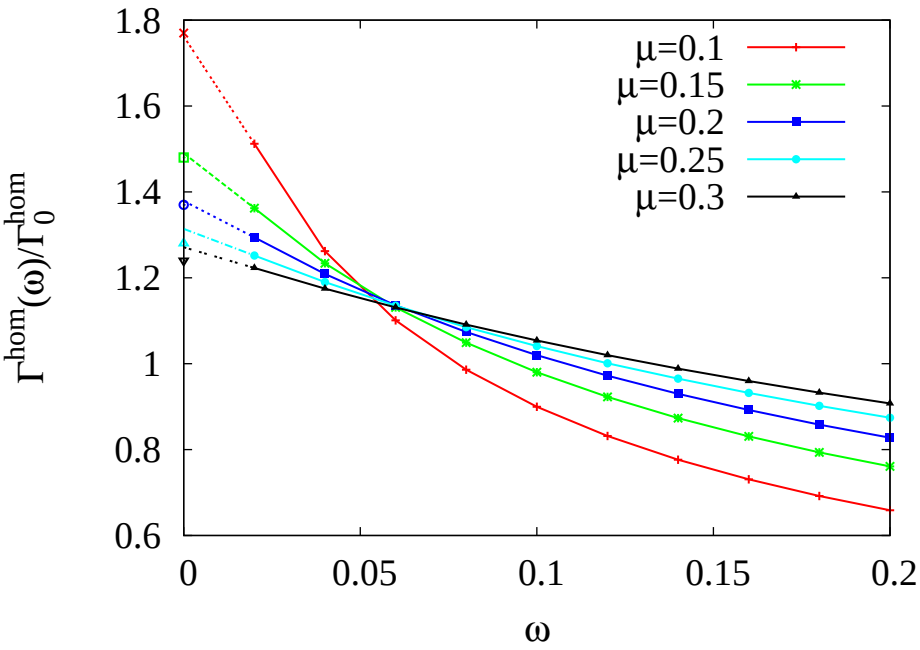

Figure 8.5: Linear extrapolation of the full conductance within the ALDA for the homogeneous electron gas for different chemical potentials. For comparison, at $\omega = 0$ the numerically calculated values calculated by P.Bokes *et al.* are shown. They agree quite well with our numerical results.

μ	0.1	0.15	0.2	0.25	0.3
r_s	4.29	3.50	3.03	2.71	2.48
$\Gamma^{\mathrm{hom}}/\Gamma_0^{\mathrm{hom}}$	1.77	1.48	1.37	1.28	1.24

Additionally, these values are displayed in figure 8.5 at $\omega = 0$. Regarding this figure one can see that the linear extrapolation of $\Gamma^{\mathrm{hom}}(\omega)$ to $\omega = 0$ yields approximately the same values.
Each chemical potential μ corresponds to a density parameter r_s, since $\frac{1}{n} = \frac{4\pi}{3} r_s^3$, $k_{\mathrm{F}} = (3\pi^2 n)^{1/3}$ and $\mu = \frac{1}{2} k_{\mathrm{F}}^2$. P. Bokes *et al.* showed that the ALDA correction is significant within the physically relevant region $2 \lesssim r_s \leq r_{s,c}$, where $r_{s,c}$ is a critical value that is caused by a pole in the irreducible polarization. It amounts to $r_{s,c} \approx 5.4$. More details can be found in [BJG06]. Hence, all chemical potentials displayed in figure 8.5 represents physically relevant cases.
For the different potentials which are investigated in this thesis I have chosen $\mu = 0.1$ which is equivalent to $r_s = 4.29$. It is a rather extreme case, for which the influence of exchange and correlation is very large.

8.2.2 Potential barrier and quantum well

Finally, I can calculate the full conductance including electron-electron interaction for different step potentials. The results for the potential barriers are presented in figure 8.6. As already observed for the homogeneous electron gas, exchange and correlation effects cause a strong enhancement of the conductance. As expected, the inclusion of exchange and correlation effects does not change the qualitative behavior between the different heights of the barrier, i.e., for a higher barrier a lower conductance is obtained. However, the relative difference between the different potential barriers is smaller than in the non-interacting case. In contrast, the conductance calculated for the different quantum wells (see figure 8.7) is higher than that of the homogeneous electron gas and the conductance for the deepest quantum well ($V = -0.1$) is the largest among all potentials considered here. This is opposed to the non-interacting case, since for this quantum well the lowest conductance was obtained (see figure 8.4). The enhancement of the conductance of the quantum wells compared to that of the homogeneous electron gas might be due to the states localized in the quantum well. For all depths V investigated in this thesis there is one localized state with positive parity at the eigenenergy E_V. The eigenergies for the different potentials are written down in the following table.

V	E_V
-0.1	-0.016
-0.075	-0.009
-0.05	-0.004
-0.03	-0.002

Since the quantum wells are very flat, the eigenstates are only weakly bound. The smoother the potential, the smaller is the difference in energy to the free states. This

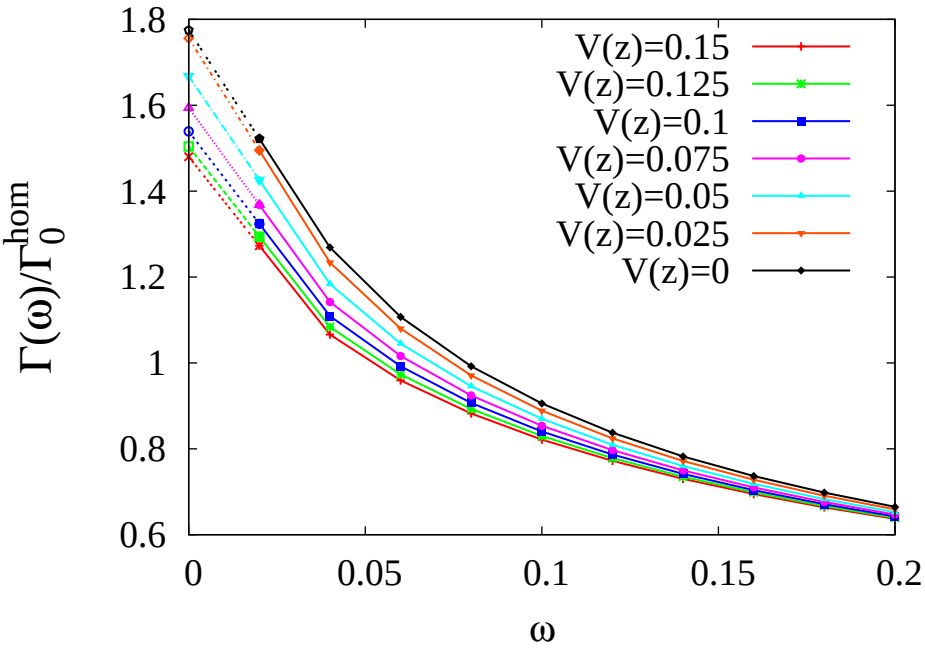

Figure 8.6: Extrapolation of the full conductance within the ALDA for the potential barrier for different values of V, but constant $\mu = 0.1$. As observed already for the homogeneous electron gas, the inclusion of exchange and correlation leads to a strong increase of the conductance. Compared to the conductance without exchange and correlation effects the relative difference between the conductances of the different potentials is reduced. In order to obtain the values for $\Gamma(0)$, I have extrapolated the curves linearly from the two points $\omega = 0.04$ and $\omega = 0.02$.

small difference might lead to numerical inaccuracies, especially for the two flattest potentials with $V = -0.03$ and $V = -0.05$ and explain that a higher conductance for these two potentials is obtained than for the two quantum wells with $V = -0.075$ and $V = -0.1$. Moreover, this fits to the observations made in the non-interacting case (see figure 8.4), where the curves $\Gamma_0(\omega)$ for the flattest potentials merely deviate to smaller values.

The general enhancement of the conductance for the quantum wells compared to that of the homogeneous electron gas under consideration of exchange and correlation effects can be explained with the help of these localized states. Electron-electron interaction of the incoming Bloch waves with the localized states might enable new transport mechanisms and (obviously) leads to an enhancement of the net conductance. However, the actual physical process is intransparent which is a consequence of the approach of TDDFT where electronic exchange and correlation enter in the exchange-correlation kernel only, but are not treated explicitly (e.g. as it is the case in the Coulomb interaction). Of course, such an enhancement of the conductance is not possible in the non-interacting case, in which for any potential the conductance

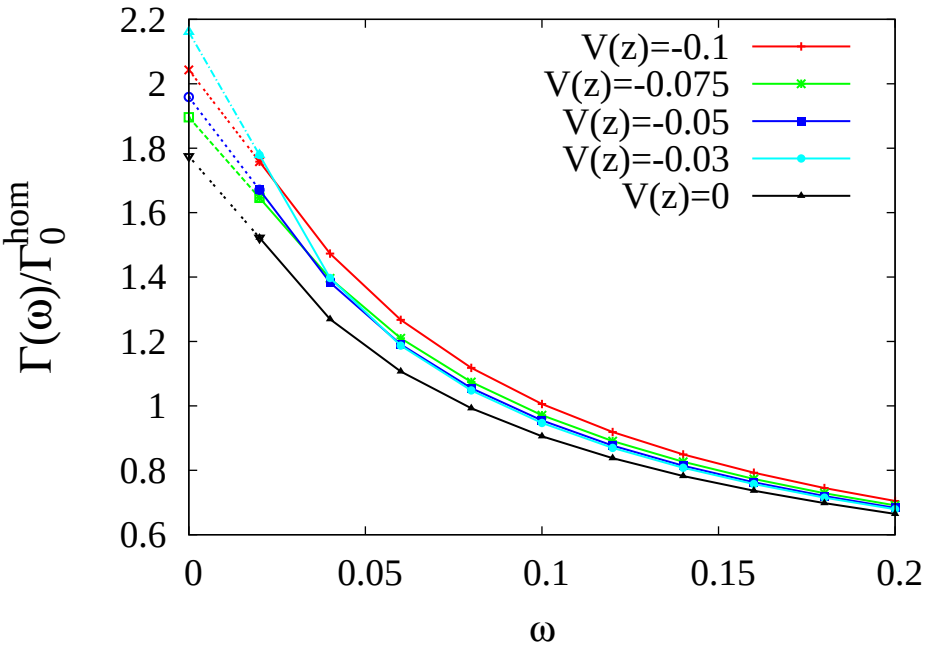

Figure 8.7: Extrapolation of the full conductance within the ALDA for the quantum well for different values of V, but constant $\mu = 0.1$. For the quantum well I even obtain a higher conductance than the one of homogeneous electron gas. This effect might be caused by localized states, which in consideration of exchange and correlation can couple to the Bloch states of the leads and thus contribute to the conductance. The fact that the conductance of the two flat potentials with $V = -0.03$ and $V = -0.05$ is higher than that of the deeper quantum wells might be due to numerical inaccuracies.

has to be smaller than that of the homogeneous electron gas.

8.2.3 Discussion

The relatively strong enhancement of the conductance especially for small chemical potentials under explicit consideration of exchange and correlation both for the homogeneous electron gas and the potential barriers and quantum wells is not yet understood. It might be due to the unusual definition of the conductance made by Bokes and co-workers as the current dependence on the total field composed of the external and the induced field. This is contradictory to the usual definition where only the external field is taken into account and surely connected to the fact that the conductance becomes zero when calculating the conductance describing the current with respect to the applied external field (see section 4.2.4).
Furthermore, it is worth to discuss the influence of the approximation of the exchange-correlation kernel $f_{\mathrm{xc}}(|\mathbf{r}-\mathbf{r}'|, t-t')$ on the conductance. I have calculated the kernel

in the most simple approximation, the ALDA. In the ALDA, the kernel is local both in time and space and thus ignores essential physical features like the nonlocal dependence on the global density distribution or the density at former times. As a consequence, the approximated kernel depends neither on the frequency nor on the wave vector in reciprocal space and is approximated by a constant

$$f_{\mathrm{xc}}^{\mathrm{ALDA}} = \lim_{q\to 0} f_{\mathrm{xc}}^{\mathrm{hom}}(q, i\omega = 0) \tag{8.2}$$

that depends only on the density.
Although the exchange-correlation kernel is in general not known, for the homogeneous electron gas an accurate parameterization of the dynamic kernel $f_{\mathrm{xc}}(q, i\omega)$ on the imaginary frequency axis is available [RA94]. It is derived from a high-order diagrammatic expansion of the polarization and, in addition, takes known sum rules into account. However, the specific element

$$\lim_{\omega\to 0} f_{\mathrm{xc}}^{\mathrm{hom}}(q, i\omega = 0) = f_{\mathrm{xc}}^{\mathrm{ALDA}} \tag{8.3}$$

required for the evaluation of the conductance is identical to the adiabatic local-density approximation, and thus leads to the same results for the conductance.
For inhomogeneous systems, however, the use of accurate parameterizations of the exchange-correlation kernel is doubtful, since the density in general is not unique, i.e. $n(\mathbf{r}) \neq n(\mathbf{r}')$ is valid. Hence, it is unclear which density to insert in the parametrization.
While for the homogeneous electron gas the ALDA leads to an exact result for the conductance, for inhomogeneous systems the ALDA remains an approximation. The magnitude of the errors in the conductance is not known, but the deviation of the exact result is assumed to increase with the deviation of the potential from the constant potential of the homogeneous electron gas. However, since in this diploma thesis only relatively weak potentials are treated, the errors made by using the ALDA are supposed to be small.

Concluding, the method for the calculation of the conductance via the irreducible polarization function proposed by P. Bokes *et al.* is very promising, since it allows to integrate electronic exchange and correlation beyond the single-particle approach of the Landauer formula. However, the practical implementation is quite complicated because of the extrapolation to the real frequency axis ($\omega \to 0$). Moreover, it is based on an usual definition of the conductance as the current dependence on the total field instead of the external field which complicates a physical interpretation of the result. Finally, the integration of electron-electron interaction in the exchange-correlation kernel (in the calculation of the irreducible polarization function) conceals the actual physical processes and, as the former argument, makes the physical interpretation difficult.

9 Summary and outlook

In this diploma thesis I investigated the effect of the electron-electron interaction on quantum transport. Generally, nanoscale transport calculations are very complex because of the involvement of many particles and the special geometry of a scattering setup. For my explorations I chose simple potential barriers and quantum wells, modeling a thin film of vacuum, an isolating material or a metal with another electron density sandwiched between two metallic leads. In this way I simplified the scattering setup while focusing on the many-body aspect.
The first part of my work deals with the calculation of the Green function in the single-particle picture assuming an effective local potential. This potential might be the Hartree-potential or the effective potential of density- functional theory, which already includes exchange and correlation effects in a local description. Since the Green-function embedding method represents one of the few possibilities to integrate the special scattering boundary conditions in feasible numerical transport calculations, I tailored the Green-function embedding method to the investigated three-dimensional setup with a one-dimensional potential. In order to evaluate the accuracy of the embedding method, I derived an analytical expression for the Green function valid for all investigated potential-step problems. This enabled me to compare the results obtained with the Green-function embedding method to the analytical ones. I showed that the deviations of the numerical results are significantly large, so that I decided to continue my calculations with the Green function calculated semi-analytically. In the following I calculated the polarization function for non-interacting electrons, given as a convolution on the complex frequency axis. For this purpose, I decomposed the Green function in a homogeneous part and a remainder, since the remainder decays much faster on the complex frequency axis than the Green function itself and the homogeneous part can be treated analytically.
In order to take dynamic exchange-correlation effects into account beyond the static contribution already included in the effective potential, I calculated the irreducible polarization. It is related to the polarization function of the non-interacting electrons through a Dyson-type equation (derived in time-dependent density-functional theory) via the exchange-correlation kernel. I approximated the kernel in the adiabatic local-density approximation (ALDA). Finally, I used the relation between the polarization and the conductance derived by Bokes and Godby [BG04] to calculate the latter both in the non-interacting single-particle picture and under the explicit consideration of dynamic exchange and correlation. The numerical results obtained in the first case agree very well with the Landauer formula and indicate the correctness of the implementation. Furthermore, the conductance for different electron densities calculated with the irreducible polarization of the homogeneous electron gas

is in good agreement with the results presented in [BG04]. I observed a systematic increase of the conductance when dynamic exchange and correlation are included. These corrections can be surprisingly large for some systems. For example, in the case of a small electron density the conductance amounts to 1.8 times the Landauer conductance.

Before the procedure of calculating the conductance via the irreducible polarization can be applied to realistic systems, some difficulties have to be overcome. First, the Green function cannot be calculated analytically and another method such as the Green-function embedding method has to be used. As shown in chapter 6, for the investigated model systems the deviations of the Green functions calculated numerically with the embedding method to the analytical results are quite large, when the real space arguments of the Green function are the same or located very close to each other. Furthermore, I showed that the accuracy of the method is very sensitive to the choice of the involved numerical parameters. Nevertheless, despite this complex interplay, a set of parameters could always be found for which the description is good. For the setups investigated in this thesis, the determined optimal parameters lead to a relatively sparse grid in the z direction, however. As the resolution cannot be increased while retaining the same accuracy of the description, this becomes a problem in the calculation of the conductance later, which requires several integrations over the z axis. Although I bypassed the problem here by continuing the calculation with the analytical Green function, in the future it is worth trying to overcome these numerical problems, since the Green-function embedding method is applicable to arbitrary potentials and realistic three-dimensional setups. The Green-function embedding method would offer the possibility to calculate the conductance for more realistic, interesting and difficult potentials.
A second question which is worth to discuss is the dependence of the irreducible polarization and the conductance on the approximation of the exchange-correlation kernel. The adiabatic local-density approximation chosen in this thesis is a very drastic approximation of the kernel. In the ALDA, the kernel is local both in the time and the space coordinates and thus ignores essential physical features like the non-local dependence on the global density distribution and on the density at former times. As a consequence, in reciprocal space the approximated kernel depends neither on the frequency nor on the wave vector. For the homogeneous electron gas for a wide range of densities n there are parameterizations of the exchange-correlation kernel $f_{\mathrm{xc}}^{\mathrm{hom}}(n, |\mathbf{r}-\mathbf{r}'|, t-t')$ available. With the help of such a parametrization it can be shown that in the case of the homogeneous electron gas the ALDA leads to the correct result for the conductance. Using the parametrized kernel $f_{\mathrm{xc}}^{\mathrm{hom}}(n, |\mathbf{r}-\mathbf{r}'|, t-t')$ in inhomogeneous systems, on the other hand, one meets a fundamental problem: In such systems the density parameter n is not unique since in general $n(\mathbf{r}) \neq n(\mathbf{r}')$ and therefore it is not clear which density to insert when evaluating the kernel. The magnitude of the errors in the conductance caused by this drastic approximation is difficult to estimate, but for the relatively flat potentials investigated in this thesis it is supposed to be rather small.

Assuming that the exchange-correlation kernel is well approximated (or numerically exact for the homogeneous electron gas) the extrapolation of the conductance to zero frequency remains a source of error. Since the frequency dependence of $\Gamma(\omega)$ even in the case of the homogeneous electron gas is not known analytically it cannot be used as a parametrization for fitting purposes. However, in the calculations made in this thesis I contented with a linear fit to obtain the conductance. The accuracy of the linear fit can be estimated with the help of the non-interacting case, where the conductance $\Gamma(\omega = 0)$ can be calculated with the Landauer formula. In order to reach a higher accuracy, either a better curve for fitting has to be found or the conductance has to be extrapolated from smaller frequencies. However, going to smaller frequencies requires higher convergence parameters and as a consequence leads to a higher computation time.
Even for the simple model systems considered here, the calculation of the conductance already turned out to be computationally very demanding. In order to avoid expensive double calculations, the Green function must calculated and stored as a function of four variables. As shown in chapter 5, in the embedding method it is first calculated for one frequency ϵ and one wave vector $\mathbf{k}_\parallel$ as a matrix of the two spatial coordinates z and z'. In contrast, the polarization function is given as a convolution over the complex frequency axis and therefore the Green function is required as a function of the frequency, too (for one $\mathbf{r}_\parallel$ and one combination of z and z'). Moreover, it is needed in real space coordinates in order to avoid a supplementary (two-dimensional) convolution concerning $\mathbf{k}_\parallel$. Concerning the parallel coordinates the Green function has to be Fourier transformed from reciprocal space to real space, since it is calculated most easily as a function of $\mathbf{k}_\parallel$. On the other hand, the polarization function is required for $\mathbf{k}_\parallel = \mathbf{0}$, and hence must be Fourier transformed back to reciprocal space. Imagining a realistic system with a three-dimensional potential the calculation time as well as the amount of data increases drastically: The Green function is now a function of eight coordinates (instead of four)! Thus, even the government of this huge amount of data constitutes a challenge. It is evident that for a practical and feasible implementation smart novel and parallel programs are required.
At the end of this diploma thesis I want to discuss once more the limits of the investigations I made here. The linear response approach is only suitable for the calculation of the static zero-bias conductance in equilibrium and does not include dynamical processes like the switch-on and the switch-off of an electric field. However, these processes are very important in nanoelectronics since most things happen on a very short time-scale. Furthermore, the model systems investigated in this thesis here are periodic in two dimensions and therefore assumed to be infinite. Thus, they model a system composed of different layers which are small only in one dimension. In contrast, in nanoelectronics most of the conducting devices are small in all dimensions.

10 Acknowledgments

This work could not have been accomplished without both the professional help and mental support of many people. First of all, I would like to thank my two advisors Arno Schindlmayr and Daniel Wortmann, who according to their different fields of research and their very different temperaments gave me a lot of new insights into the interesting world of many-body physics and electronic transport. In particular, I want to thank you, Arno, for your deliberate and mature comments concerning my work. Although during this year your time was often very rare, you took always some time to answer my questions. Moreover, your very critical proof-reading was very helpful and gave me a deeper insight in many-body physics. Great thanks to you, Daniel, for your creative, helpful ideas, your patience and your encouragement in times of my greatest exasperation. You gave me always some brainchildren how to get out of an impasse.

I am grateful to Prof. Dr. Stefan Blügel who — without knowing me at all — offered me the possibility writing my diploma thesis in the 'Theory I' institute at the research center of Jülich and who took over the 'Erstgutachten'. Furthermore, I would like to thank Prof. Dr. Stefan Heinze from the University of Hamburg here as the second examiner of this work. Without his willingness to do so I could not have come to the 'Theory I' institute of Jülich.

Big thanks goes to my three room-mates Andreas Dolfen, Andreas Gierlich and Manfred Niesert for creating the enjoyable working atmosphere and for assisting me in all kinds of problems. Without your technical support I would not have accomplished this work. Furthermore, I would like to thank you for the very helpful proof-reading of my work and the constructive comments.

My thanks also goes to Lena Vedmedenko, my fellow student from the university of Hamburg. Looking back to the times of our studies, I am very thankful for our helpful discussions, for the steadiness of our common work and the mutual support. Knowing always that I can count on you, I will not miss you. I know that it is very rare to find someone with whom one can work together for quite a long time. Although we had not much contact during the time of my diploma thesis, the very few discussions were very encouraging for me.

Coming to an end I would like to thank my family and friends. Although having no idea what I am doing they were never in doubt about a successful end of this work. My special thanks goes to you, Philipp, for your encouragement, your patience and your helpful comments. Especially when I was desperate and hopeless, you fetched me back to earth and gave me new hope. Finally, without you I would not have come to Jülich and would not have spent this enjoyable and educational year here.

Bibliography

[AG98] F. Aryasetiawan and O. Gunnarson.
The *GW* method.
Reports on progress in Physics, 61:237–312, 1998.

[ARDSO98] Stefan Albrecht, Lucia Reining, Rodolfo Del Sole, and Giovanni Onida.
Ab initio calculation of excitonic effects in the optical spectra of semiconductors.
Phys. Rev. Lett., 80(20):4510–4513, May 1998.

[Bar61] J. Bardeen.
Tunnelling from a many-particle point of view.
Phys. Rev. Lett., 6(2):57–59, Jan 1961.

[BB06] S. Blügel and Gustav Bihlmayer, editors.
Computational Nanoscience: Do it yourself!, volume 31 of *NIC series*.
NIC-directors, 2006.

[BG04] P. Bokes and R. W. Godby.
Conductance and polarization in quantum junctions.
Physical Review B (Condensed Matter and Materials Physics), 69(24):245420, 2004.

[BILP85] M. Büttiker, Y. Imry, R. Landauer, and S. Pinhas.
Generalized many-channel conductance formula with application to small rings.
Phys. Rev. B, 31(10):6207–6215, May 1985.

[BJG06] P. Bokes, J. Jung, and R. W. Godby.
Quantum conductance of homogeneous and inhomogeneous interacting electron systems.
ArXiv Condensed Matter e-prints, April 2006.

[CA80] D. M. Ceperley and B. J. Alder.
Ground state of the electron gas by a stochastic method.
Phys. Rev. Lett., 45(7):566–569, Aug 1980.

[CBLC96] Leonor Chico, Lorin X. Benedict, Steven G. Louie, and Marvin L. Cohen.
Quantum conductance of carbon nanotubes with defects.
Phys. Rev. B, 54(4):2600–2606, Jul 1996.

[EWK04] F. Evers, F. Weigend, and M. Koentopp.
Conductance of molecular wires and transport calculations based on density-functional theory.

Physical Review B (Condensed Matter and Materials Physics), 69(23):235411, 2004.

[FBM04] G. Fratesi, G. P. Brivio, and L. G. Molinari.
Many-body method for infinite nonperiodic systems.
Physical Review B (Condensed Matter and Materials Physics), 69(24):245113, 2004.

[FW03] A.L. Fetter and J.D. Walecka.
Quantum Theory of Many-Particle Physics.
Dover, 2003.

[GSS87] R. W. Godby, M. Schlüter, and L. J. Sham.
Quasiparticle energies in gaas and alas.
Phys. Rev. B, 35(8):4170–4171, Mar 1987.

[Hed65] Lars Hedin.
New Method for Calculating the One-Particle Green's Function with Application to the Electron-Gas Problem.
Phys. Rev., 139(3A):A796–A823, Aug 1965.

[HK64] P. Hohenberg and W. Kohn.
Inhomogeneous electron gas.
Phys. Rev., 136(3B):B864–B871, Nov 1964.

[HL86] Mark S. Hybertsen and Steven G. Louie.
Electron correlation in semiconductors and insulators: Band gaps and quasiparticle energies.
Phys. Rev. B, 34(8):5390–5413, Oct 1986.

[HT95] Kenji Hirose and Masaru Tsukada.
First-principles calculation of the electronic structure for a bielectrode junction system under strong field and current.
Phys. Rev. B, 51(8):5278–5290, Feb 1995.

[HTM+02] S. Heinze, J. Tersoff, R. Martel, V. Derycke, J. Appenzeller, and Ph. Avouris.
Carbon nanotubes as schottky barrier transistors.
Phys. Rev. Lett., 89(10):106801, Aug 2002.

[Ing81] J. E. Inglesfield.
A method of embedding.
Journal of Physics C, 14:3795–3806, 1981.

[Ink84] John C. Inkson.
Many-body theory of solids.
Plenum Press, 1984.

[KDP80] K. v. Klitzing, G. Dorda, and M. Pepper.
New method for high-accuracy determination of the fine-structure constant based on quantized hall resistance.

Phys. Rev. Lett., 45(6):494–497, Aug 1980.

[Kon64] J. Kondo.
Resistance minimum in dilute magnetic alloys.
Progress of Theoretical Physics, 32(1):37–49, 1964.

[Kor47] J. Korringa.
Physica, 1947.

[KR54] W. Kohn and N. Rostoker.
Solution of the schrödinger equation in periodic lattices with an application to metallic lithium.
Phys. Rev., 94(5):1111–1120, Jun 1954.

[KS65] W. Kohn and L. J. Sham.
Self-consistent equations including exchange and correlation effects.
Phys. Rev., 140(4A):A1133–A1138, Nov 1965.

[Kub59] R. Kubo.
Some aspects of the statistical-mechanical theory of irreversible processes.
In W. E. Brittin and L.G. Dunham, editors, *Lectures in Theoretical Physics*, volume 1. Interscience, 1959.

[Lan57] R. Landauer.
Spatial variations of currents and fields due to localized scatterers in metallic conduction.
IBM Journal of Research and Development, 1(3):223, 1957.

[Mah90] Gerald D. Mahan.
Many-Particle Physics.
Plenum Press, second edition, 1990.

[Mat97] J. Mathon.
Tight-binding theory of tunneling giant magnetoresistance.
Phys. Rev. B, 56(18):11810–11819, Nov 1997.

[MS59] Paul C. Martin and Julian Schwinger.
Theory of many-particle systems. i.
Phys. Rev., 115(6):1342–1373, Sep 1959.

[PBE96] John P. Perdew, Kieron Burke, and Matthias Ernzerhof.
Generalized gradient approximation made simple.
Phys. Rev. Lett., 77(18):3865–3868, Oct 1996.

[PCV+92] John P. Perdew, J. A. Chevary, S. H. Vosko, Koblar A. Jackson, Mark R. Pederson, D. J. Singh, and Carlos Fiolhais.
Atoms, molecules, solids, and surfaces: Applications of the generalized gradient approximation for exchange and correlation.
Phys. Rev. B, 46(11):6671–6687, Sep 1992.

[PGG96] M. Petersilka, U. J. Gossmann, and E. K. U. Gross.
Excitation energies from time-dependent density-functional theory.
Phys. Rev. Lett., 76(8):1212–1215, Feb 1996.

[PW92] John P. Perdew and Yue Wang.
Accurate and simple analytic representation of the electron-gas correlation energy.
Phys. Rev. B, 45(23):13244–13249, Jun 1992.

[RA94] C. F. Richardson and N. W. Ashcroft.
Dynamical local-field factors and effective interactions in the three-dimensional electron liquid.
Phys. Rev. B, 50(12):8170–8181, Sep 1994.

[RG84] Erich Runge and E. K. U. Gross.
Density-functional theory for time-dependent systems.
Phys. Rev. Lett., 52(12):997, Mar 1984.

[ROB+02] J. Reichert, R. Ochs, D. Beckmann, H. B. Weber, M. Mayor, and H. v. Löhneysen.
Driving current through single organic molecules.
Phys. Rev. Lett., 88(17):176804, Apr 2002.

[RZM+97] M. A. Reed, C. Zhou, C. J. Muller, T. P. Burgin, and J. M. Tour.
Conductance of a Molecular Junction.
Science, 278(5336):252–254, 1997.

[Sch51] Julian Schwinger.
On the green's functions of quantized fields.
Proceedings of the National Academy of Sciences, 37(7):452–459, 1951.

[Sch06] Arno Schindlmayr.
Time-dependent density-functional theory.
In E. Koch H. Müller-Krumbhaar R. Spatschek R. G. Winkler S. Blügel, G. Gompper, editor, *Computational Condensed Matter Physics*, volume 32 of *Reihe Materie und Material/Matter and Materials*, pages A4.1–A4.19. Schriften des Forschungszentrums Jülich, 2006.

[TVD98] Sander J. Tans, Alwin R. M. Verschueren, and Cees Dekker.
Room-temperature transistor based on a single carbon nanotube.
Nature, 393:49, 1998.

[Was03] R. Waser, editor.
Nanoelectronics and Information Technology.
Wiley-VCH Verlag, 2003.

[WGAW00] L. Jönnson W. G. Aulbur and J. W. Wilkins.
In H. Ehrenreich and F. Spaepen, editors, *Solid State Physics*, page 1. Academic, 2000.

[WIB02] D. Wortmann, H. Ishida, and S. Blügel.

Embedded green-function approach to the ballistic electron transport through an interface.
Phys. Rev. B, 66(7):075113, Aug 2002.

[Wor03] Daniel Wortmann.
An Embedding Green Function Approach for Electronic Transport through Interfaces.
PhD thesis, Forschungszentrum Jülich, 2003.

[ZS80] A. Zangwill and Paul Soven.
Resonant photoemission in Barium and Cerium.
Phys. Rev. Lett., 45(3):204–207, Jul 1980.

Selbständigkeitserklärung

Hiermit versichere ich, die vorliegende Arbeit selbständig und nur unter Zuhilfenahme der angegebenen Quellen und Hilfsmittel angefertigt zu haben. Ich bin mit einer zukünftigen Ausleihe meiner Diplomarbeit einverstanden.

Jülich im Juli 2007

(Swantje Heers)